A Novel Approach to Programmable Imaging Using MOEMS

A Thesis

Submitted to the Faculty

of

Drexel University

by

Vasileios T. Nasis

in partial fulfillment of the

requirements for the degree

of

Doctor of Philosophy in Electrical and Computer Engineering

November 2007

Dedications

...to my parents Thomas and Koula Nasis and to my wife Allison.

Acknowledgments

I would like to express my heartfelt gratitude to my advisor, Dr. Timothy P. Kurzweg and to my Co-advisor Dr. R. Andrew Hicks, for their inspiration and guidance over the preparation of this thesis and all my graduate research endeavors. It is due their consistent support that I have been able to finish my graduate studies at Drexel University successfully.

Thanks also to the other members of my thesis committee, Dr. Kostas Daniilidis, Dr. Yougmoo Kim and Dr. Adam Fontecchio. In particular, i would like to thank Dr. Daniilidis for giving me a lot of ideas arround computer vision that i was able later on to implement to my research. Also I would like to thank Dr. Mohana Shankar and Dr. Nihat Bilgutay for their guidance and help during my graduate and undergraduate studies at the Electrical and Computer Engineering Department of Drexel University.

Over the course of the past eight years as member of Drexel's family i have had the honor to work with many distinct individuals who have helped me and inspired throughout all this time. So i would like to thank them all.

Above all, I would like to thank my parents, all my family and my wife for their love and support all this time.

Table of Contents

List of Tables

List of Figures

Abstract

A Novel Approach to Programmable Imaging Using MOEMS

Vasileios T. Nasis

Timothy P. Kurzweg, Ph.D

New advancements in science are frequently sparked by the invention of new instruments. Possibly the most important scientific instrument of the past fifty years is the digital computer. Among the computers many uses and impacts, digital imaging has revolutionized images and photography, merging computer processing and optical images. In this thesis, we merge an additional reconfigurable micro-mechanical domain into the digital imaging system, introducing a novel imaging method called Programmable Imaging. With our imaging method, we selectively sample the object plane, by utilizing state-of-the-art Micro-Optical-Electrical-Mechanical Systems (MOEMS) of mirror arrays. The main concept is to use an array of tiny mirrors that have the ability to tilt in different directions. Each mirror acts as an "eye" which images a scene. The individual images from each mirror are then reassembled, such that all of the information is placed into a single image. By exact control of the mirrors, the object plane can be sampled in a desired fashion, such that post-processing effects, such as image distortion and digital zoom, that are currently performed in software can now be performed in real time in hardware as the image gets captured. It is important to note that even for different sampling or imaging functions, no hardware components or settings are changed in the system.

In this work, we present our programmable imaging system prototype. The MOEMS chipset used in our prototype is the Lucent LambdaRouter mirror array. This device contains 256 individually-controlled micro-mirrors, which can be tilted on both the x and y axes $\pm 8^o$. We describe the theoretical model of our system, including a system model, capacity model, and diffraction results. We experimentally prototype our programmable imaging system using both a single mirror, followed by multiple mirrors. With the single mirror imaging, we explore examples related to single projection systems and give details of our required mirror calibration. Using this technique, we show mosaic images, as well as images in which a single pixel was extracted for every mirror tilt. Using this single pixel approach, the greatest capabilities of our programmable imaging are realized. When using multiple mirrors to image an object, new features of our system are demonstrated. In this case, the object plane can be viewed from different perspectives. From these multi-perspective images, virtual 3-D images can be created. In addition, stereo depth estimation can be performed to calculate the distance between the object and the image plane. This depth measurement is significant, as the depth information is taken with only one image from only one camera.

1. Introduction

1.1 Motivation and Significance

New advancements in science are frequently sparked by the invention of new instruments. We have seen repeatedly such examples throughout history, including significant inventions of the telescope, the microscope, the cyclotron and the transistor. Conceivably, the most important scientific instrument of the past fifty years is the digital computer. Among its many uses and impacts in sciences, the coupling of computers and optics created a whole new era, in imaging, known as *digital imaging*.

Since, the beginning of photography, the imaging paradigm has changed little, as it is still based on the principle of the pinhole camera, also known as camera obscura. As shown, in Figure 1.1 the *Conventional Camera* has a detector (film or Solid State) and a lens that essentially captures the light rays that pass through its center of projection or effective pinhole. In other words, the conventional camera performs a sampling of the complete set of rays, or the light field, that resides in an object plane.

Imaging systems that differ from the traditional lens-film paradigm have recently been appearing in increasing numbers. New imaging methods through the use of

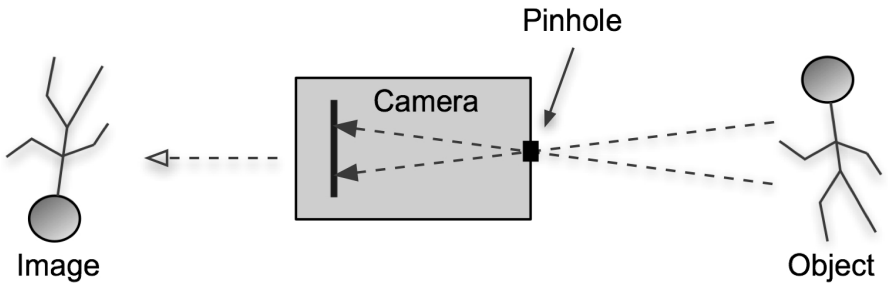

Figure 1.1: System design of a *conventional* camera

computers have revolutionized our ability to observe and analyze natural and man-made worlds. Computational cameras can produce images that are fundamentally different from the traditional perspective images and they enhance the quality and the information of an image. However, the hardware and software of a computational camera is designed to produce a particular type of image. The nature of this image cannot be altered without significant redesign of the system. One of the earliest examples of computational imaging is coded aperture imaging, which dates back to 1961 by Mertz and Young [3]. Coded aperture imaging uses many pinholes to increase the signal-to-noise-ratio (SNR) for intrinsically weak sources when the radiation can be neither reflected nor refracted [4]. Effectively, many copies of the object plane is multiplexed into an image plane. This complex image is then decoded, typically by a computer, to form a reconstructed image.

Computational imaging uses the optical system design to perform a specific imaging task. Computational cameras sample the light field in radically different ways to create new and useful forms of visual information [5]. As opposed to a traditional camera, computational cameras embodies the convergence of the camera and the computer. As shown, in Figure 1.2, computational imaging uses new methods to map rays in the light field to pixels on the detector in an unconventional fashion. For example, the computational camera can assign a ray to a particular pixel *photosite* (pixel on the sensor) rather than having the ray travel to a path determined by the properties of the lens, as it would happen in a conventional camera. In the case of coded aperture imaging, many copies of the object (one from each pinhole) is encoded onto the image sensor. The computer decodes the image, by knowing the aperture mask. More examples of new imaging applications and systems can be found in the excellent survey by Levoy [6].

Since, the captured image is optically coded, interpreting it in its raw form may be

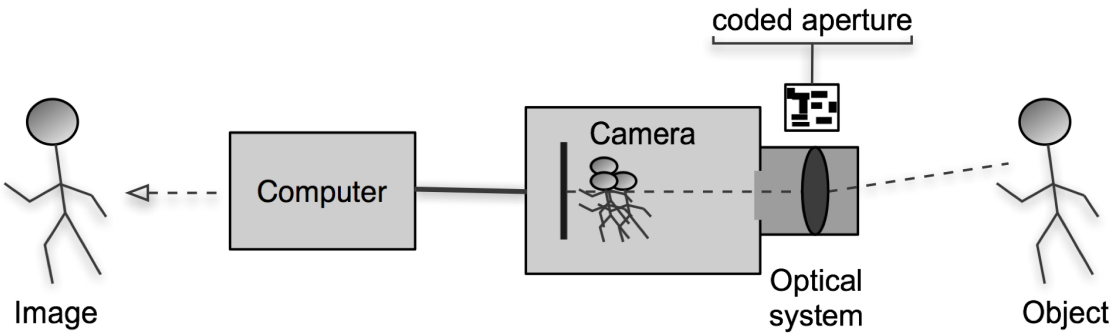

Figure 1.2: System design of a typical *computational* camera.

difficult. However, the computational module knows the details of the system hence, it can decode the captured image to produce new types of images that could benefit a vision system-either a human observing the images or a computer that analyzes the images to interpret the scene.

All of the previously mentioned systems are static, that is, the system and optical elements do not change. In this thesis, we identify the need for a computational imaging system that could be adaptable and reconfigurable. To meet this need, we introduce *Programmable Imaging*, a completely reconfigurable computational imaging system. In this thesis, we introduce a new approach to programmable imaging with the use of micro-electro-optical mechanical systems (MOEMS) of mirrors. In Figure 1.3, we show the Lucent LambdaRouter, which is the MOEMS device used throughout this thesis. We show that when MOEMS are used in imaging, they can create imaging systems that can be reconfigurable on the fly without modifying any of its hardware components. In addition, we demonstrate how MOEMS allow us to perform image processing tasks in hardware, that otherwise would have required intense computational algorithms to perform the tasks in software.

As an example of our imaging technique and capabilities, envision of an imaging system that simultaneously could capture an image in multiple ways *without* the

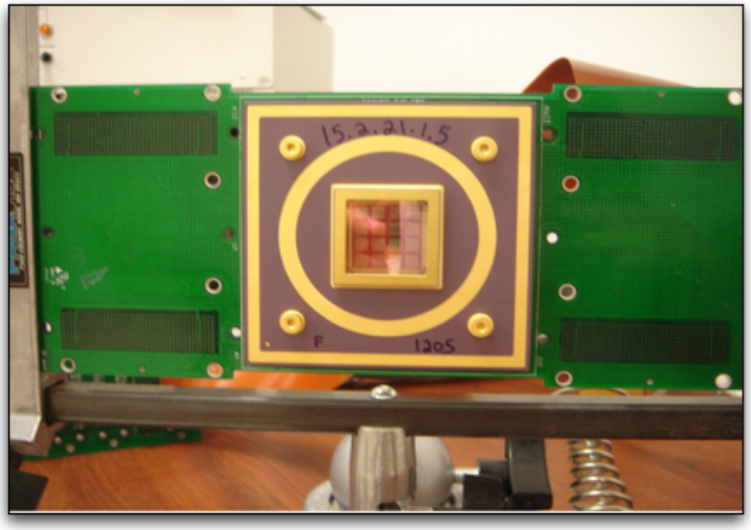

Figure 1.3: A 256 (16x16) mirrors MOEMS array chipset of the Lambdarouter.

need of modifying any of its hardware components and *without* sacrificing any image quality parameters. Then a such system could produce images like the ones shown on Figures 1.4, and 1.5. This propose type of a camera could capture the same object at different zoom levels and different aspects of it. Moreover, it could also capture the object from many different points of view. The application of such cameras could be numerous and could applied anywhere from consumer electronics to sophisticated security and monitoring systems.

We next introduce some of the fundamental parameters of imaging, which we will use in this thesis to characterize our *Programmable Imaging system*.

1.2 Imaging parameters used throughout thesis

Since the beginning of photography, people have always looked to improve the quality of imaging by seeking to invent new methods to increase the *resolution*, the *Field of View* (FOV), the *depth of field*, the *dynamic range*, and the *spectral analysis* of the captured image. In this thesis we focus on only three of these parameters:

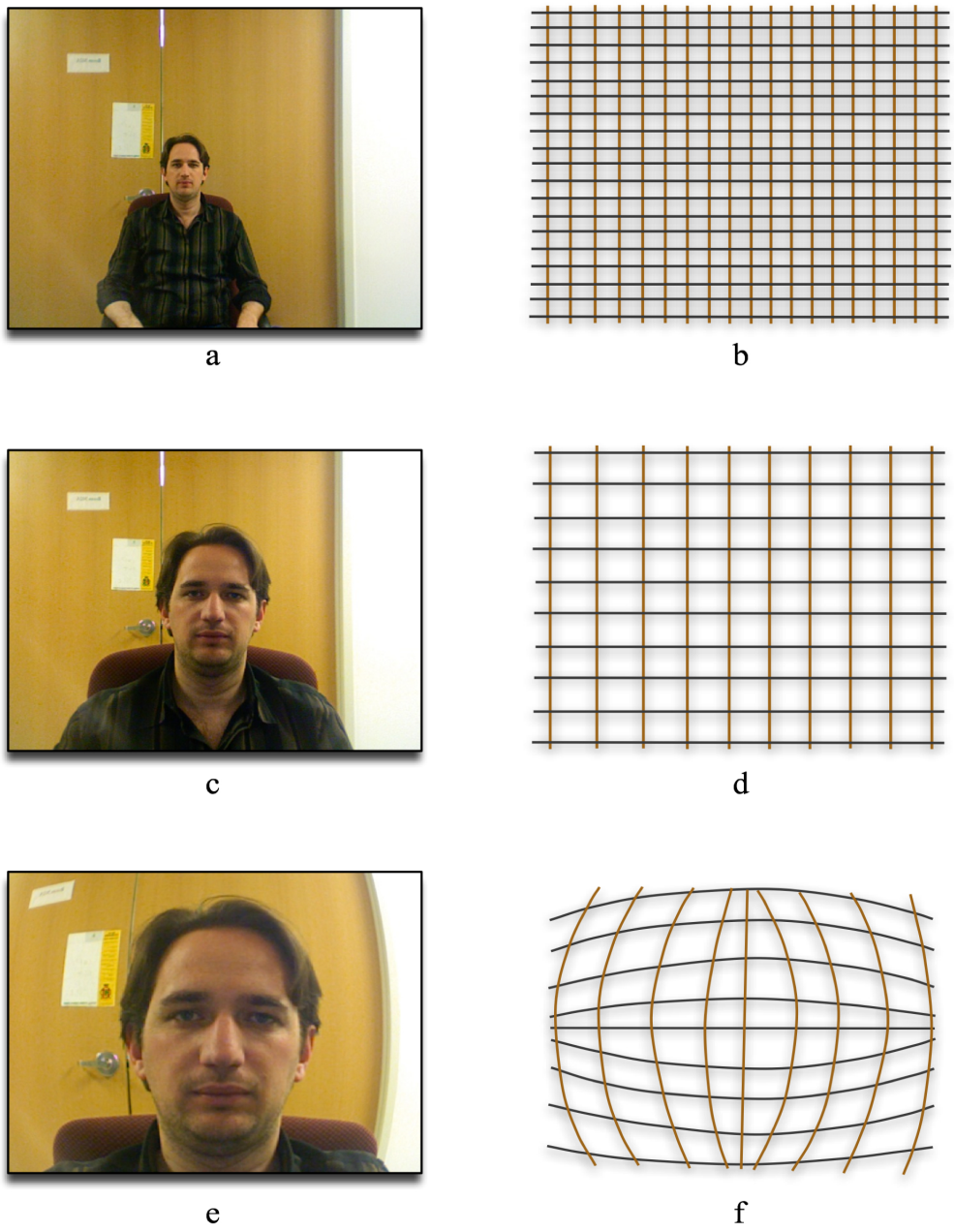

Figure 1.4: On this Figure we see different images that our conceptual camera could capture without changing at anytime its hardware configuration. It can not only capture the same object at different zoom levels, but also it could distribute the captured pixels in such way that could mimic different optical systems (e.g. fisheye lens) as we see on captures *e* and *f*.

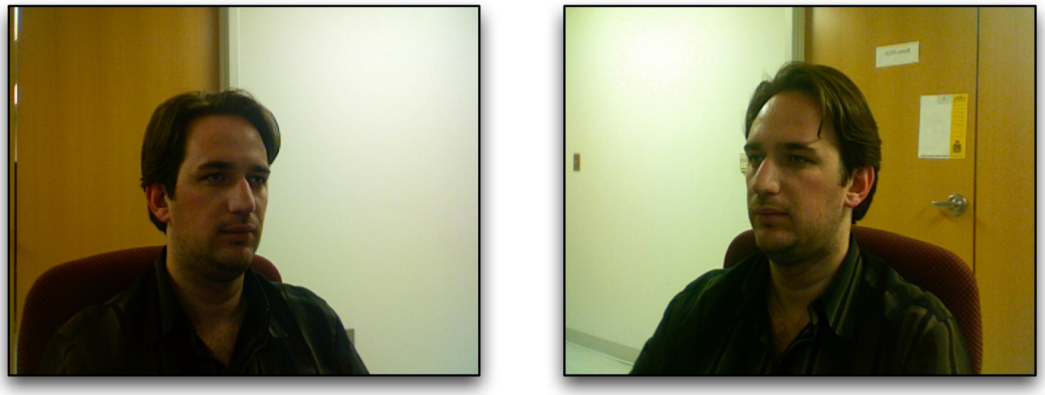

a b

Figure 1.5: On this set of Figures we can see how the same imaging that was described earlier could capture multi-perspective images.

resolution, *field-of-view (FOV)* and *depth estimation* [7].

Below we provide a brief overview of each of these components, and present some key concepts in these imaging areas that has been developed over the years.

1.2.1 Resolution

Resolution is possibly the most noticeable parameter that characterizes the quality of an image. For the longest time, the optical and sensor communities have been striving to increase the resolution of imaging systems. Even though resolution describes the detail an image holds, this parameter can be defined in different ways. Below we give a brief explanation of some the different classifications of resolution in imaging.

Spatial resolution measures how closely lines can be resolved in an image. This type of resolution depends on the properties of the system that creates the image. For practical purposes, the clarity of an image is given in lines per inch.

Spectral resolution is defined by how color images distinguish light of different wavelengths. Multi-spectral images resolve even finer differences of wavelength

to reproduce color images due to their capacity towards higher spectral resolution.

Temporal resolution is defined by the time resolution, or the number of frames that the camera can capture per second. For example, movie cameras and high speed cameras can resolve events at different point in time, resulting in a high temporal resolution.

Radiometric resolution is the capacity of the system to represent or distinguish difference of intensity. Radiometric resolution is measured is measured on number of levels quantization levels or number of bits. In practice, the effective radiometric resolution is typical limited by noise level, rather than by the number of bits.

In Chapter 3, we discuss the spatial resolution of our system and how it is determined. In Chapter 4, we experimentally validate our theoretical calculations. We will show that the resolution of our design does not depend on a single component, but in the whole system configuration.

1.2.2 Field of View (FOV)

One of the first things noticed in an image is the field of view. Most imaging systems are rather limited in their fields of view. They can only capture a small fraction of the complete sphere around their location in space. Clearly, if a camera could capture the complete sphere or even hemisphere, it would profoundly impact the capability of the vision system that uses it. French philosopher Michel Foucault explored at great length the psychological implications of being able to view everything at once in his work about *panopticon* [5].

About a century ago the *fisheye* lens was introduced, a type of lens that increases dramatically the field of an imaging system up to 220^o. As shown in Figure 1.6, a

(a) Fisheye Lens

(b) Fisheye lens ray diagram

Figure 1.6: Fisheye lens is one of the most common lenses used for wide field panoramic imaging.

fisheye lens is a wide angle imaging apparatus that uses meniscus (crescent-shaped) lenses to severely bend light rays into the camera, particularly, the rays that are in the periphery of the field of view. However, it is difficult to design a fisheye lens with a field of view that is much larger than a hemisphere while maintaining high image quality.

Therefore, new methods had to be developed to deal with this challenge. One proposed solution is *catadioptrics* which is an approach that combines the use of lenses and mirrors [8]. Figure 1.8(a) shows an example of a wide-angle catadioptric cameras. As can be seen, a catadioptric camera is created by an attachment to a conventional camera, which includes a relay lens and paraboidal mirror. As the figure shows, the camera's field of view increases significantly to greater than a hemisphere since it has a 220^o field of view in the vertical plane and 360^o field of view on the horizontal plane [5]. The most obvious problem with catadioptric systems is the obstruction-the black spot in the center where the mirror sees the relay lens also refereed as the blind spot of the camera.

Figure 1.8 shows an example of an image taken with a catadioptric camera. Notice

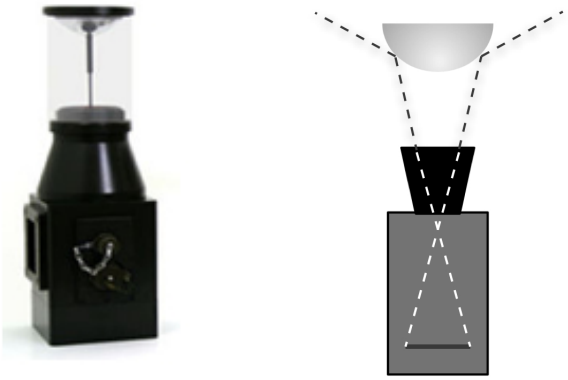

(a) Catadioptric Lens

(b) Catadioptic lens ray diagram

Figure 1.7: Catadioptric lens and diagram of a catadioptric optical system.

that the top image is warped and stretched. It is key to note, that additional post processing in software is required to make the image rectified, as shown in 1.8(b). Also note, that using our programmable imaging, no post processing will be required to create the rectified image.

Perhaps, the most crucial problem with catadioptric systems and fisheye lenses is the uneven image resolution and light distribution on the captured image, due to distortions introduced by the mirror or the lens respectively. For example, Figure 1.8(a) shows an example of an image taken with a catadioptric camera. Notice that the top image is warped and stretched. The fisheye has even power distribution throughout its field of view and offers higher resolution towards the optical axis. On the other side, catadioptric systems offer higher resolution towards the periphery of the lens rather that towards the optical axis.

Since the camera's computational module knows the optical compression of the the catadioptric system or fish-eye lens, with the use of specific algorithms it can map big parts of the highly distorted images in perspective images. This can be seen in

the rectified image, seen in 1.8(b), that is created from the original data. It is key to note, that additional post processing in software is required to make the image rectified. Also note, that using our programmable imaging technique described in this thesis requires no post processing to create the rectified image.

Over time, other techniques have been developed that contribute to increasing the field of view of an image. A common method that is used is *Image Mosaicing*. With image mosaicing, a sequence of images are taken from the same point of view. Using sophisticated software algorithms, these individual images are stitched together by allowing neighboring images that share common fields of view to merge together to form a new image with a larger field of view. In Figure 1.9, a two-frame mosaic image of Drexel University's Great Hall has been formed from two separate images.

By comparing image mosaicing with other image methods discussed previously, we see that while mosaicing methods require the scene to be static during the capture process, a single shot camera (e.q. fisheye, catadioptric) can capture images in highly dynamic environments. However, the common disadvantage of all of the mentioned techniques is the fact that all of them require software post processing in order to enlarge the field of view of the image.

In Chapters 4 and 5 of this thesis, we will see how the FOV of our imaging system can be modified by only controlling the scanning span of the micro-mirrors. More importantly, we will provide calibration methods that allow us to use catadioptric systems or any other wide FOV lenses in conjunction with our micro-mirrors, in order to create a system that allows the real time capture of rectified and wide FOV images, without the need of any software post processing.

(a) Catadioptric image

(b) Rectified catadioptric image

Figure 1.8: An example of an image taken with a catadioptric camera and its rectification. It easily identifies the obstruction (black circle in the middle of the image), which is a problem that is common in such systems. In addition, we can identify disproportionate distribution of energy and data points by observing the periphery of the rectified image. *(Courtesy of Dr. R.A. Hicks)*

Figure 1.9: Image Mosaicing. Blending of two images to create a new image with a wider Field of View

1.2.3 Depth

The word depth in the imaging community has two definitions, depending on who uses the term. For a photographer, depth refers to the *Depth of Field* of an image, which is the amount of distance between the nearest and farthest object which both appear in focus. However, the word depth for a computer scientist has a different meaning, which refers to *Depth Estimation*. Depth estimation is the calculation of the distance between the image plane and the object plane. In this thesis, using multiple mirrors, we show that we can provide depth estimation.

Scene reconstruction is an old and challenging problem that aims to create a 3D model of a scene, given only 2D images of the scene. An important early application of scene reconstruction was in autonomous robot navigation. Multimedia computing has generated renewed interest in the problem and has shifted the emphasis to generation new, *virtual* views of the scenes. Applications of multimedia computing include virtual reality, games, and special effects for motion pictures.

As computing power increases, more complex algorithms can be executed in a short period of time. That has allow the development of more complex algorithms that can generate very realistic 3D reconstructions. The depth estimation algorithms can be divided into two major groups: a) object plane perception and b) camera settings.

1.2.3.1 Object Plane Perception

With our two eyes, we view an object with two separate images. Our brain fuses the two images to produce a sensation of depth. The same technique holds true for images taken from multiple perspectives, resulting in a depth estimation from an object plane to the image plane. This defines the most classical approach in depth estimation, which is *Stereo* [9]. With stereo two images can be used to estimate the distance to an object plane. Based on stereo, a newer approach has been developed which is depth estimation from *motion*. The common requirement in all stereo perception methods is that the camera settings remain constant throughout the whole depth estimation procedure. Typically, only the camera moves its position.

1.2.3.2 Camera Settings

Other approaches to the depth estimation problem keep the camera still, but change its settings. In this case, depth of image can be used to do depth estimation. As it was addressed above, the depth of an image indicates the *circle of confusion*, or else the area that the object plane can move and still appear as its in focus. Therefore, by knowing the specifications of your lens system and by changing the settings of your camera, such as moving the image plane, very valuable information can be extracted that could lead to estimating the distance of the object plane. Much research in this field has produced a number of different variations of the general idea, which has

resulted in very robust methods for 3D reconstruction of an object [9].

In Chapter 5, we show how our imaging system can be used for depth estimation, by using Stereo depth estimation techniques. In this case, we will take different perspectives of an object, by using images from different mirrors in an array.

1.2.4 Dynamic Range

While digital cameras have improved dramatically with respect to spatial resolution, they remain limited in terms of the number of discrete brightness values they can measure. Lets consider the following example, a scene that includes a person indoors and lit by room lamps, while standing next to a window where the sun brightly lights the scene outside. If the cameras exposure time is increased to ensure the person appears well lit in the image, the window would be washed out, or saturated. On the other hand, if the exposure time is lowered to capture the bright outdoor scene, the person will appear dark in the image. This occurs because digital cameras typically measure 256 levels, in other words, they have 8 bits of brightness of each color channel which is simply not enough to capture the rich brightness variations in most real scenes.

In addition, the size of each photosite (photodiode cell of a digital image sensor) comes and take a very significant role in the dynamic range of a camera. As market trends are pushing for smaller cameras the same time the image sensor size decreases. That though requires that every photosite becomes smaller and that results in a tradeoff between sensor *quality vs. sensor* size.

In recent years, and as computation power has increased exponentially, much work has been published on this field providing sophisticated methods on how to increase dynamic range in digital cameras. In a conventional camera, all pixels on the image sensor are equally sensitive to light and that results to the problems that described

above with dynamic range. A popular way to increase the dynamic range is to capture many images of the scene using different exposures and the use software to combine the parts of the different exposed images. The major downside of this method is that it requires the scene to be more or less static and as result with this method you cannot combine parts that contain fast moving objects, similar problem that occurs also with image mosaicing. Alternatively another way of increasing dynamic range is by introducing a sensor with photosites of different sensitivity. Various researchers have come up with clever approaches which includes using assortments of pixels or image sensors with different sensitivities either by placing an optical mask with cells of different transmittances on the sensor(s) or by having interspersed sets of pixels exposed on the scene over different integration times.

1.2.5 Spectrum

The range of frequencies that can be captured from a sensor is another important factor of digital imaging. Most common ways of extracting different frequency ranges is by putting different filters on top of the sensor. This is how most of the digital cameras work today. With filters such as Red, Green and Blue and with the help of some algorithms a full color image can be regenerated (see Figure 1.10(a)). More recently a new revolutionary technology introduced FOVEON X3 allows sensors to capture different wavelengths without the need of any filters (see Figure 1.10(b)). Various wavelengths penetrate different depths of the substrate of the image sensor which then get translated into different colors.

The spectrum range though is not only important for a good quality of pictures since it is very useful in other applications. A number of different optical filters can be introduced in front of an image sensor to separate diffuse and specular reflections from the scene and detect material properties. In fact, multiple imaging dimensions

(a) CCD Image Sensor

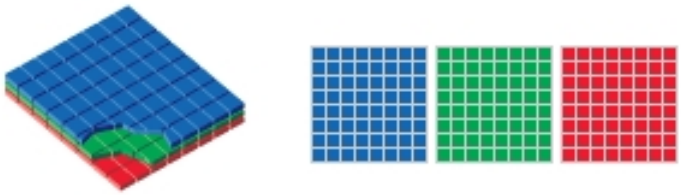

(b) Foveon Image Sensor

Figure 1.10: Two of the most common substrate image sensors. *(courtesy of Foveon Inc.)*

can be explored simultaneously by using complex optical filters.

1.3 Programmable Imaging

The limitations of existing computational imaging methods and the need for better control of the data and new imaging capacities has led to the development of a new field called *Programmable Imaging* [5]. A Programmable Imaging system uses a reconfigurable optical system, which can vary in terms of its radiometric or geometric properties, to form an image. In Figure 1.11, we see a typical diagram of a programmable imaging system. We see that the controller modifies the camera settings and can instruct the image processor to manipulate the received image accordingly. The result is a single imaging system that can emulate the functionalities of several

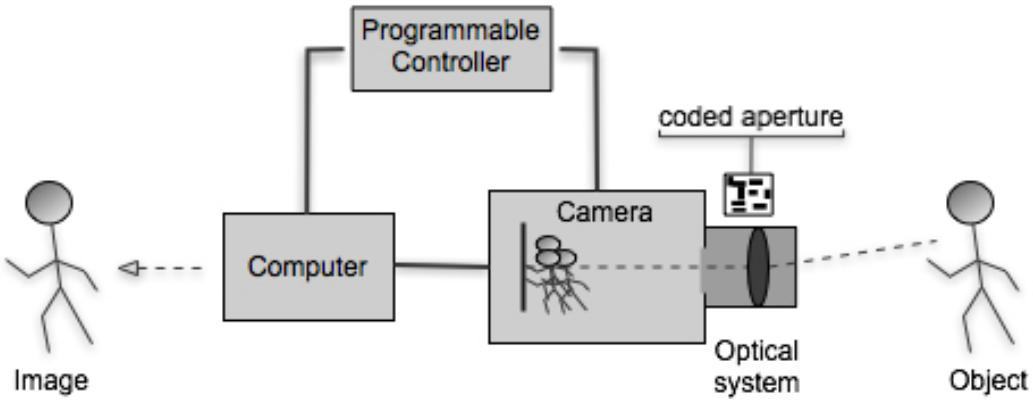

Figure 1.11: System design of a *Programmable* Camera

specialized systems.

The programmable camera that we introduce in this thesis allows us to sample the image of the object plane in a dynamic and reconfigurable way. That is a major advantage because this feature can be used to eliminate any image distortion and allow varying to the FOV and resolution of the image as needed. Such a flexible imaging system has two major benefits: first, the user is free to change the role of the camera as needed and second, we can begin to explore the notion of a purposive camera so, as time progresses, it always produces the visual information that is most pertinent to the task.

Programmable imaging with MOEMS gives a new dimension to imaging capabilities and has started a new era of innovation. It allows us to perform tasks that so far were not possible or they could only be achieved by post processing methods.

1.4 Thesis Contributions

In this thesis, we explore programmable imaging from a different perspective by utilizing analog MOEMS mirrors into an imaging system. We show that MOEMS mirrors incorporated into imaging systems can create new capacities in the field of

imaging that otherwise would have required multiple complex systems, post processing methods, or could not have been achieved before.

By using MOEMS mirrors, we introduce an imaging approach that makes a correspondence for every pixel on the object plane to the image plane. This is achieved by introducing a reconfigurable MOEMS element into the ray path of the two planes. We have studied the system through extensive simulations and experimentation to determine its imaging capabilities and performance.

We show that even a single pixel sensor is capable of producing high quality images. This study can be very significant for the future development of micro-systems. CCD and CMOS image sensors are close to reaching their limits by trying to squeeze more and more photosites into a small real estate [10]. Our approach could be used in order to gather multiple data points from a single photosite.

By taking advantage of the MOEMS reliability and controllability, we show that we can manage, in a unique way, the sampling of the object plane. We can control the field of view, as well as the resolution of the image. But more importantly, we can sample the object plane in a specified way. For example, our imaging sampling technique can compensate for any distortions caused by different components of the imaging system or can view the system as if different lenses were on the camera. All of this imaging can be done in hardware and in real time. In other words, images that are currently produced with post processing software methods can now be performed directly in hardware.

We further contribute to the research by exploring imaging with MOEMS mirror arrays. MOEMS technology allows the development of many independent system on the same substrate. As a result, we studied and developed methods for multi-perspective imaging with MOEMS. In addition, imaging with MOEMS array has allowed for faster object plane scanning by sectoring the object plane to multiple

micro-mirrors. Another aspect of imaging with MOEMS arrays is that the multiple perspective images allow for the calculation of depth estimation, using classical stereo technique. In this thesis, we show how this unique feature is used in 3-D image reconstruction.

The prototype system that we have developed in our lab has been used to validate our theory with proof of concept experiments. Future work in the field will include image quality enhancement, faster imaging, and the development of new applications.

We summarize our specific contributions in thesis in the following bulleted list:

- Developed theory for our *programmable imaging technique*, which enables dynamic and reconfigurable sampling of the object plane without changing any hardware components or settings of the imaging system.
- *First* and *only* research team to image through MOEMS micro-mirror device and MOEMS array of micro-mirrors, without the need of any special signal processing methods.
- Developed methods for sampling the object plane using both a single and a multiple pixel extraction techniques.
- Created first ever programmable imaging camera using MOEMS.
- Performed calibration of the imaging system enabling exact pixel sampling.
- With the use of a MOEMS mirror array, developed a technique to capture multi-perspective images, providing virtual reality 3D images and depth estimation, through the use of a single camera.
- Identified potential limits and use of the technology.

1.5 Thesis Overview

In this thesis, *Chapter 1* introduced our research idea and presented key features of imaging and of our system. These ideas are extensively explained throughout the thesis. *Chapter 2* introduces the reader to world of MEOMS by explaining about the different types of MOEMS devices and how they operate. Current applications of MOEMS are also discussed. In *Chapter 3*, we introduce our Programmable Imaging technique by discussing our system design and providing a theoretical approach to the benefits and the unique features of the imaging technique. In *Chapter 4*, we experimentally present our work of programmable imaging with a single MOEMS element. We build off of the single mirror by experimentally showing multiple perspective imaging off of a mirror array in *Chapter 5*. These experimental results validate our research and the benefits of our approach. We conclude this thesis in *Chapter 6*, by summarizing our work, detailing our contributions, and proposing future work in this growing and exciting field.

2. Background: MOEMS and Imaging

They are better than our natural senses, they can go to places that we wouldn't dream of going, they can react faster than we could even imagined and they surround us at every moment of the day: Micro-Electro-Mechanical Systems (MEMS). They are measured in microns and they are some of the smallest devices ever manufactured in commercial quantities. Today, they can be found in consumer goods *(e.g mobile phones)*, in the automobile industry *(e.g. airbags)* and in medical devices *(e.g. implantable applications)*.

MEMS is the integration of mechanical elements and electronics on a common silicon substrate created through micro-fabrication technology. While the electronics are fabricated using integrated circuit (IC) process sequences (e.g CMOS, Bipolar, or BICMOS processes), the micro-mechanical components are fabricated using compatible *micro-machining* processes that selectively etch away parts of the silicon wafer or add new structural layers to form the mechanical and electromechanical devices [11; 12; 13; 14].

What started as an experiment in Westinghouse Research Labs in Pittsburgh by Dr. Harvey Nathanson resulted today in a $5 billion global industry [15]. For about a decade, starting from 1965 Dr. Nathasons' team developed a number of silicon based MEMS devices starting with vibrating beams. The first such device was called *resonating gate transistor*, long before the MEMS field was established [1].

The resonating gate transistor *(RGT)* was a one millimeter long device that responded to an extremely narrow range of electrical input signals. It transmitted the signals within the selected range to an output circuit while ignoring other frequencies. Thus serving as a bandpass filter. As we can see in Figure 2.1, [1] the RGT

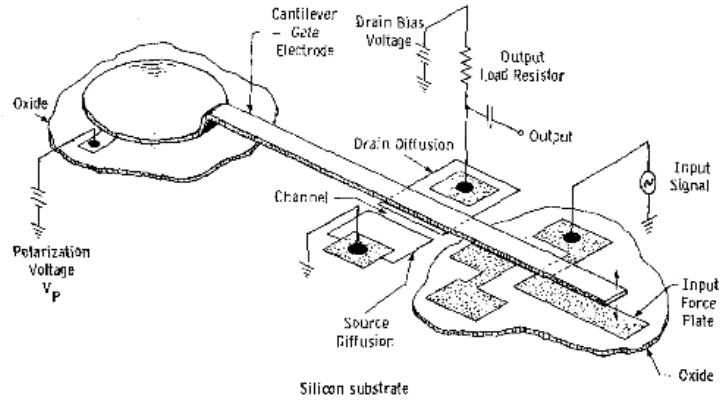

Figure 2.1: Resonant Gate Transistor-The first MEMS device ever fabricated [1].

employed an electrostatic field between the suspended end of a conductive cantilever and a silicon substrate, to which the other end of the cantilever was affixed. The suspended part of the cantilever, when it was vibrated by an electrostatic force, would move closer to and further from the substrate and as result was rapidly increasing and decreasing the resistance of the transistor.

The cantilevers size determined its resonant frequency. As a result, any time the input signal to the system was the same as the resonant frequency of the cantilever, then the cantilever would vibrate. Otherwise, any other input would had been discarded from the cantilever.

As integrated circuits rapidly developed the end goals and the focus began on commercialization [16]. When MEMS processing was first developed during the 1980s, the MEMS devices where inherently small, due to the two-decades commercial development of integrated circuits. Bulks sensors and actuators, which for almost half century had suffered from large size, where now recast as micro-sensors and micro-actuators using MEMS technology. Eventually, MEMS became the solution for miniaturization, reliability, and repeatability. During the 1980s, MEMS was a source of curiosity which simulated many innovative ideas and lead to development of new tools for many

scientific purposes.

Around the same time as MEMS, and as the interest in optical communications was growing, another technological branch was developing called *micro-optics* [17; 16; 13]. Its advancement was limited by bulk optical components being too large for system requirements. During the development of MEMS, micro-optics including lenses, sources, and actuators, were also developed by the successful adaptation of available IC fabrication techniques [18]. Since, then micro-optics have been used in many diverse applications, both for miniaturization of conventional systems and for many novel and unique uses made possible by the unique properties of micro-optics components.

2.1 Micro-Optical-Electromechanical-Systems (MOEMS)

Recently, industrial needs for commercial research and development in optical systems, including telecom and optical communication, demanded device miniaturization that led to the merging of the two technologies: *MEMS* and *Micro-Optics*. The teaming of these technologies, combined with microelectronics created the rich enabling technology of Micro-Optical-Electromechanical-Systems (MOEMS), as seen in Figure 2.2. All three constituent technologies in MOEMS allow for batch processing, while micro-optics and MEMS-also involving both micro-machining and embossing-makes MOEMS highly interesting for commercial applications [16].

MOEMS are a relatively new innovative technology that started in the late 1980s. The technology has advanced, that a recent report by NEXUS indicated that the MOEMS market is a rapidly growing one with a growth rate of 1.6 billion dollars per year. For 2007 the market size is reaching 4 billion dollars [15; 19].

Over the years MOEMS have found applications in many fields besides telecommunications, including imaging, bar code scanners and gyroscopes. In this chapter,

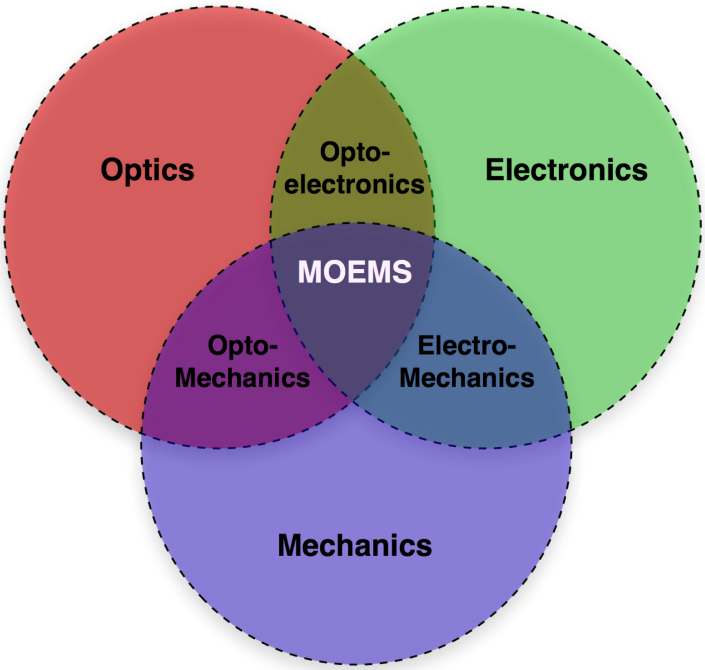

Figure 2.2: MOEMS - A field created from the interaction of micro-optics, micro-mechanics and micro-electronics *(courtesy of DARPA)*

we discuss the basic theory behind MOEMS and the different types of devices. We briefly discuss the current applications of MOEMS and their markets. In particular to this thesis, we will explore their use in imaging and discuss the previous work that was performed in the field.

2.2 Types of MOEMS

A typical MOEMS device is composed generally from micro-actuators, signal processors, and control electronics, as shown of Figure 2.3. The processor first receives a command from the outside world to perform a task, and then sends the command to the control electronics. Upon receiving this command the micro actuator mechanically alter or displace the the optical component to complete the task. In some systems (e.g. Micro-Scanners) there is a micro-sensor that monitors the displacement

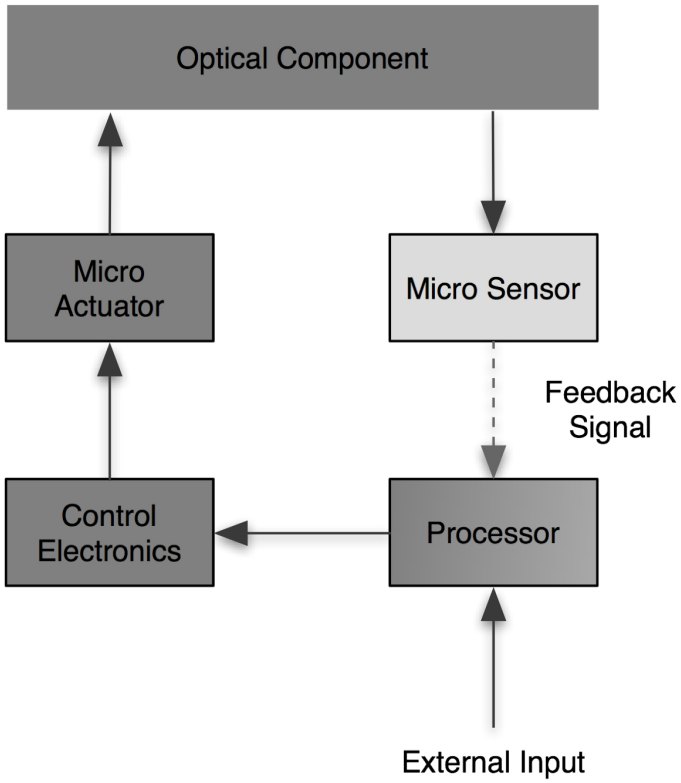

Figure 2.3: MOEMS system diagram. MOEMS are system on chip devices which are composed of many different components.

of the optical component and feeds that information back to the processors. From all the components of MOEMS the one that plays the most crucial role is the *micro-actuator* and according to the type of the micro-actuator we can classify the MOEMS into different categories.

Depending on the application, there are different types of micro-actuators that can be classified in the following categories: *electrostatic* [20; 21], *thermal* [22; 23], *piezo-electric* [24; 25; 26], *shape memory alloy (SMA)* [27; 28], and *eletromagnetic* [29; 30], *solid-liquid phase change* [31],*thermopneumatic* [32],*microbubble* and *microsteam* [33]. The ones that qualify for optical applications, and have some degree of compatibility with conventional lithography-based silicon processing, are electrostatic, thermal, piezolelectric, SMA, and magnetic actuators. Apropos the category of the micro-

actuator, there are four critical parameters common to all of them: the output force $\mathbf{F}$ [1] , displacement $\mathbf{u}$, volume v, and response time t. Another useful parameter to compare different actuator mechanisms is work output per unit volume, defined as

$$W = \frac{\mathbf{F} \cdot \mathbf{u}}{v} \tag{2.1}$$

Typically, as the displacement provided by an actuator increases, the available force at the displacement decreases [16]. Therefore, it is helpful to evaluate the peak displacement with no loading force, and the peak force with no displacement. Several performance parameters for electrostatic, thermal, piezoelectric, SMA, and magnetic actuators are summarized in Table 2.1. Each category of the micro-actuators has its own advantages and disadvantages, but one always can be chosen to fulfill requirements of a specific application.

Generally, electrostatic actuators require high actuation voltage though their power consumption is negligible. They deliver small output force and displacement, while their speed can be several kHz in quasi-static or in resonant mode [20; 21]. As a result, this family of actuators is useful for these applications that require high speed such as, MOEMS scanners and Digital Mirrors Devices (DMD). The thermal actuators can provide both high force (several mN) and large displacement (several hundred μm), but its speed is greatly limited by the cooling during each actuation cycle. It is very significant, though, from a power perspective that its actuation can be kept below 15V, something very rare in MOEMS [22; 23]. That parameter is very important since the disadvantages that MOEMS have is the required high voltage in order to operate. In this thesis, the Programmable Imaging is performed with electrostatic mirrors.

Another category of micro-actuators is piezo-electric actuators. These actuators

[1] bold letters indicate vectors

can achieve large deflections ($\sim 10\mu m$) but the output force is only a few tens of μN, which means that actuator components need to be very small in order to be able to move. The piezo-electric actuator can achieve speeds is in the range of 1-10kHz [24; 25; 26]. In contrast, SMA micro-actuators are capable of generating a large force of (200 mN) over a long displacement ($80\mu m$). However, the response speed is only in the range of 20Hz [27; 28]. Lastly, magnetic actuators can generate both attractive and repulsion actuation. They offer forces up to several tens of mN and very large displacements $< 1mm$ while they can achieve speeds up to 100KHz. However, since they are current based devices, steady power consumption is required [29; 30].

Further Classification of MOEMS, from the point of view of the optical applications, is based on the direction of the actuation towards the substrate: *in-plane* and *out-of-plane* actuators [16].

2.2.0.1 In-plane actuation

In-plane actuation is a motion that takes place parallel to the substrate. It is preferred for certain kinds of applications, since each optical component as well as each micro-actuator is easily integrated and passively aligned by using precise lithographically defined structures. Furthermore, they make the packaging process of the optical subsystems or the whole system easier. Several devices, such as the optical switch and the optical variable attenuator, have been developed using in-plane movable mirrors or blocks [34; 35; 36].

2.2.0.2 Out-of-plane actuation

Out-of-plane actuation is a process that results in motion out of, or perpendicular to, the substrate plane. It has been widely used in optical applications, such as programmable grating for displays, deformable micro-mirrors for adaptive optics,

mirrors for tunable lasers and torsional mirrors for optical switching, scanning and modulation. Usually these particular type of devices consist of plates hinge-supported micro-mirrors, which are suspended in parallel above the substrate. The plates or mirrors can be moved either up and down, or torsionally so as to form an angle to the substrate under actuation. Optical functionality can be realized with out-of-plane switching [16; 37; 38; 39; 40; 41].

Three-dminensional 3D actuation is also being investigates for silicon-based self-assembled optical platforms, micro-robotics and etc. Several approaches to 3D actuation have been developed and one of these method is to use a combination of in-plane and out-of-plane actuators [42; 43; 44; 45; 16].

In this thesis, we focus on *Electrostatic Out-of-plane Actuators* since the MOEMS that we use in use for our Programmable Imaging belong in this category. Below we provide a brief description of how these actuators operate depending on forces acting on them and the type of motion they cause.

2.2.1 Electrostatic Actuators

The displacement of a force of a specifically designed structure can be generated by utilizing the coulombic attraction force between two oppositely charged bodies [46]. This is a well established mechanism that has been used in many forms of actuators for many years for various applications. In all cases, the electrostatic force can be calculated from the stored energy (U_E) in the electrostatic system. If the effective capacitance of the device is C, and the applied voltage is V, then the stored energy of this system is given by

$$U_E = \frac{1}{2}CV^2 \tag{2.2}$$

Table 2.1: Comparison of electrostatic, thermal, piezoelectric and SMA actuators

Actuator Type	**Disp.** (μm)	**Output Force** (μN)	**Actuation voltage** (V)	**Speed** (Hz)	**W/v(J/m^3)**
Electrostatic	$0.1 - 30$	$0.1 - (1x10^3)$	$\approx 50 - 120$	$3x10^3$	$7.0x10^2 - 1.8x10^5$
Thermal	$10 - 100$	$10 - (1x10^3)$	< 20	$10^2 - 10^3$	$4.6x10^5$
Piezoelectric	≈ 10	$10 - (1x10^6)$	$20 - 10^3$	$10x10^3$	$1.2x10^5 - 1.8x10^2$
SMA	$10 - 570$	$(10 - 200)x10^3$	$1 - 3$	20	$2.5x10^7 - 6.0x10^6$
Magnetic	Up to 10^3	Up to 10^5	< 10 mA (current)	$10^2 - 10^4$	$1.6x10^3 - 4.0x10^5$

Then the electrostatic force is

$$F = -\nabla U_E \tag{2.3}$$

The three axis components of the force can be written as

$$F_x = -\frac{\partial U_E}{\partial x},\ F_y = -\frac{\partial U_E}{\partial y},\ F_z = -\frac{\partial U_E}{\partial z} \tag{2.4}$$

Since both C and V are variable if the device actuates, Eq. 2.4 can be modified to

$$F = -\frac{1}{2}V^2\nabla C - \frac{1}{2}C\nabla(V^2) \tag{2.5}$$

If V is fixed during actuation, then Eq. 2.5 can be simplified to

$$F = -\frac{1}{2}V^2\nabla C \tag{2.6}$$

Equation 2.6 is the basic equation to calculate the output force for most of the existing electrostatic actuators. For simple case of two charged plates, there are usually *three* basic type of relative motion. This types of motion are *perpendicular*, *lateral*, and *torsional* movement. Details of these motions are provided in Appendix C.

Two of the most well known MOEM devices, Texas Instruments'DMD (Digital Micromirror Device) and Lucent's LambdaRouter, are based on actuation through electrostatic attraction. The DMD, shown on Figure 2.4, was introduced in the 1980's. It was the first commercially utilized electrostatic torsion actuation device that is found in many consumer products, including TVs and video projectors. The DMD is an array of reflective mirrors where each one can be tilted up to $\pm 10^o$ and as results it can achieve the *digital* or else *on/off* states of each micro-mirror. Although designed to be a display element we have seen it today in many other applications

such as, lithography, coded apertures and others. We will discuss about some of the DMD imaging application later in this chapter.

The WaveStar, also based on electrostatic torsional actuators, was developed at Bell Labs for the LambdaRouter network swtich. This device is shown in Figure 2.5, and is the MOEMS device used for imaging in this thesis. Each of the micro-mirrors on this array can be tilted on two-axis independently and the can take over 100,000 individual states with $\pm 8^o$ of tilt. The particular micro-mirror array was developed for telecommunications purposes and it was used as a matrix switch engine for *LambdaRouter*.

With the understanding of electrostatic actuation, and the introduction of some of the most developed devices, we discuss some of the applications of these electrostatically actuated MOEMS in the next section.

2.3 Applications of MOEMS

Until recently MOEMS, have been primarily used for telecommunication networking and displays. As introduced in the last section, Texas Instruments, pushed the MOEMS technology towards the display industry [47]. Dr. Larry Hornbeck with his invention and vision of the digital micro-mirror device (DMD) opened up new opportunities at TI and a whole new market in the display industry that made Texas Instruments the leader in the field.

As the DMD started to become commercial, the increasingly high demands of data in telecommunications opened up a new commercial market for MOEMS. Optical communications met these demand with effective use of wavelength by advancing wavelength division multiplexing (WDM) and dense wavelength division multiplexing (DWDM) techniques. Using fiber optics for optical transmission lines requires light concentrators, beam shapers, optical transformers, beamsplitters, and beam scan-

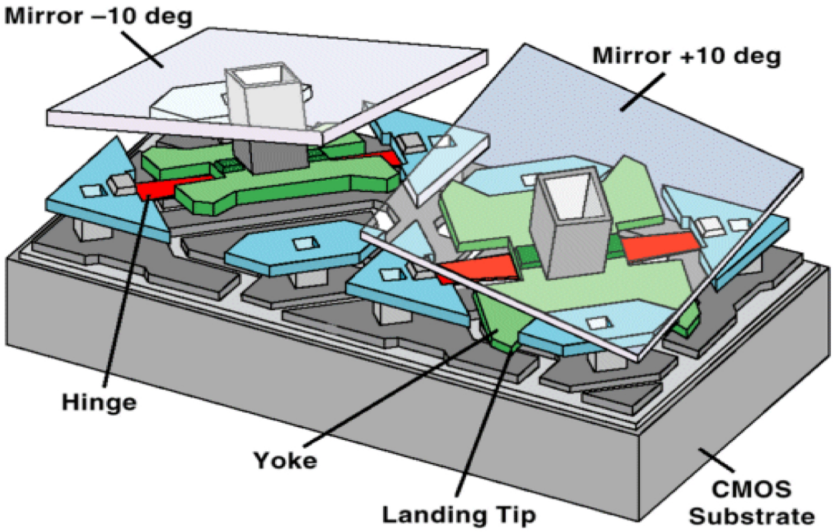

(a) Structure of a DMD.

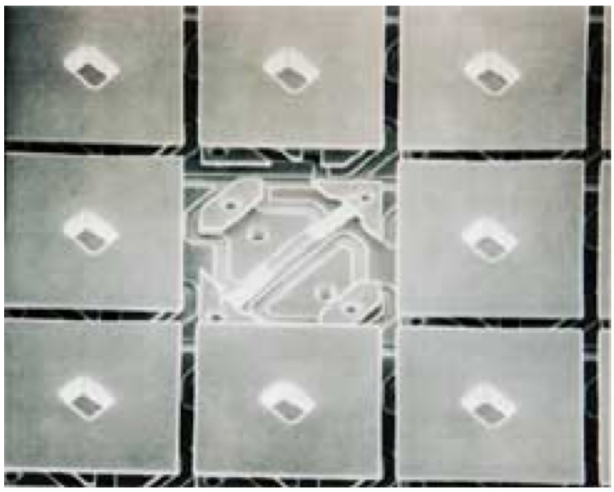

(b) Overview of DMD.

Figure 2.4: DMD is a technology developed by Texas Instruments and is the main component of the DLP consumer products such as, TV, projectors and etc.*courtesy of Texas Instruments*

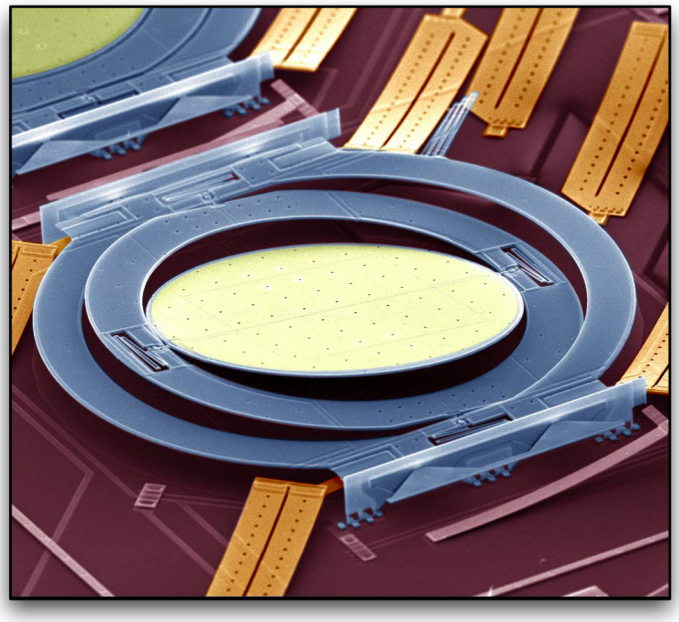

(a) A single mirror of the array.

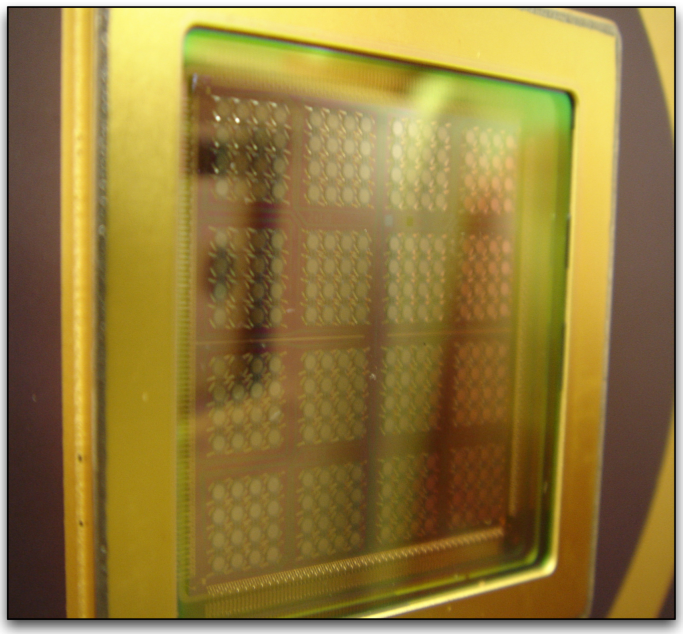

(b) Overview of MOEMS array

Figure 2.5: Lambdarouter was developed by Lucent technologies for use in optical switching.

ners. However, for the success of these optical telecom systems, optical switching is required. All-optical switching reduces the costly transfer from the optical domain for interconnect to the optical domain for switching. As result, during the explosion of the telecommunications industries in the late 1990's, MOEMS development for telecommunications needs was increasing exponentially [16; 48].

However, in the early 2000 the sudden downturn of telecom industry changed the MOEMS landscape. Many of the MEMS companies that were focused only on telecom applications either closed down or stopped MOEMS development. A few companies survived and took their mature technology and applied it to other fields and markets. Today MOEMS applications include bar code readers, spectrometers, maskless lithography, adaptive optics, head-up displays, and IR imagers [49; 17; 50; 51; 52].

In the next section, we give a brief overview of some of the most common applications of MOEMS in various fields. The reader can find more detailed information about the uses of MOEMS and its markets in the references found in the next section.

2.3.1 MOEMS in Optical Network Switching

A switch defines the very essence of the word *network*. From the time Alexander Graham Bell invented telephone to today, switching technology has changed dramatically from manual to electronic and recently to optical. Increasing demand for larger bandwidth in telecommunication forced technology to explore new alternatives in switching and routing of data.

In the mid of 1990's, Bell Laboratories, the research and development arm of Lucent Technologies, demonstrated an all optical cross-connect optical switch using MOEMS. This switch later on became known to the world as *Lambdarouter*. Lucent and other companies later on such as, Calient Networks and Xros (now a part of Nor-

tel Netoworks) selected MOEMS for building optics-cross connects because it yields small, inexpensive devices that can be incorporated with very large scale integrated circuits. Most important, MOEMS can yield micro-machines that are robust, long lived and scalable to large numbers of devices on wafer. The technology also is exceptionally matched to optics applications because it easily accommodates the need to expand or reconfigure the number of pathways through the switch [16].

To direct a wavelength along a pathway in the network, the MOEMS switch uses tiny micro-mirrors positioned so that each is illuminated by one or more of the optical wavelengths carrying a stream of information within a single fiber. For example, a stream of photons in a wavelength coming in through an input port hits series of micro-mirrors that send it out through one of many output ports, depending on which route it is supposed to take. Sophisticated controllers that mange the motion of the mirrors make decision when a stream of light arrives on how the mirror needs to tilt in order to bounce the beam to appropriate output [53].

The Lambdarouter is based on the above principle. The incoming lightwave gets filtered into separate wavelengths, each of which hits one of the 256 tilted input mirrors. The wavelengths bounce off the input mirrors and get reflected off another mirror onto output mirrors that then direct the wavelength into another fiber. The entire process lasts a few milliseconds which is fast enough for the most demanding switching applications [54].

The size of the individual switching elements make the MEMS approach extraordinarily attractive. Each micro-mirror is a half millimeter in diameter and they rest one millimeter apart. All 256 of them are fabricated on a $2.5cm^2$ piece of Si.

As a final product, the Lambdarouter was introduced in July of 2000. It offered more than 10 Tb/s of total switching capacity, 10 times the traffic over the most heavily used segments of the internet. Each of the 256 input-to-output channels can

support speeds of 320Gb/s-128 times faster than current electronic switches. These mirrors were the pinnacle of the technology. The size, reliability, and repeatability were amazing. However, as the telecom market crashed, these mirror were used for other applications, including the programmable imaging work performed in this proposal.

2.3.2 MOEMS in Display

MOEMS technology by definition combines MEMS and micro-optics, therefore it is well suited for the manipulation of light. There are number of different ways to scan, steer, or modulate the light beams with small electromechanical structures. In this section, we illustrate how light steering and light modulations using MOEMS can be used for display capabilities.

The MOEMS display technologies can be divided into three categories:

- *Retinal Scanning Display (RSD):* A technology based on 2D-scanner-based display technology.
- *Grating Light Valve (GLV):* An example of 1D scanner and 1D-pixel array display technology.
- *Digital Micro-mirror Display (DMD):* The most well known MOEMS display technology based on 2D pixel-array.

Retinal Scanning Display (RSD) The first displays that were commercially available were the cathode ray tube (CRT). This were actually scanning beam displays since an electron beam was scanned on to a phosphor screen and was result was emitting light. Based on the similar idea combination of 1D or 2D MOEMS devices, with the use of color LASERs for light sources, can create 2D raster scanned images.

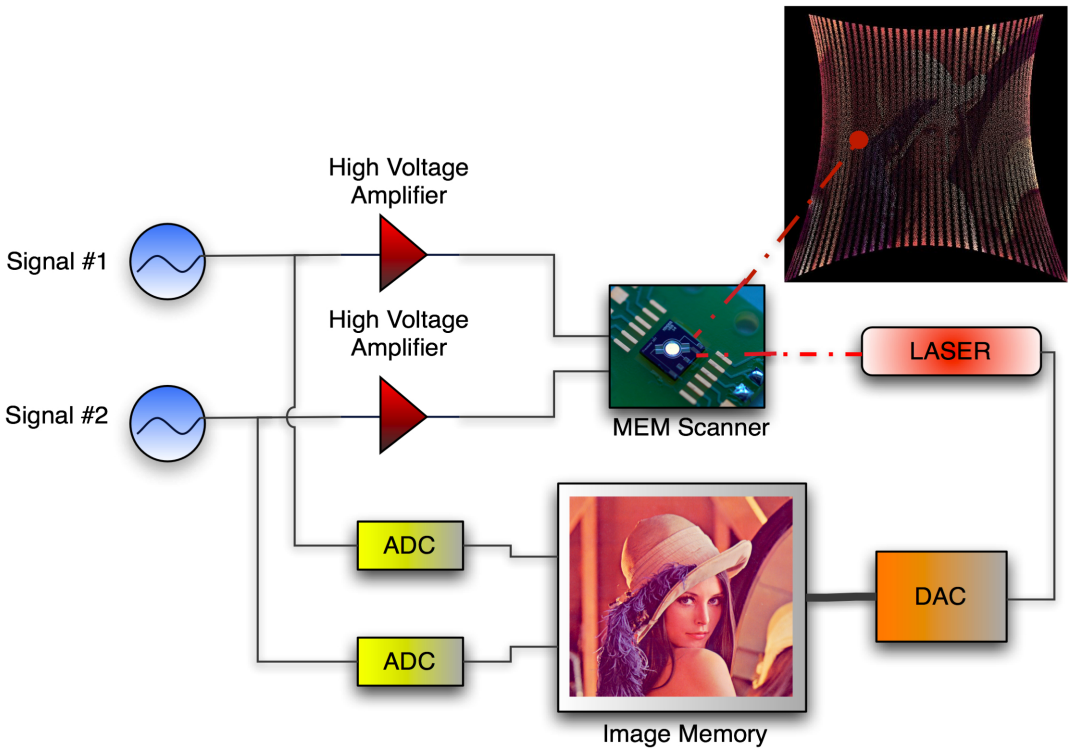

Figure 2.6: A system configuration of a MOEMS LASER projection system.

Research institutes such as, Fraunhofer ISIT, Fraunhofer IPMS and companies such as Microvision have been developing miniaturized projection system based on the idea of LASER projection displays that use bi-axial raster scanning MOEMS. In this case as well the light gets modulated as it hits the surface of the micro-mirror and a pixel by pixel the image gets projected. On Figure 2.6 it is a shown a system design of such projectors which can achieve resolutions of HDTV quality (1920x1080)pixels [17; 16].

RSD's are wearable scanning display systems that create a virtual image at the viewer's retina. RSD technology was invented at the University of Washington Human Interface Technology (HIT) LAB in the early 1990s. It was originally called the Virtual Retinal Display (VRD) and used acousto-optics scanners.

Microvision is one of the leaders on the field and has been developing RSD technology demonstrators and products based on MOEMS scanners for various military applications such as, their product NOMAD [49; 52].

Grating Light Valve (GLV) displays are reflection type diffraction grating. The gratings is made up of a 1D array of microbridges, where alternating microbridges in the array deflected up and down in response to an electrostatic changing the grating phase. The grating phase controls the amount of diffracted light intensity that goes into different diffraction orders. In the display implementation the pixel intensity modulation is achieved by optical spatial filtering of the undesired diffraction orders.

The GLV concept was invented at Stanford University in the early 1990s and the technology was transfered to Silicon Light Machines. In 2000, Sony licensed the GLV technology for developing display applications. Currently, there are no GLV-based commercial products. Silicon Light Machines developed technology demonstrators based on the GLV technology and reported performance of high resolution projection display [55; 56; 16].

The projection system uses three 1080-pixel linear GLV chips, one for each color, and a galvanometric scanner. The GLV array is oriented vertically, and the line image is scanned horizontally. The $110in$ diagonal projection has HDTV resolution (1920x1080) with up to 96Hz refresh rate. A system diagram of a such projector it is shown in Figure 2.7

Digital Micro-mirror Display (DMD) The natural interface to digital video is a digital display, which accepts electrical bits as its input and converts them into optical bits in its output. The digital to analog processing function is performed in the mind of the observer.

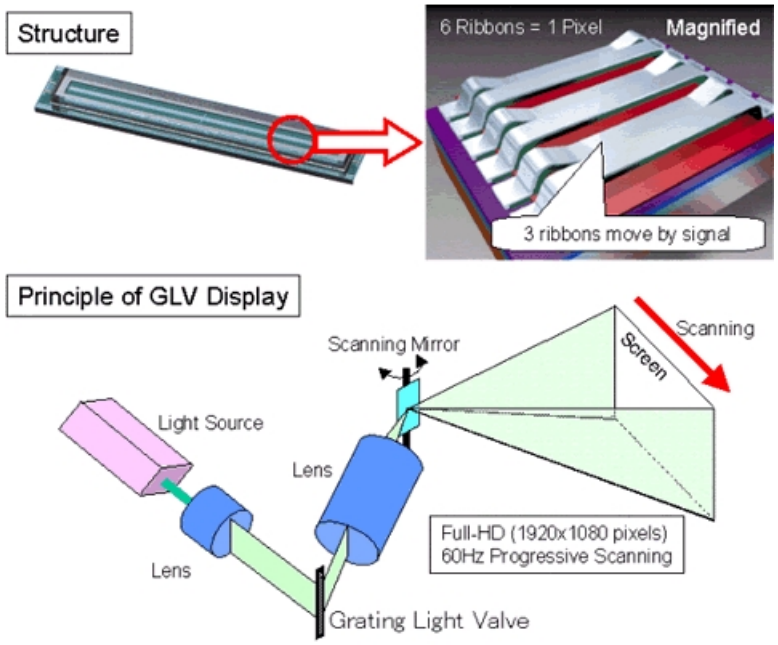

Figure 2.7: A system configuration of grating light valve (GLV). *(courtesy of Sony.)*

Texas Instruments has developed such a display with the inventions of the Digital Micro-mirror Device (DMD). This digital mirror device (DMD) works as a light switch and is designed and fabricated by CMOS like processes over a a CMOS memory wafer. Each light switch has an aluminum mirror, 16 μm^2, that can reflect light in one of two directions depending on the state of the underlying memory cell. As the memory state changes from 0 to 1 the mirror tilts from -10^o to $+10^o$ respectively (see Figure 2.4). By combining the DMD with a suitable light source and projection optics, the mirror reflects incident light either into or out of the pupil of the projection lens. Thus the state 1 of the mirror appears bright and the state 0 appears dark and this way the grayscale is achieved by binary pulse modulation of the incident light [57; 58]. Color is achieved by using color filters either stationary or rotating in combinations with one or more DMD chips. A system design of a DMD projection system is shown

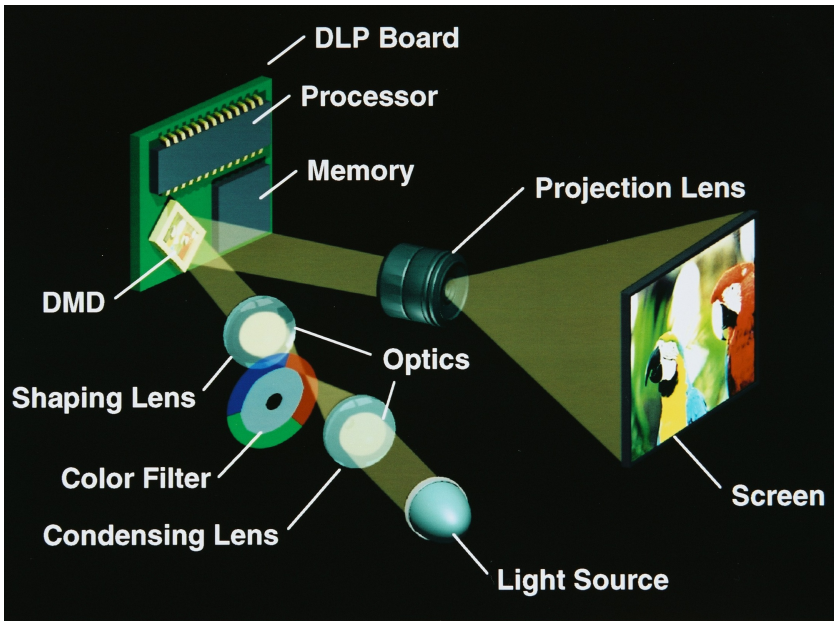

Figure 2.8: A system configuration of a digital light projection (DLP) system. *(courtesy of Texas Instruments.)*

in Figure 2.8.

The DMD is an example of successful MEOMS technology that has led to various commercial products. DMD-based digital light projection (DLP) entered the projection market in 1996, and now they are in volume production for up to SXGA resolution (1280x1024). The DLP technology was developed to serve several markets such as portable projectors, movie theaters (digital cinema), and more recently large screen TV sets for home theater entertainment [58; 47; 16].

2.3.3 MOEMS in Imaging

MOEMS haven't only achieved to miniaturized projection systems but they have also allow researchers to develop new imaging methods. MOEMS have enhanced and enrich the capacities of computational imaging and have define a new era in digital imaging. The focus of our work in this thesis is the use of MOEMS for imaging.

In this section we present two efforts from other researchers in developing imaging systems that are using MEOMS.

2.3.3.1 Compressive Imaging

Compressive Sensing is an emerging field based on the revelation that a small number of linear projections of a compressible signal enough information for reconstruction an processing.

Based on that idea, Kellys et al. using a DMD device have developed a single pixel camera that captures images using a method called *compressive imaging method* [59]. This approach is based on new digital image camera that directly acquires random projections of the signal without collecting all pixels/voxels. As shown, in Figure 2.9 the camera architecture employes a digital micro-mirror array to perform optical calculations of linear projections of an image onto pseudo-random binary patterns. Incident light field (corresponding to the desired image) is reflected off the DMD array whose mirror orientations are modulated in a pseudo-random pattern. Each different mirror pattern produces an encoded image that is imaged by the image sensor. Some unique features of systems include the ability to obtain an image with a single detection element while sampling the image fewer times than the number of pixels. In addition, since the system relies on a single photon detector, it can be adapted to image at wavelengths that are currently impossible with conventional CCD and CMOS imagers.

Experimental results have shown the validity of the idea on the other hand, the same data, shows the poor resolution performance of the camera. Even though the required number of projections is smaller than the numbers of pixels of the image for scenes with a lot of complexity that is not the case. In conclusion, this method relies heavily in on computing power and in finding the best projection patterns that will

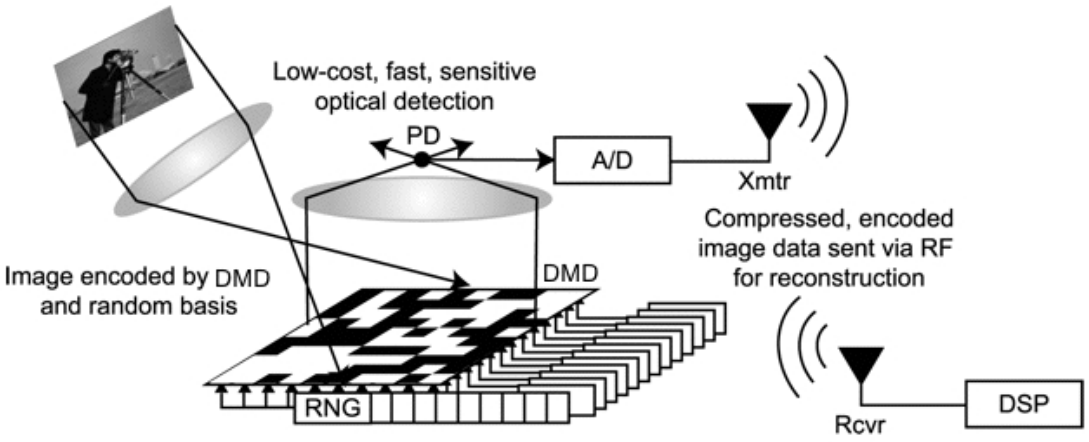

Figure 2.9: A system configuration for the single pixel camera that uses compressive imaging methods.*(courtesy of Rice University)*

result on the least losses of information.

2.3.3.2 Programmable Imaging

Programmable Imaging is an approach which provides a human user or vision system significant control over the radiometric and geometric characteristics of the system the flexibility is achieved using a programmable MOEMS mirror or array of them. The orientations of the micro-mirror(s) of the array can be controlled with a high precision over space and time. This enables the system to select and modulate rays from the light field based on the needs of the application at hand.

Nayar et al. in [60] shows that using a single DMD you can developed an imaging system with multiple imaging capabilities. As shown, in Figure 2.10 the scene is first projected onto and focus the DMD plane. This means that the cone of light from each scene point received by the aperture of the imaging lens is focused onto a single micro-mirror. When all the mirrors are oriented at 10^o, the light cones are reflected in the direction of the re-imaging lens which focuses the image received from by the

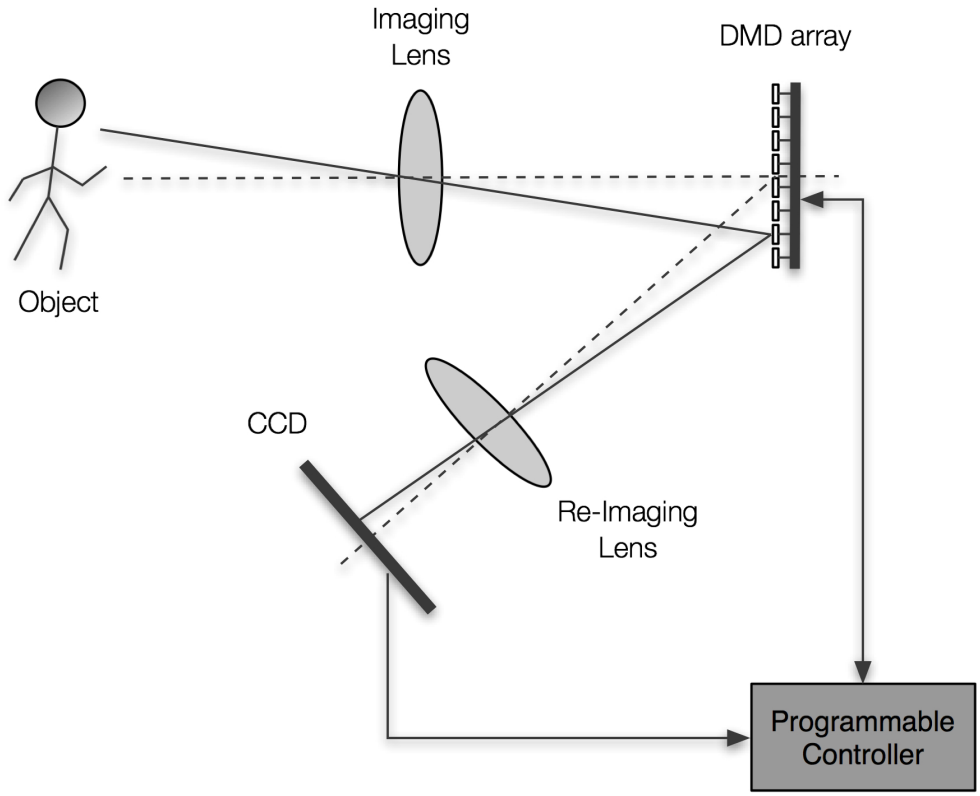

Figure 2.10: A system configuration for the single pixel camera that uses compressive imaging methods.

DMD onto a CCD image detector. Otherwise, they are reflected internally on a dark surface where they get absorbed and don't participate in the formation of the image. Even though the micro-mirrors of the device can only take two states it is shown that this capacity can be used to developed a programmable imaging system that had a variety of functionality such as, high dynamic range imaging, feature detection, and object recognition.

The existing methods imaging methods with MOEMS have a very little control over the information that is captured. In other words, they are still based on the tra-

ditional lens-sensor paradigm which dates back to the pinhole camera. The methods, that we have seen so far they extract information from the captured image rather than controlling the content of the scene that get imaged.

2.3.3.3 Programmable Imaging - Our Approach

In this thesis, we present our approach to programmable imaging with MOEMS. We show that by incorporating MOEMS into an imaging system we can control the way the scene gets sampled. This camera design introduces new capacities in digital imaging that otherwise would require complex system and post processing of data.

In the following chapters we will show how to control resolution, FOV, zoom, depth estimation, correction of optical distortions and other based on the very unique feature of our camera design which is *dynamic image sampling*.

3. Imaging with MOEMS: A new Paradigm in Digital Imaging

As we have already mentioned in Chapter 1, conventional cameras have no control over the sampling of the object plane. The image sensor simply registers the image that is focused by the lens onto the image plane. As a result, any manipulation of the image has to be done with software post processing methods. This paradigm has dominated the field since the beginning of imaging. Over the years, as computing power increased exponentially, image processing methods have been developed to allow post processing capabilities, which include: *resolution*, *sampling pattern*, and *field of view (FOV)*.

In this chapter, we provide the theory of our work for dynamically, controlling how the image is sampled through the use of a micro-optical-electro-mechanical-systems (MOEMS) mirrors. In the following chapters, we present experimental results that validate our proposed system. We show that many of the image processing techniques that so far could only be performed with post processing algorithms, can now be built into the imaging process of our system. This allows an increase in image performance metrics, as well as introducing new imaging functionality that cannot be found in current imaging systems.

3.1 Proposed system model

In theory, any point-to-point mapping can be established between the object and the image planes with the presence of a reflecting surface within the system [61]. As it is shown in Figure 3.1, to realize a given correspondence one can imagine placing a flat mirror in the optical path, and tilting it appropriately to map the ray from a point on the object plane (point of an imaging object) to a corresponding image plane

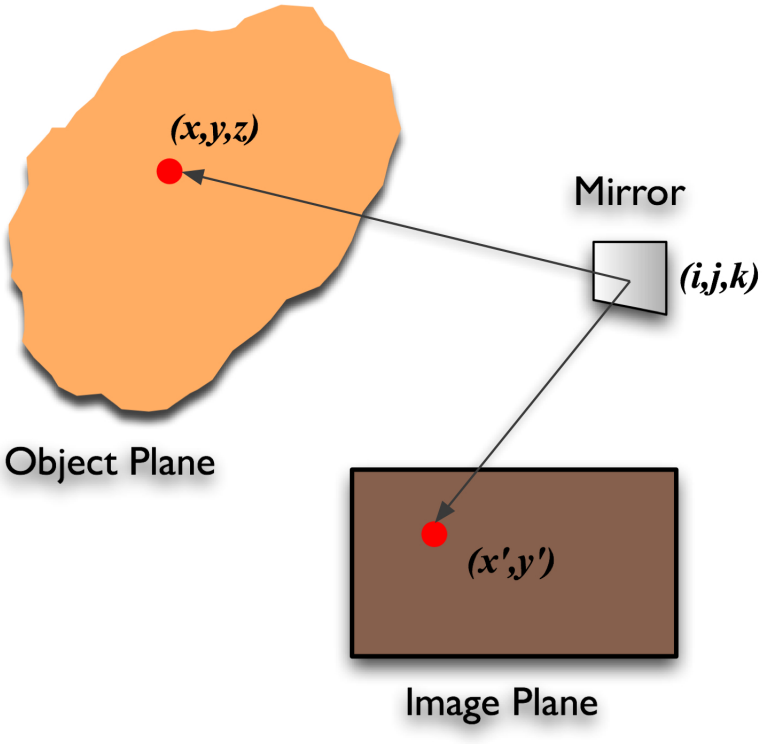

Figure 3.1: Theoretical approach in imaging through a mirror.

(CCD element). It is clear that the ray length is not important from a geometrical point of view, however, from an optics point of view, this length can affect the image quality, In other words, we can, in principle, map any point on the object to the image plane as long as the mirror can achieve any position/tilt.

In this thesis, we replace this flat, ideal mirror with a MOEMS mirror as shown in Figure 3.2. Therefore, by properly orienting a micro-mirror, it should be possible to realize any correspondence between a point on the object plane and a photosite on the CCD image plane. MOEMS mirrors have highly repeatable states (ie, tilts), therefore, once a mirror is calibrated in a tilt between a point on the object and image planes, that correspondence can be achieved over and over again.

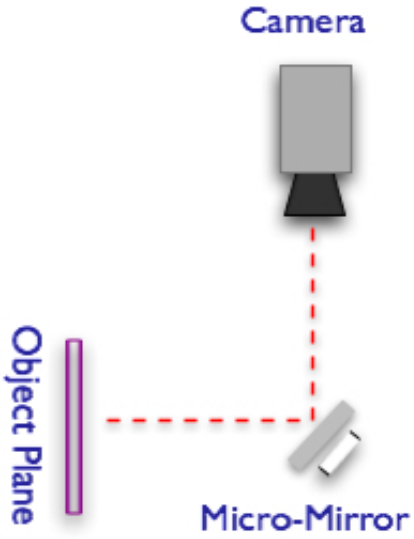

Figure 3.2: Imaging System model using MOEMS

3.2 Image Formation

When considering our optical system, the mirror simply acts as a tiny aperture in the system. Therefore, the optical system described in Figure 3.1 can be replaced with a simple pinhole optical model as shown in Figure 3.3, where every point on the object plane will get mapped in the image plane after each ray passes through the center of the pinhole. A point in the object plane is given as $\vec{P} = (X\ Y\ Z)^t$, in three dimensions. This object point is projected in two dimensions on the image plane as $\vec{p} = (x\ y)^t$, which is the position of the point on the image sensor.

According to the pinhole camera model, under perspective projection, light rays travel from a point in the three dimensional world through a pinhole until they intersect the sensor plane. The perspective projection equations are given by [9]

$$x = \frac{d_s X}{Z} \quad y = \frac{d_s Y}{Z} \tag{3.1}$$

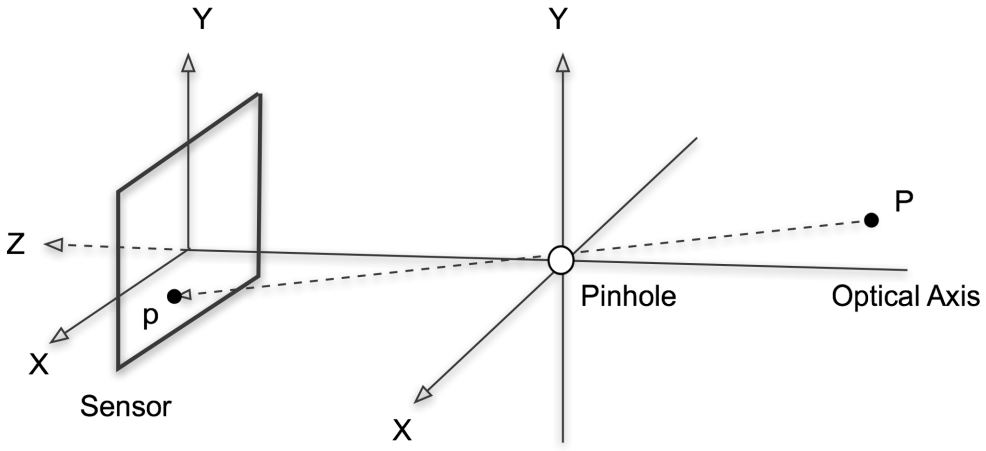

Figure 3.3: Pinhole camera. Illustrated is the projection of the point $\vec{P}$, in the three dimensional world under perspective projection on two dimensional plane. Under perspective projection, light rays pass through a small pinhole.

where, d_s is the distance from the pinhole to the sensor plane along the optical axis. The projective projection equations may be derived simply from a similar triangle argument.

Although the perspective projection equations are non-linear, they may be expresses in a matrix form using the homogeneous equations [9]:

$$\begin{pmatrix} x_s \\ y_s \\ s \end{pmatrix} = \begin{pmatrix} d_s & 0 & 0 & 0 \\ 0 & d_s & 0 & 0 \\ 0 & 0 & 1 & 0 \end{pmatrix} \begin{pmatrix} X \\ Y \\ Z \\ 1 \end{pmatrix} \tag{3.2}$$

where, the final image coordinates are given by $(xy)^t = (\frac{x_s}{s}\frac{y_s}{s})^t$

As we see in Figure 3.2, the general setup of our actual system is composed from an image sensor, a lens, the MOEMS device, and the object plane. Modeling the light path using geometrical optics, we can derive a model that allows us to explore our system's imaging capacity.

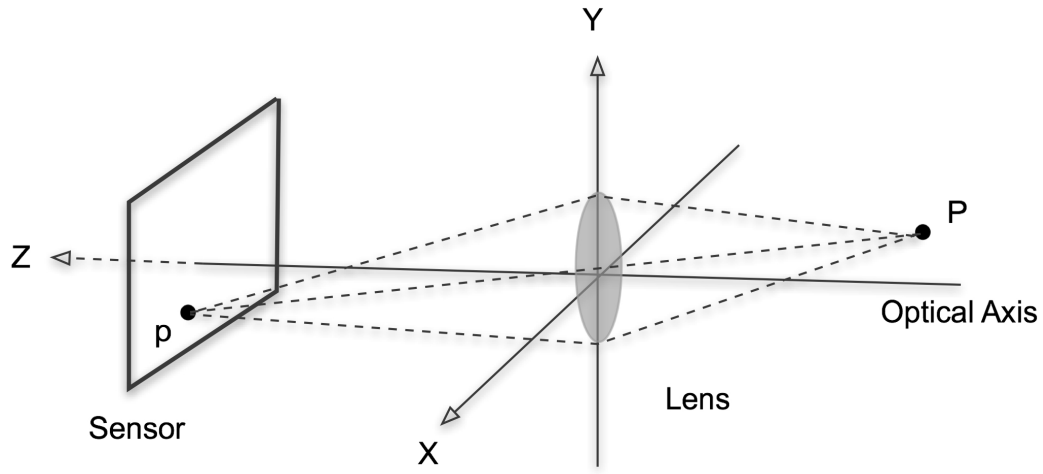

Figure 3.4: Thin Lens model. Illustrated is the projection of the point $\vec{P}$, in the three dimensional world under thin lens model. A lens collect light emanating from each point in the world from a continuum of directions and focuses them to a small region on the sensor plane.

We begin with the simple thin lens model that is widely known in the optics and vision community and it is shown on Figure 3.4. The main assumption is that the lens is thin and the aperture position coincides with the lens. All light rays that are radiated by scene point $\vec{P}$ and pass through the lens are refracted by the lens to converge at point $\vec{p}$ on the image plane [9].

Light emanates from a point in all directions, and the pinhole camera model described about captures this light from a single direction. On the other hand, a lens collects light from many directions and focus is it to a small area on the image plane.

The relationship between the focal length of the lens f and the distance d_s and d_o between the lens and the image plane, as well as, the lens and the object plane, respectively, are given by the following formula.

$$\frac{1}{d_o} + \frac{1}{d_s} = \frac{1}{f} \tag{3.3}$$

Each point $\vec{P}$ on the object plane is projected onto a single point $\vec{p}$ on the image

plane, causing a clear and *focused* image to be formed. Points away from the focal point are images as blurred circles with a radius r:

$$r = \frac{R}{\frac{1}{f} - \frac{1}{Z}} \left| \left(\frac{1}{f} - \frac{1}{Z} \right) - d_s \right| \tag{3.4}$$

where R is the radius of the lens. This relationship is easily derived from the imaging geometry. In this case, we can assume that the properties of the camera and the micro-mirror can be treated as one thin-lens system together.

Under this model the projection of a point $\vec{P} = (X\ Y\ Z)^t$ in the world is centered about the point $(x\ y)^t = \left(\frac{d_s X}{Z}\ \frac{d_s Y}{Z}\right)$. Note that the pinhole model under perspective projection is simply a special case of the thin-lens model.

As in all case of perspective, the thin-lens equations are linear and can thus be written in matrix form:

$$\begin{pmatrix} l_2 \\ a_2 \end{pmatrix} = \begin{pmatrix} 1 & 0 \\ -\frac{1}{R}\left(\frac{n_2 - n_1}{n_2}\right) & \frac{n_1}{n_2} \end{pmatrix} \begin{pmatrix} l_1 \\ a_1 \end{pmatrix} \tag{3.5}$$

As illustrated in Figure 3.2, the micro-mirror in our system acts like an aperture stop (ie, an entrance pupil), that does not coincide with the lens. By introducing the micro-mirror at the focal length of the lens, it will change the properties of the optical system to a *telecentric lens*. Telecentricity is a property that special lenses have, where the chief rays for all points across the object or image are collimated (see Figure 3.5).

The fact that the optical system has become a telecentric lens creates some very special properties for our system [62; 63]. First of all, the nominal and effective focal length of the conventional lens model that were $f/2a$ and $d_i/2a$, respectively, are now both equal to $f/2a'$, as seen in Figure 3.5. This means that the $F/\sharp$ of our system will strictly depend on the size of the micro-mirror and the focal length of the lens.

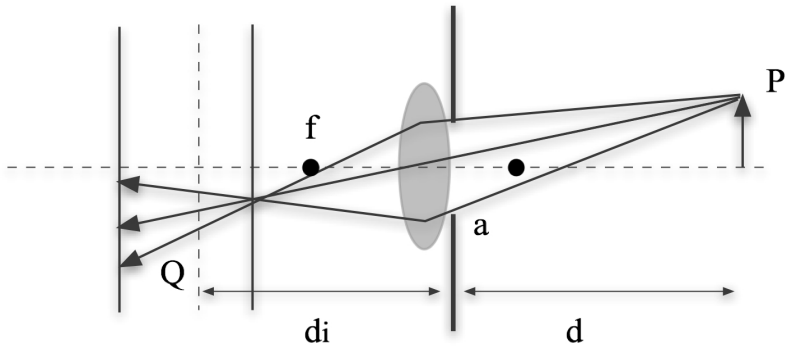

(a) Conventional Lens.

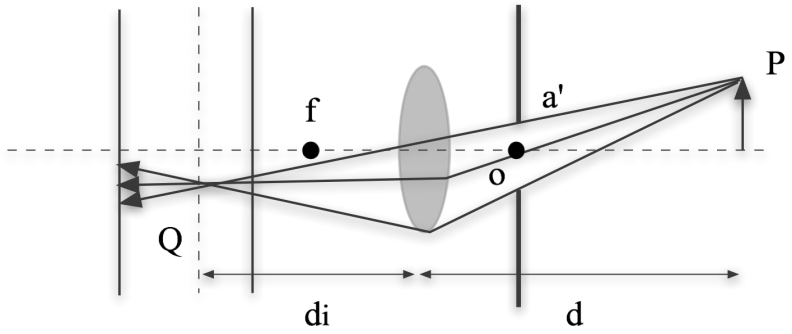

(b) Image-side Telecentric Lens

Figure 3.5: Telecentric optics achieved by adding an aperture at the focal point of a conventional lens. This simple modification causes magnification to be invariant to the position of the sensor plane.

This is a very important property, since it helps us realize that as the micro-mirror tilts on the *X Y Z plane*, its 2D projection will result in an optical system with a variable $F/\sharp$. This $F/\sharp$ depends on the angle of tilt of the micro-mirror, and the system will have a constant focal length. This telecentric property also plays a role in the resolution of the system, as we will see later in this chapter.

Finally, another important property of our system is its large depth of field. This does not have to do with the telecentricity of our system, however it has to do with the fact that most telecentric systems have a very small entrance pupil, due to their narrow filed of view. As a result, a greater depth of field is achieved. This property

is very important considering that even if the micro-mirror is constantly moving on the *X Y Z plane*, the object plane will remain in focus on the image sensor.

The optical properties discussed above also apply to the case when the thin lens model is replaced by a compound photographic lens. In this case, the lens has its own built-in *iris*. In optical systems with multiple components and multiple aperture stops, the stop that is considered the *system* aperture stop is the one whose image can be seen from the object plane at the smallest angle [2]. In other words, the system aperture stop is the limiting aperture of the system, typically, the smallest aperture in the system. In the case of our micromirror imaging system, the role of the system aperture stop is taken by the micro-mirror.

3.3 Image Quality Evaluation

The performance characteristics of an imaging systems optical system can be represented in many ways. Often the final optical performance specifications are given in terms of:

Modulation Transfer Function (MTF): It is perhaps the most comprehensive of all optical system performance criteria, especially for image forming systems. It represents the transfer of modulation from the object to the image by the lens as a function of spatial frequency.

Spot Diagram: It is the geometrical image blur formed by the lens when imaging a point object.

Encircled energy: It is energy percentage plotted as a function of image diameter. When a point source gets imaged on the image plane, it creates a spot. Encircled energy determines how spread the spot is and as a result the energy. It is used to determine the pitch of CCD pixels depending on the imaging application.

Image quality though, most of the times, is thought of as *resolution* or how close two objects can approach each other while still being resolved or distinguished from one another. Image quality can also be thought of as image sharpness, crispness, or contrast.

It is important to realize that imagery is never perfect since it is limited by diffraction, geometrical aberrations, and other factors. Also it is important to perceive that the image quality or resolution of an imaging system is not totally dependent on the optics, but may include the sensor, electronics, display device, and/or other components that make up the system. As a result, in this chapter we are not specifying the exact performance of our system, but rather predict its behavior and define its boundaries. In this thesis, we are presenting a new method for imaging and not an imaging device. As a result, measuring the MTF, Spot Diagram, and Encircled energy of our system makes no sense because we don't present a fixed design. Therefore, when are discussing image quality we need to address the factors that affect the image quality and they will exist in any imaging system that will be designed according to our system model and not to a particular set up. These factors are *resolution* and *irradiance*.

3.3.1 Spatial Resolution

The term *Spatial Resolution* or else *Resolving Power* is the equivalent to image quality since it is the first parameter that comes to mind. It describes the ability of an optical system to separate two closely spaced point sources as they get projected through the same aperture.

It is safe to assume that like any other optical system, our system will suffer from *diffraction*. Diffraction is a phenomena or effect resulting from the interaction of light with a limiting edge or aperture [2]. In the case of our micromirror imaging system,

diffraction occurs from the micro-mirror. As rays travel toward the image plane, the edges of the aperture effectively cut the light. This edge, which in many case as well as in our case, is an aperture stop that warps around the optical axis that is resulting in a diffraction pattern. If the aperture stop that causes the diffraction pattern is circular, then the diffraction pattern is known as the *Airy Disk*, which can be seen in Figure 3.6.

As long as any geometrical aberrations in an imaging system are smaller than the diffraction blur, then the image is well represented by the *Airy Disk*. This form of optics is called *Diffraction Limited Optics*. It is important for a designer to know the exact diffraction-limit of the system, as it results in the optimization of the imaging system.

There are two important components in a diffraction-limited optical system: 1) the physical diameter of Airy disk, 2) the angular diameter/ substance of Airy disk. The physical dimension of the Airy disk relates the aperture size of an optical system to the focal length and the wavelength of the ray, as given in [2]

$$Airy\ Disk = 2.44\,\lambda\,F/\sharp \tag{3.6}$$

For the visible portion of the spectrum, one can approximate the Airy disk size, which is in direct proportion with the F-number.

The other parameter of the Airy disc of equal importance is the angular diameter, expressed in radians. As we can also see in Figure 3.7, the angular substance of the Airy disk decreases in proportion to the diameter of the increase of focal length.

$$Angular\ Diameter\ of\ Airy\ Disk = \frac{2.44\lambda}{aperture\ diameter} \tag{3.7}$$

From the above and taking into consideration that the micro-mirror(s) we use

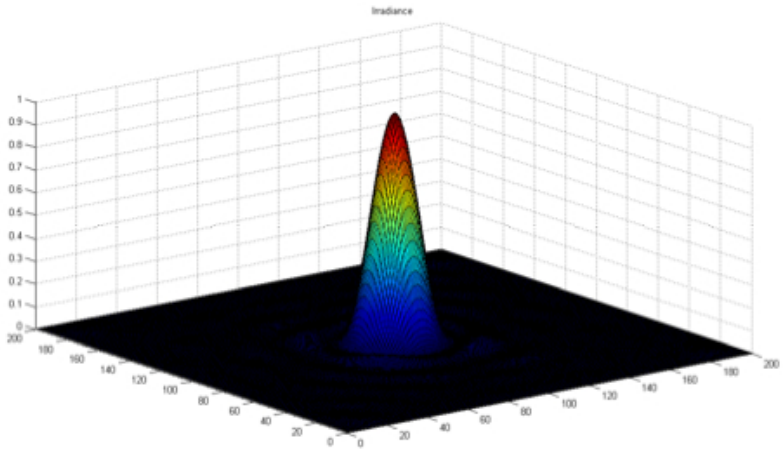

(a) Amplitude of a diffracted light source

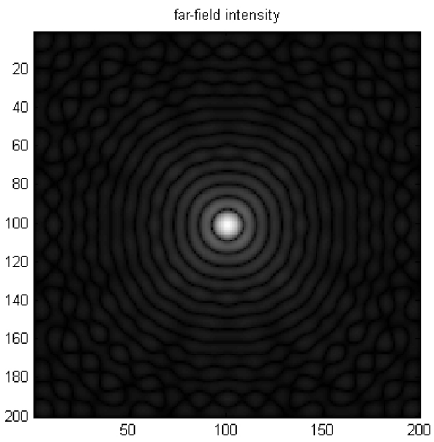

(b) Top view of diffracted light source

Figure 3.6: Diffraction pattern at Fraunhofer distance of a point source traveling through a circular aperture. The main circle in the center of Figure 3.6(b) is the airy disk.

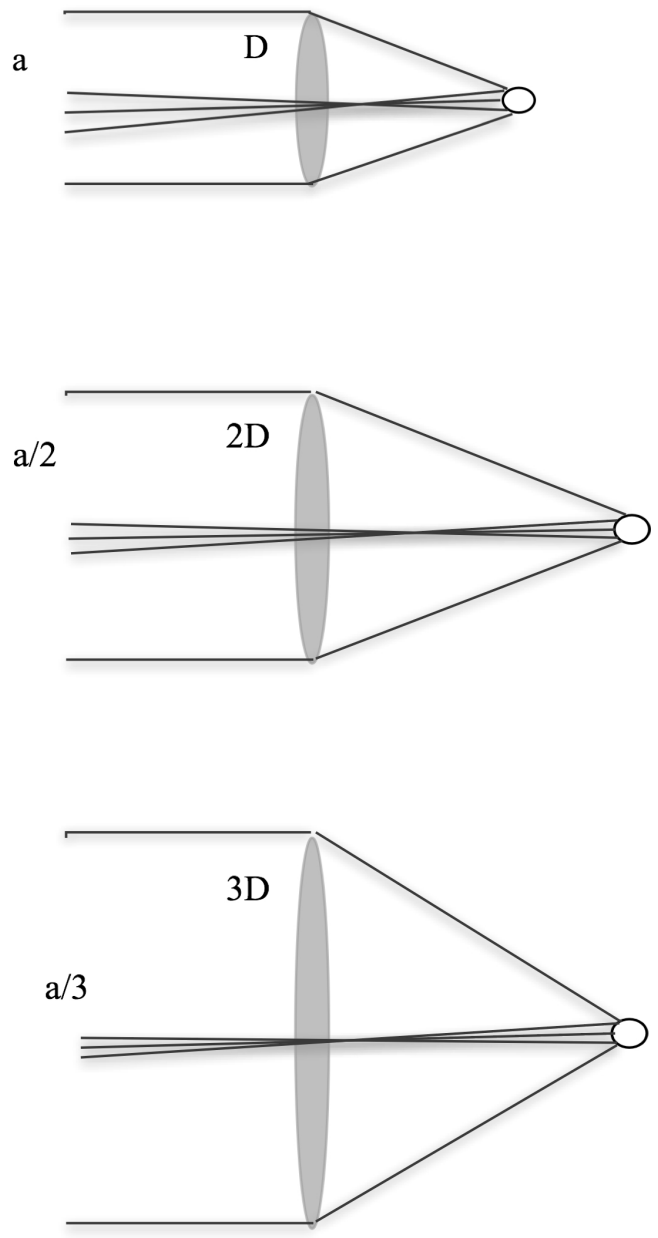

Figure 3.7: Clarifying illustration of Diffraction Limited imagery. Relationship between angular diameter and focal length of an optical system. [2]

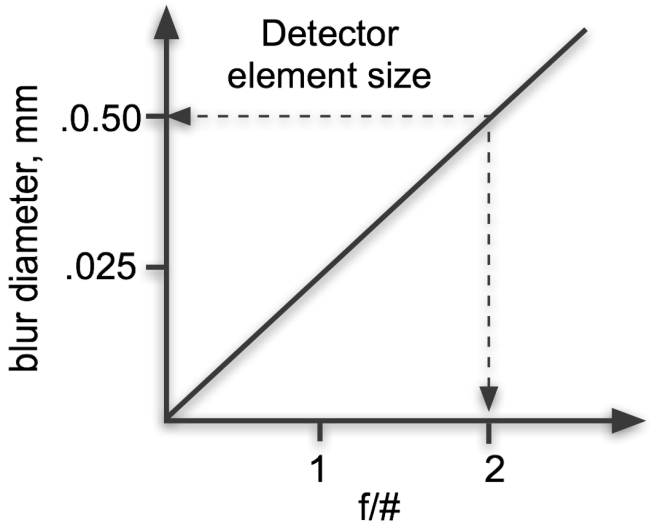

Figure 3.8: CCD Detector size vs. Object blur size relationship. [2]

throughout the thesis have a $650\mu m$ diameter and the lens of the camera is 75mm. Then the $F/\sharp$ is 12.5 and that will result in an Airy Disk of $15.25\mu m$ with an Angular Diameter of $\sim$ 0.002 radians. A rule of thumb for good digital imaging results is to match the Airy disk of your optical system with the pixel pitch of the CCD. In our case, the camera we use has pixels' pitch of $7.5\mu m$, which means that it is much smaller than the Airy disk of the system. That results in an energy leak to neighboring pixels. This relationship between detector elements size and blur diameter is shown in Figure 3.8

As we have already mentioned, the resolution of an optical system is defined on how close two point sources can be in order to be identified on the image plane as two separate points. We saw above that a point source, as it propagates through an aperture, develops a diffraction pattern that gets mapped on the image plane. In the case of two point sources then we have two such diffraction patterns on the image plane. The closest the peaks of these patterns can come together and still be resolvable is equal to the size of the airy disk of the system and it is called *Raleigh*

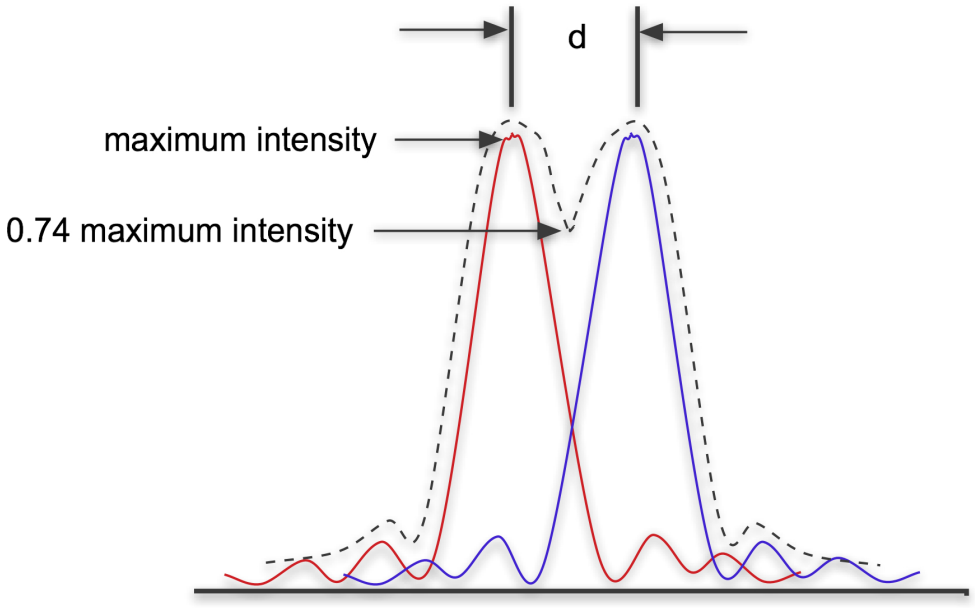

Figure 3.9: Raleigh criterion. The minimum distance that two point sources can have on the object plane in order for their diffraction patterns, on the image plane, to be resolved.

criterion. As shown in Figure 3.9, the maximum intensity of the two resultant points sources is equal to 0.74 of the maximum intensity of the two peaks.

$$d = 1.22\,\lambda\,f/\sharp \tag{3.8}$$

Another important quality that can be used to explain the image quality of our imaging method is the System Irradiance.

3.3.2 System Irradiance

All of the above assumed that the mirror was still at all time in one position. As we have explained though, the mirror will be scanning the object plane by taking different tilts. That tilting will result is changing the amount of the reflection of the mirror, which of course will affect the irradiance in the system.

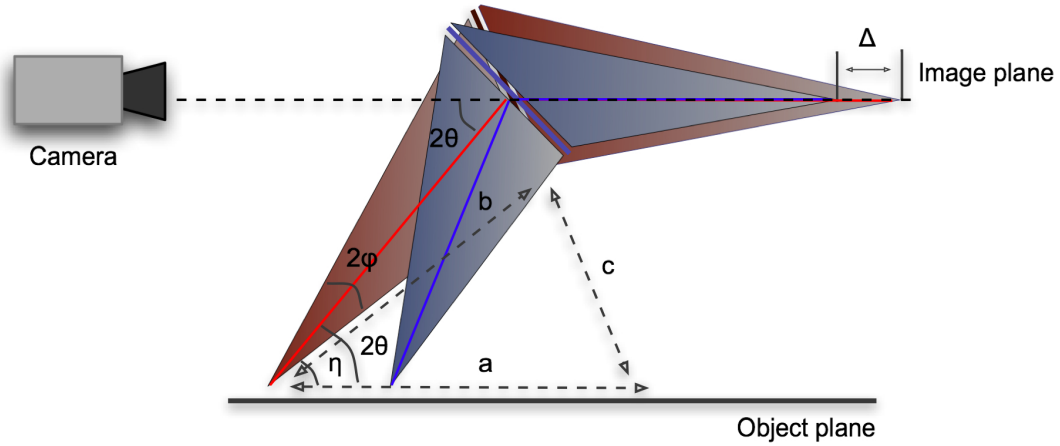

Figure 3.10: Ray tracing for different tilts - Change in system irradiance

One way to determine this irradiance affect in our system is by applying ray optics into our system's model as show on Figure 3.10. As we see, depending on the tilt there is going to be a relationship between the amount of tilt of the mirror and the amount of light that will be reflected off the mirror. This relationship is expressed below.

By plotting the amount of tilt of the mirror versus the amount of light transferred through the micro-mirror, we come up with a relationship that indicates how uniform the irradiance in our system is. For the best performance, as shown in Figure 3.11, the mirror must be tilted at a bank of 35^o with respect to its vertical axis.

$$a = d\left(\frac{cos(2\theta)}{sin(2\theta)} + \frac{sin(\theta)}{cos(\theta)}\right) \tag{3.9}$$

$$c = \frac{d}{cos(\theta)} - \frac{d}{2} \tag{3.10}$$

$$cos(\eta) = \frac{a - c * sin(\theta)}{\sqrt{a^2 + c^2 - ac * sin(\theta)}} \tag{3.11}$$

$$2\phi = 2(2\theta - \eta) \tag{3.12}$$

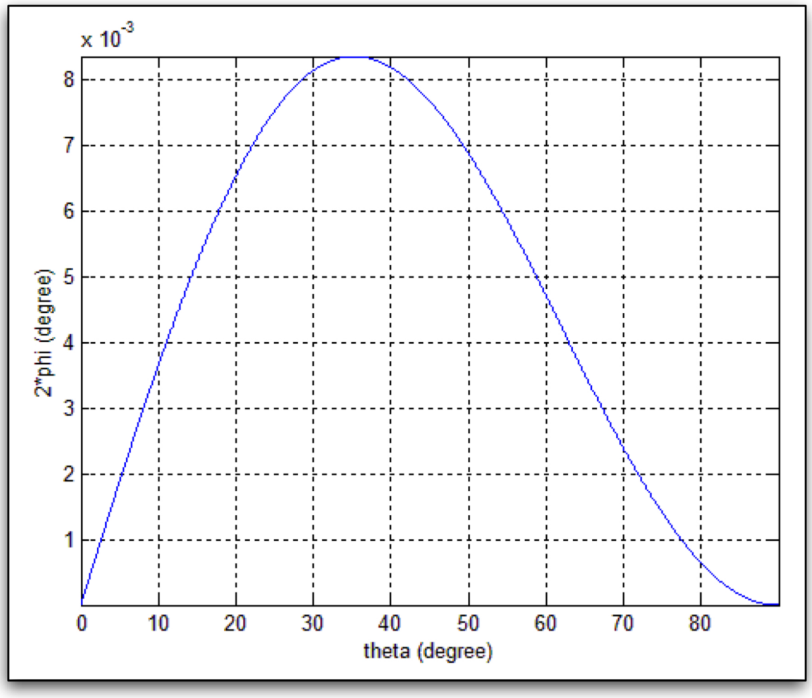

Figure 3.11: Irradiance vs Mirror Tilt

Another important observation is that while the mirror tilts, the position of the imaginary object is going to be shifted as well. This will create the so-called circle of confusion of our system. This will define the minimum depth of field that our system needs to have in order to not generate images in and out of focus while it takes different tilts.

$$\Delta = d\left(\frac{1}{sin(2\theta - 1)})\right) \tag{3.13}$$

3.4 Summary and Contributions

In this chapter we presented our system model of imaging through micro-mirrors from an optical point of view. We identified some of the properties that are introduced as we place a micro-mirror in the light path of the lens and the object plane.

We found that micro-mirror in to the whole optical system plays the role of an

optical stop or else F-stop. However, when we place that stop at the focal point of the lens of the image sensor then we have a telecentric imaging system. In addition, due to the size of the micro-mirror it increases the depth of field of the optical system.

We examined qualitatively the imaging performance of our system. We identified the parameters which are more crucial in determine the quality of imaging, regardless of the other components involved in the optical configuration. We found that for the given setup that we have the theoretical maximum resolution that it can achieve is about $15\mu m$ and in addition we calculated the highest irradiance that we could get our of our system for a given system configuration. We found that when the mirror is tilted at an angle of 35^o from its vertical axis we can extract the highest irradiance. We observed also that for tilts $\pm 8^o$, common degree of tilting for MOEMS devices, the irradiance of the system remains almost constant. That means that the quality of data that gets extracted from the mirror as it tilts, it has the same characteristics.

Next, we examine the performance but also the imaging capacity and method of imaging using our model of programmable imaging with our actual system prototype.

4. Experimental Imaging with a Single MOEMS Mirror

In the previous chapters, we provided an overview on how a micro-optical-electro-mechanical systems (MOEMS) of mirrors can be used in imaging systems. We discussed MOEMS operation and their applications. Moreover, we have shown how they are used in current imaging systems with their presence and the innovative features they offer. However, so far we have taken only a theoretical approach into consideration. In this chapter, we discuss in depth experimental imaging with MOEMS and present our imaging system prototype. In addition, we present our proof of concept results, which validate our system theory. Throughout this chapter, we identify the benefits that MOEMS bring in the field of imaging and particularly in field of *programmable imaging*.

A Programmable Imaging camera can image an object in a reconfigurable fashion and providing the user a desired image capacity. An example of such a programmable imaging system is shown in Figure 4.1. This system consists of an image sensor (camera) that images the object plane through a controllable micro-mirror. As oppose to a conventional camera system, the micro-mirror allows the image sensor to capture the object plane in a programmable way. In other words, as the micro-mirror tilts only sections of the object plane get projected on the image plane of the sensor and get recorded. In this example, three images are produced from the programmable camera, seen at the top of Figure 4.1. The image on the left shows a standard image of the object plane, while the middle image shows a zoom-in to a particular region. On the right, a image is provided by the programmable camera that looks as if the object plane is seen through a fish-eye lens. It is critical to note that *no* changes were made to the hardware of thesystem to capture the different images. Only, the

mirror movement was reconfigured. From this image, one of the applications of a programmable imaging system is realized. In this case, the resulting images appear as if a three different lenses were used in the system. In fact, no lenses were changed, thereby demonstrating that programmable imaging can act as a *dynamic lens*.

In this chapter, we demonstrate the programmability of our imaging system by showing the ability to make any correspondence between the object plane and image plane by tilting the micro-mirror in a predetermined fashion. This feature allow the user to dynamically control the sampling pattern, field of view and resolution of the image.

4.1 Experimental Setup

In Figure 4.1, we illustrated the system model of our proposed imaging system and some initial results. In Figure 4.4, we show the actual experimental prototype of our imaging system. The image sensor used is a *Sony DFW-V300*[1] CCD camera with a *75mm focusable Double Gauss Macro Imaging Lens from Edmund Optics*[2], which has a narrow field of view. The camera is connected, through an IEEE-1394 Matrox Frame grabber, to an imaging PC (running Windows XP), which is running *MATLAB* and the *Image Acquisition Toolbox* in order to capture snapshots and import the images into *MATLABs'* environment for processing, as shown, on Figure 4.2. The MOEMS mirrors used in our prototype is *Lucents' LambdaRouter chipset*.

The driver of the micro-mirrors device is connected to a PC (running Windows NT) which, through a custom application, controls the tilt of each mirror separately. The two PCs are connected via an IEEE802.3 connection and they are synchronized through a simple file creation/deletion scheme. This way when any of the micro-mirrors run a scanning profile the camera knows when a new tilt occurs in order to

[1] see Appendix A.1 for the specifications of the image sensor
[2] see Appendix A.2 for the specifications of the particular lens

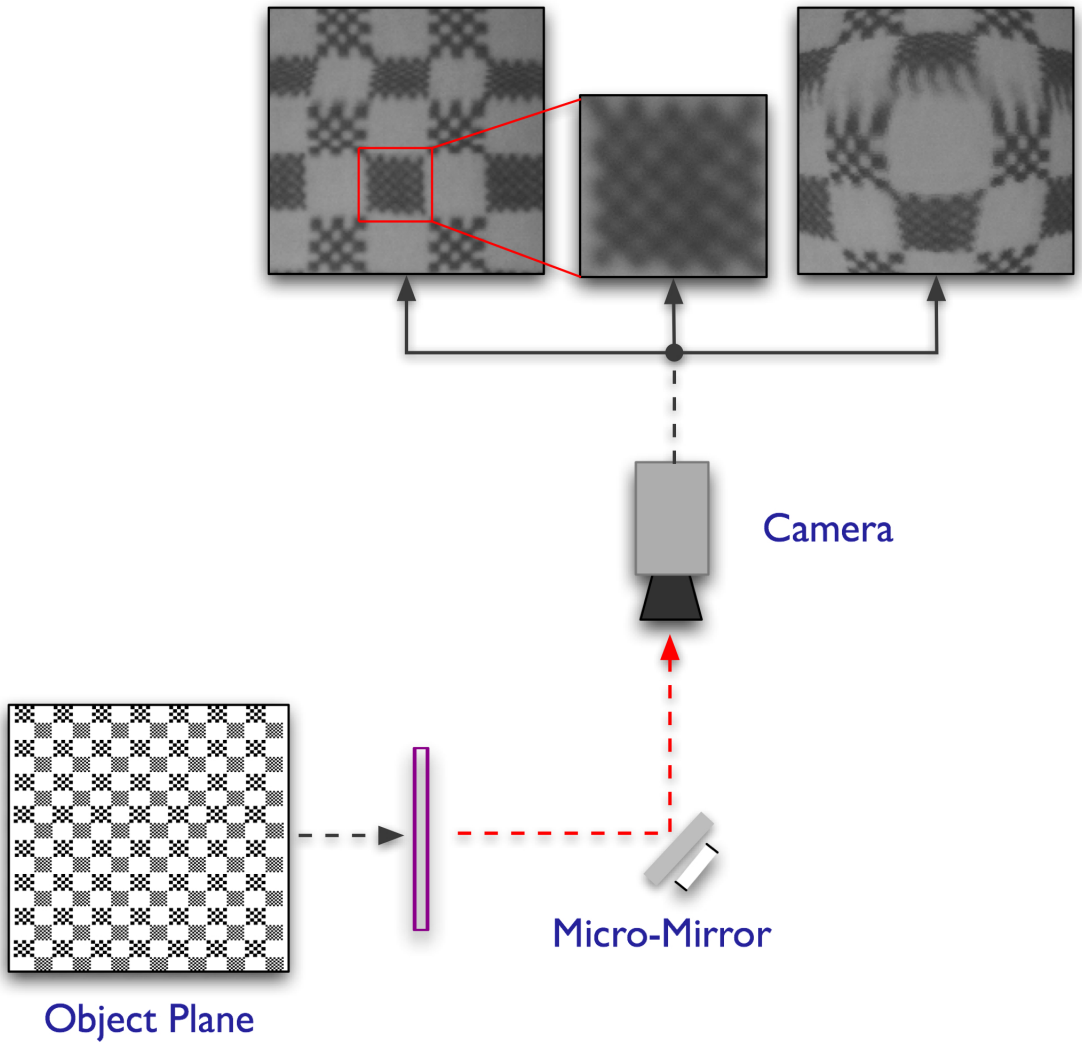

Figure 4.1: System diagram of our proposed MOEMS camera configuration. Our imaging system gives the ability to image the object plane in different ways by varying field-of-view, resolution and sampling pattern.

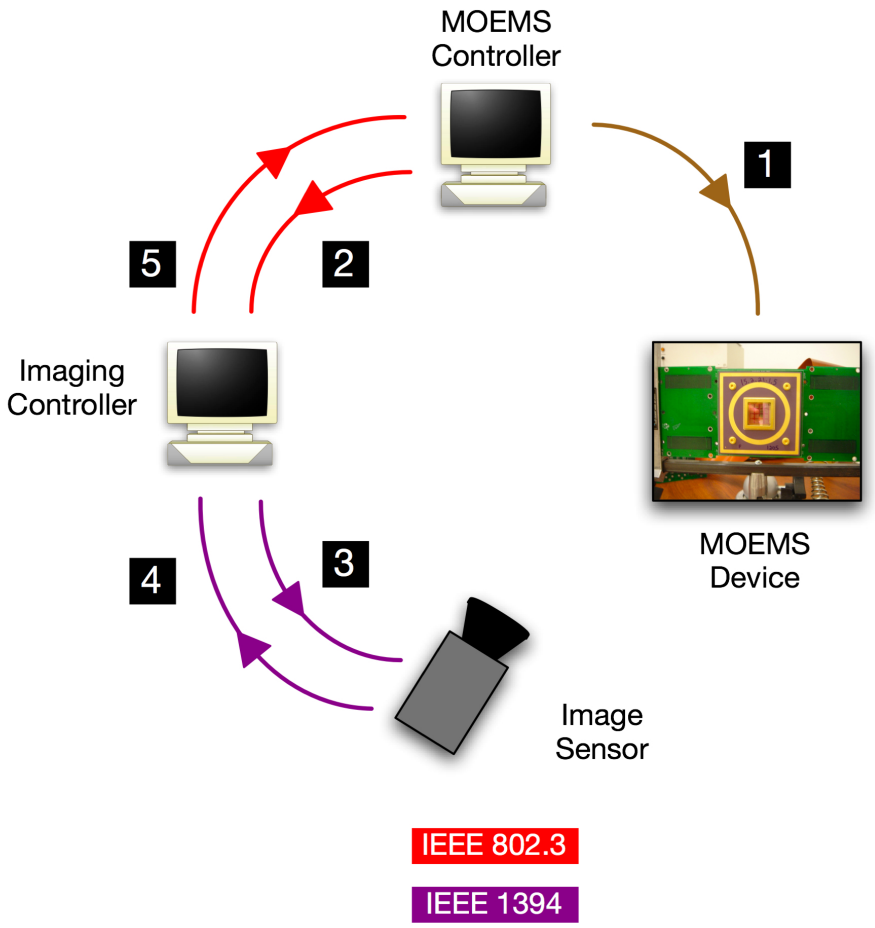

Figure 4.2: System diagram of our proposed MOEMS camera operation flow.

capture a snapshot.

Lucent Technologies has generously provided us, through an extended loan, with the *LambdaRouter*[54; 64; 65]. The Lambdarouter chip consists of a MOEMS mirror array with a total of 256 mirrors in a square 16x16 configuration (see Figure 1.3). Each mirror has a diameter of $650\mu m$ and has two degrees of freedom $\pm 8^o$ of tilt in both X-Y axes. Each micro-mirror is electrostatically actuated via a set of four electrodes that are under the mirror and its frame, as seen in Figure 4.5. When voltage is applied to a given electrode, the mirror plate or frame is electrostatically attracted and tilt towards the side of the electrode. The 8^o tilt corresponds to a

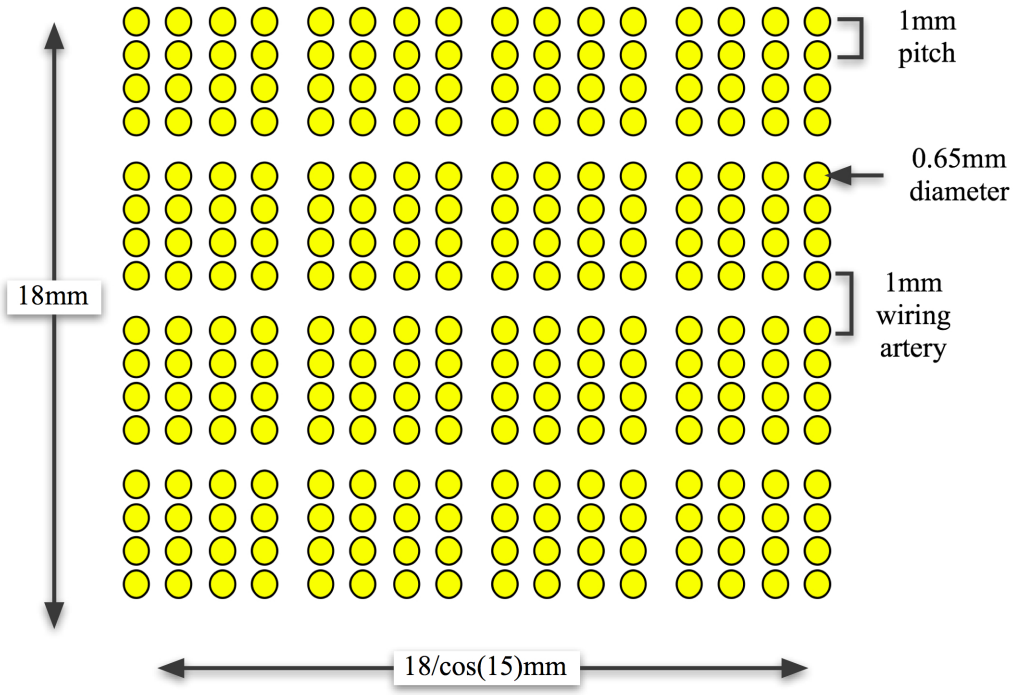

Figure 4.3: The Lambdarouter chipset is composed of 256 surface machined two axis steering mirrors. The schematic shows the layout of the mirrors which are $650\mu m$ in diameter on a 1-mm pitch with wiring arteries every fourth row and column. One axis is stretched by 3.5% to account for the 15^o skew of the chip system

voltage of approximately 200 Volts on the electrode. It is important to note, that the LambdaRouter was originally fabricated to enable all-optical switching for a large telecom switching infrastructure, not for imaging. Later in this chapter, we will provide some of the challenges of using this MOEMS device for imaging. In this chapter, we focus only on the actuation of one mirror in the array to perform our imaging. In Chapter 5, we will see experimental results where more than one mirror is used for imaging.

Continuing with the system described in Figure 4.4, it is seen that the camera focuses through the micro-mirror onto the object plane. We originally use an object plane composed of a checkerboard pattern consisting of $5mm$ squares, each broken into four sub-subsquares, two of which contain smaller checkerboard patterns, with

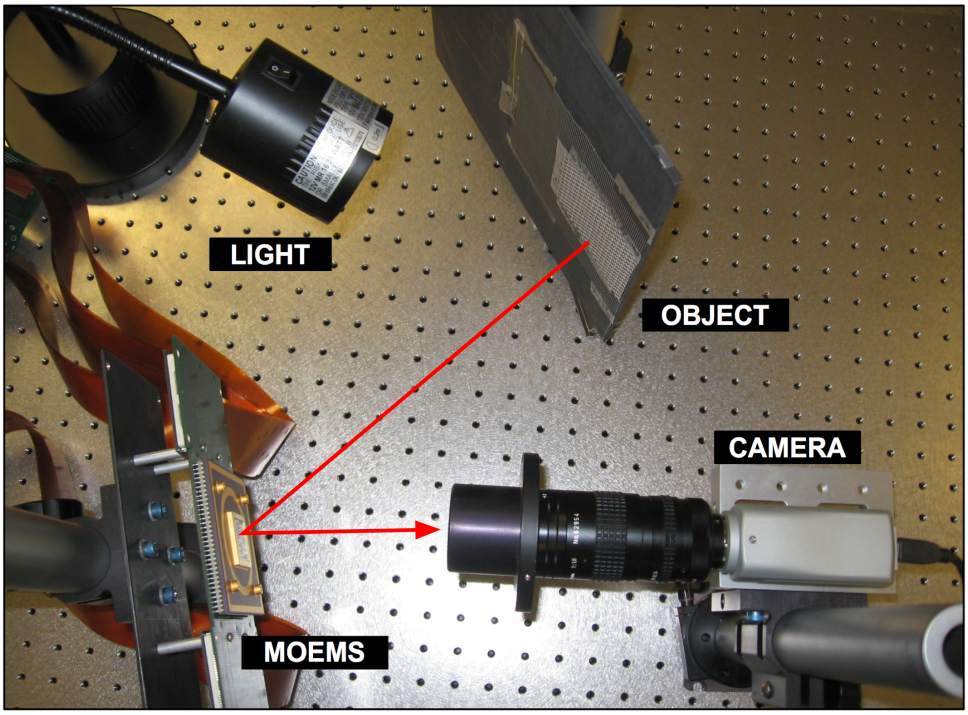

Figure 4.4: Overview of our imaging system prototype. With this experimental set up one or more micro-mirrors can be used simultaneously to image the object plane.

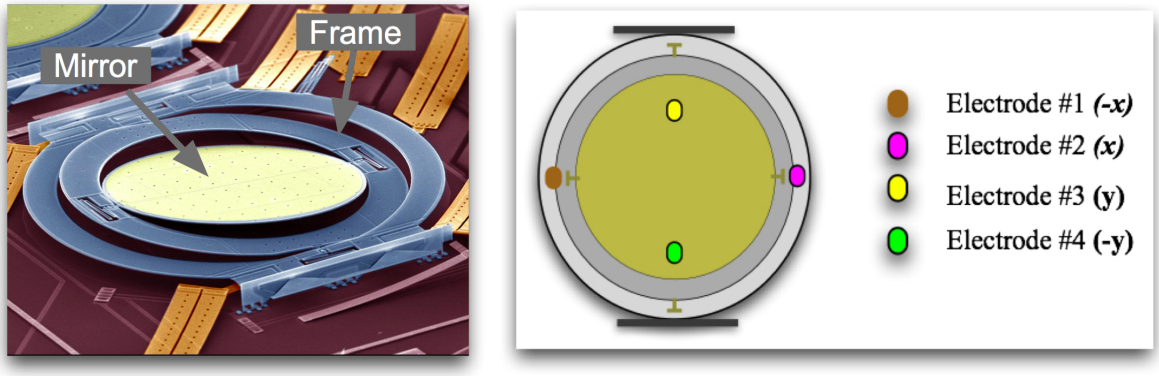

Figure 4.5: Lucents' Lambdarouter micro-mirrors are actuated electrostatically with electrodes that located underneath the mirror plate and the frame of the mirror. Each set of electrodes is causing a single axis motion and combined they offer two degrees of freedom motion flexibility to the micro-mirror

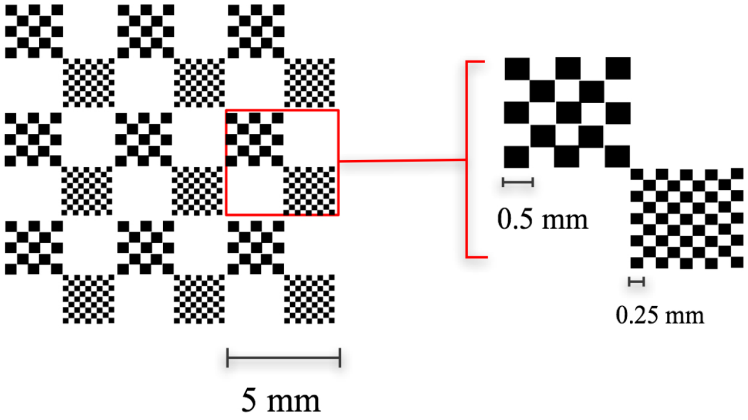

Figure 4.6: Object plane used for imaging and for camera calibration. The checkerboard pattern target consists of $5mm$ squares, each broken into four sub-subsquares, two of which contain smaller checkerboard patterns, with checkers of $0.5mm$ and others of $0.25mm$

checkers of $0.5mm$ and others of $0.25mm$ as shown in Figure 4.6. We use this pattern for two reasons. It allows us to calibrate our system and it is also a standard way to experimentally calculate the spatial resolution of our imaging system. Both of these topics will be discussed later in this chapter.

Lucents' Lambdarouter chip was designed to be used in a large all-optical network switch. Therefore, the micro-mirrors were packaged in order to no only protect them from any physical damage, but also to filter out any ambient light while increasing the efficiency of the optical light used in the all-optical network switch. Therefore a protecting overglass cover is placed over the mirror array. This cover has an antireflection multi-layer coating, acting as a notch filter, specified at the optical communication wavelength of 1550nm. As a result, we conclude that the Lambdarouter chipset, as provided to us, is not an optimal device for imaging in the visible range of 400-720nm. As can be seen in Figure 4.7, there is a large glare in the visible wavelengths from the coating on the overglass [3]. This glare was a challenge to overcome in our exper-

[3]see Appendix B for further discussion of the effect of the overglass in our system

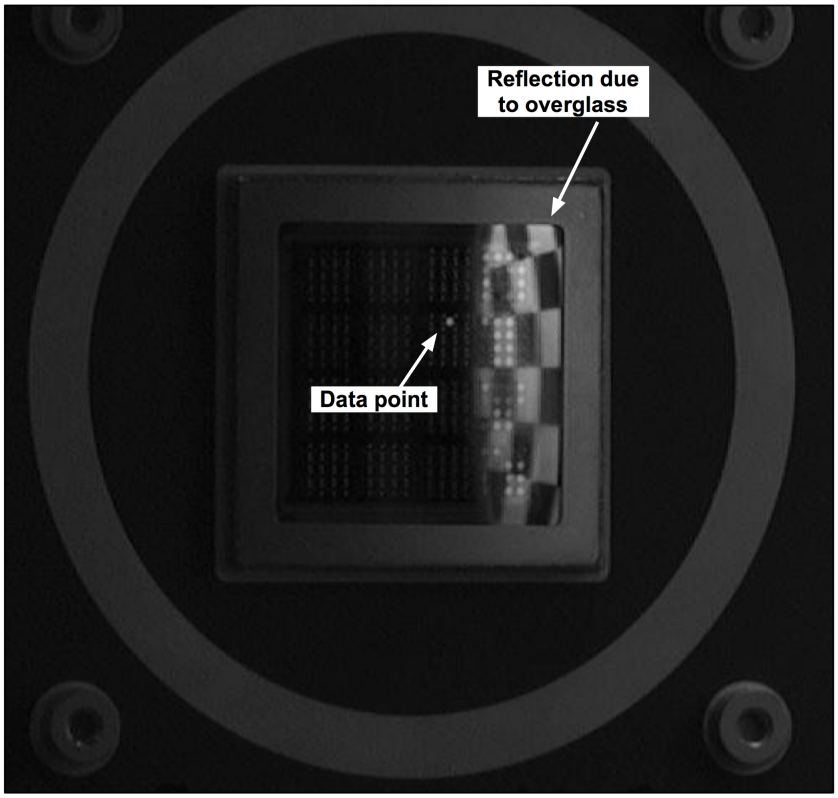

Figure 4.7: A screenshot of Lucents' Lambarouter MOEMS array of micro-mirrors. It is very visible the reflection of the object plane on the ovreglass protection, as well as, the active mirror that scans over a white checker. With careful placement of all the components of our system we can bypass/eliminate much of the reflection effect caused by the overglass.

imental prototype, as it limited the position of the object plane. Therefore, one of the most crucial aspects of our imaging system is the precise topology of the different components of our system. By carefully choosing the positions of the components, we can eliminate, as much as possible, the reflection of the overglass covering the micro-mirrors in order to allow light to penetrate the overglass and reflect off of the mirror to the image sensor.

4.2 Image Formation

In this section, we describe the details of capturing programmable images through the micromirror. We begin the discussion with an overview of the process. Recall from Figure 4.1, the object plane is focused through the micro-mirror onto the image plane. In Figure 4.8, three images of the object plane are shown, each corresponding to a different voltage set in the X and Y directions. Each voltage set applied to the mirror electrodes corresponds to a specific mirror tilt due to the electrostatic attraction forces between the electrode and the mirror. To create an image, the micro-mirror progressively scans through the object plane, with different and unique voltage sets applied to the electrodes. For each mirror tilt, an image snapshot is taken (as shown in Figure 4.8) and from these snapshots, desired image information is extracted and assembled into a single image. We have examined two image formation approaches, by using multiple and single pixel extraction. Details of these two approaches are presented below [66].

4.2.1 Multiple Pixel imaging method

One of the most common way to produce wide field of view images is through the process of image *mosaicing*, which we overviewed in Chapter 1. Recall, the main idea behind this method is to pan and tilt the camera while capturing still images at each position. Using various post processing algorithms, a high field of view image is created.

Conversely, in our programmable imaging system, instead of moving the camera, we tilt the micro-mirror in different positions capture a snapshot for each position, as seen in Figure 4.9. It is well known, and also shown in Figure 4.10, that the part of an image close to the edges of the circular aperture of the mirror suffer from diffraction and vignetting. As a result, from each frame we extract a certain section of the image

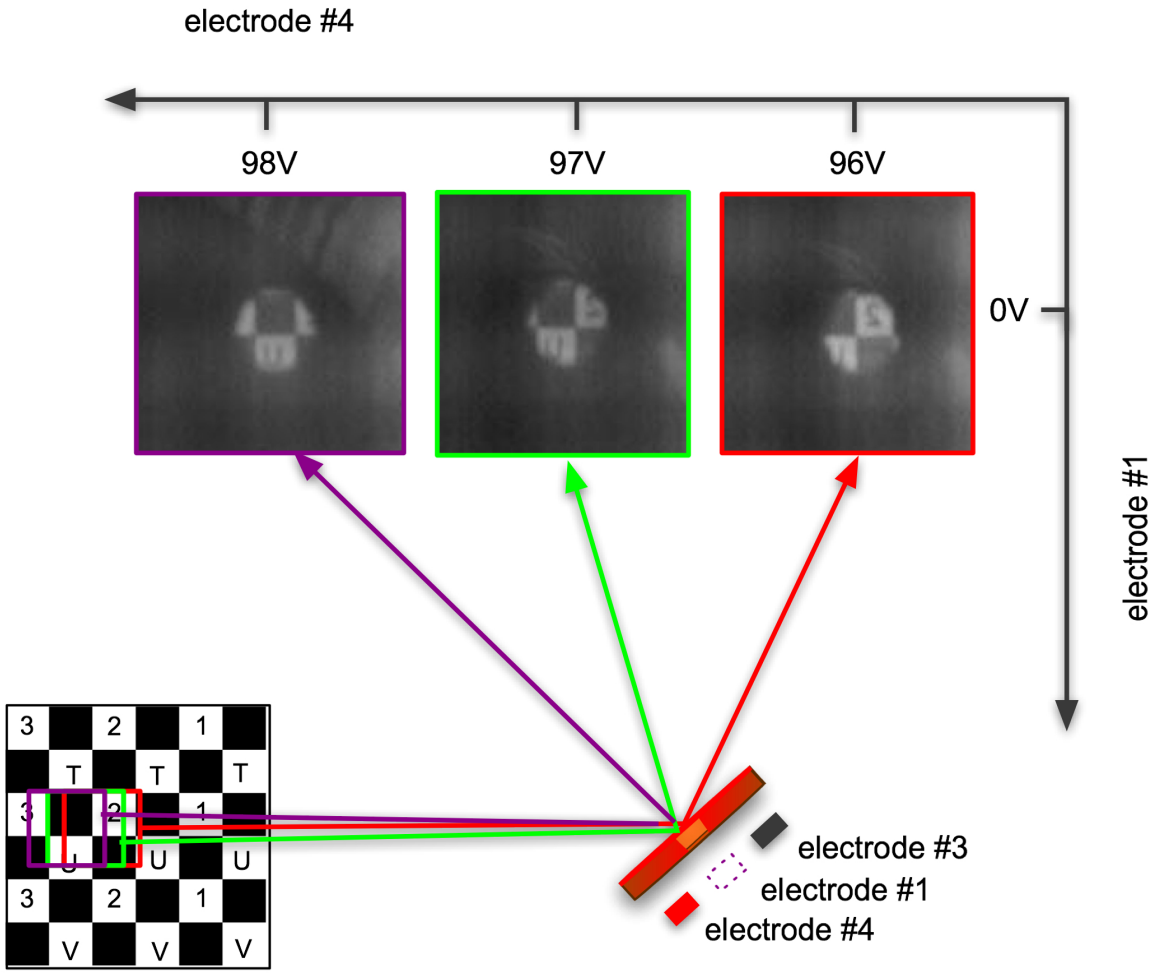

Figure 4.8: Micro-mirror scanning procedure and imaging. The mirror tilts by electrostatic forces that get developed between the mirror and the electrodes underneath. As voltage applied on an electrode the mirrors' tilt changes as well. For each tilt we capture a screenshot of which certain portion of it is used to form the final image of the object plane.

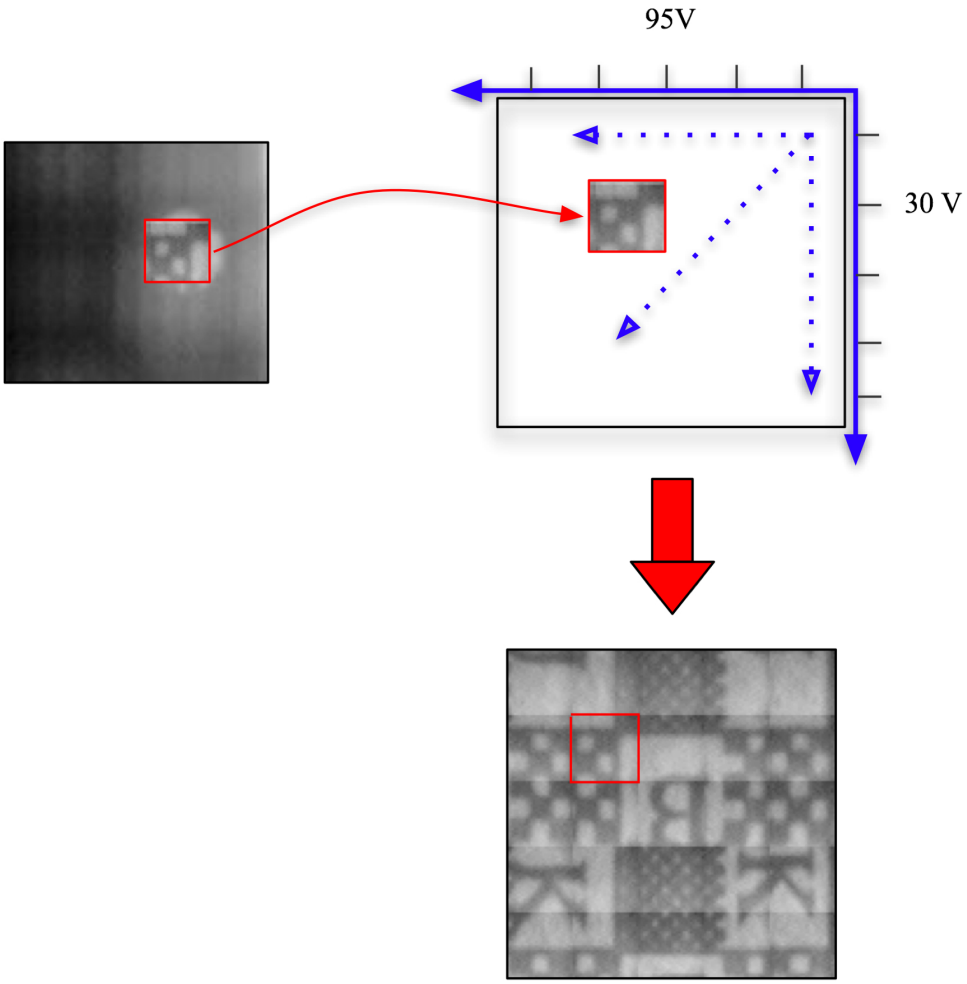

Figure 4.9: Multiple Pixel imaging method - pieces of data are sampled separately, with every tilt of the micro-mirror, and mapped precisely on the image plane in a mosaic fashion

that excludes this effects, as shown in Figure 4.9. In this example, each block of extracted image data is 25x25 pixels. By careful system calibration and exact mirror tilts, each of these extracted images can fit together to forming a single image. In [67], we presented this idea and showed how our imaging system can create mosaics and as result to increase the FOV of the imaging sensor.

Our method results in creating image mosaics that increase the field of view and the spatial resolution of the image, similar to what image *mosaicing* methods can

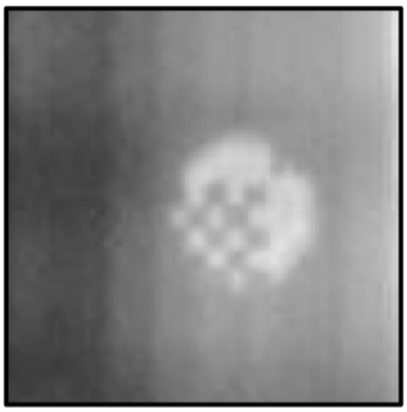

Figure 4.10: Screenshot of the micro-mirror at some tilt while scanning the object plane. Close to the periphery of the circular image we can identify elements of diffraction and vignetting cause by the circular micro-mirror.

achieve today. The difference though between conventional mosacing and our programmable method can be divided into two categories.

First, in conventional image mosaicing techniques, there is a need to capture all of the snapshot images and then perform software post processing to obtain the data. In our case, we build the final image in real time, by just extracting the required pixel for each block. Second, in conventional image mosaicing techniques, the captured images need to have a FOV overlap of close to 50% in order to find common data (image) points between neighboring images, such that the mosaicing algorithms will perform well and produce acceptable results [68]. In our case, no FOV overlap is required between neighboring images. More importantly, classical mosaicing has no information about the camera system that took the images of the object plane. In our case, the system (ie, tilt of the mirrors) is known, allowing us to quickly and easily use mosaic to capture the object plane.

Our method proves that image mosaicing can be achieved without the need of post processing but with precise data sampling. The required sampling is achievable in our system, as there is no physical camera movement as in conventional image

mosaicing, just the tilt of the mirror. Our technique can be used in applications where the imaging sensor has very narrow field of view. The MOEM device can be used to extend the field of view of the system while performing mosaicing on the fly without any post processing. This is a very beneficial function since it lets us sample parts of the object plane precisely, in a *programmable* way.

However, with blocks of data in our mosaicing technique, complete dynamic sampling of the object plane is not possible. Therefore, we must decrease the size of the image corresponding to each mirror tilt. To meet this end, we next introduce image formation method which is programmable imaging by extracting a single pixel from each mirror tilt.

4.2.2 Single Pixel imaging method

As shown in our theoretical system configuration in Figure 4.11, it is possible to make a correspondence between any point on the object plane with any point on the image plane by placing and tilting a mirror appropriately within their ray path. We take this a step further by proposing that for every mirror tilt, we extract one pixel, this way enabling an image sensor of only a single pixel. If we have enough mirror tilts, and thereby enough extracted pixels, we could image the object plane.

Similarly to the multi-pixel method that we presented above, for the single pixel extraction case, the mirror once again scans the object plane. However, now only one pixel is extracted from the image snapshot corresponding to each mirror tilt. By scanning the entire object plane, a complete image can be rendered by placing the pixels next to each other, as shown in Figure 4.12. The importance of this single pixel method is the fact that we can choose every pixel that is used in the image. This allow us to observe the object plane in any desired reconfigurable fashion since we know for every pixel the exact voltage applied on the mirror and the exact tilt of the

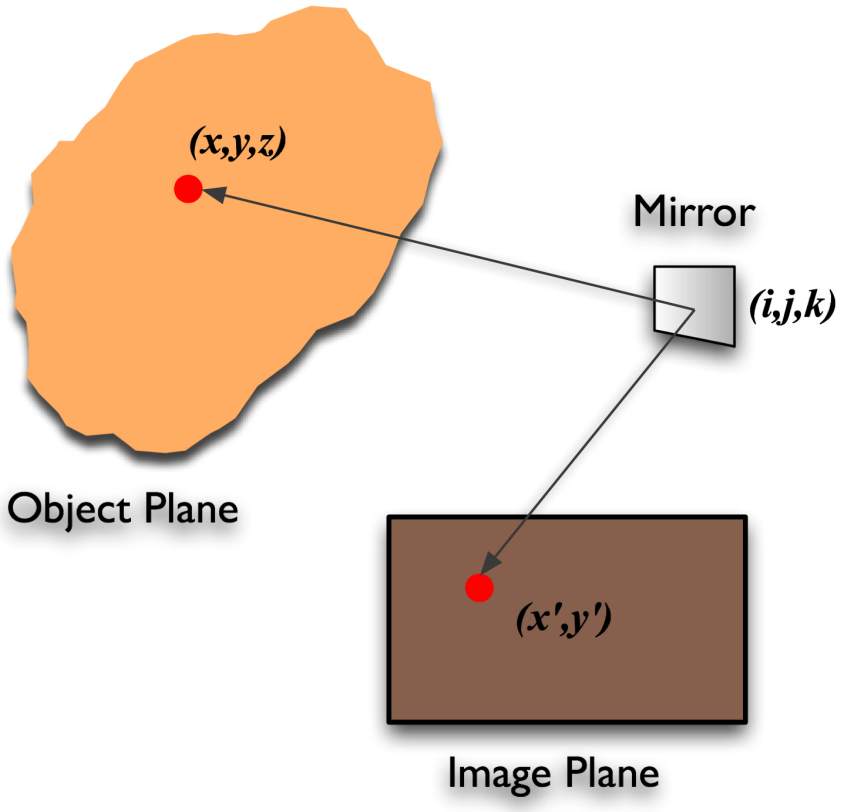

Figure 4.11: A theoretical approach - Correspondence between points on the object plane and image plane.

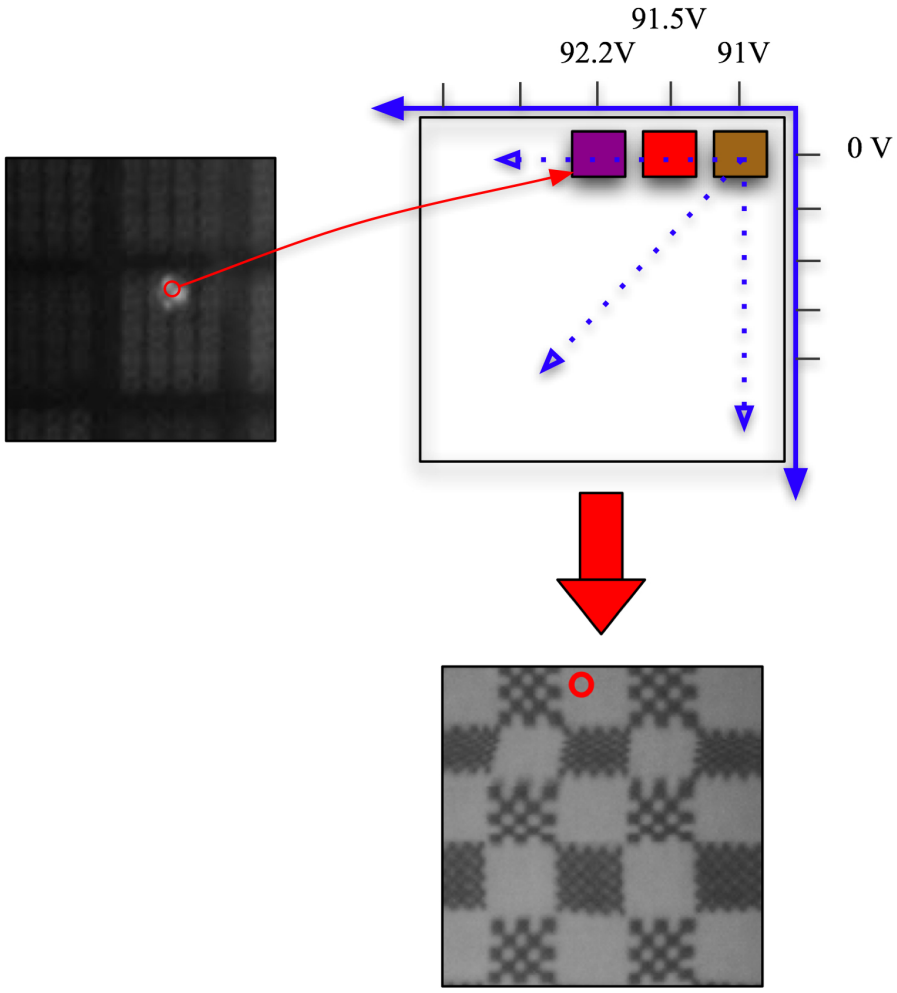

Figure 4.12: Single Pixel image formation - As the mirror tilts a single pixel is extracted and mapped accordingly on the image plane.

mirror. In other words every pixel has its own identification.

Depending on the MOEMS device used, there is a limitation on how many distinct states the MOEMS mirror can take, as well as, the scanning profile that can perform. For the particular device used in this thesis, the *Lucents' Lambdarouter*, each distinct micro-mirror can take over 100,000 distinct states on the entire XY-plane [54]. The limitation in this case comes from the digital-to-analog conversion (D/A) electronics, rather than the mechanical capacity of the MOEMS. Theoretical, the mirror can support an infinite number of states.

4.3 Imaging System Calibration

In order to take advantage of our systems' ability to sample the object plane in a dynamic and reconfigurable fashion, we require a very precise calibration of our imaging system in order to perform desired point-to-point correspondences between the object plane and the image plane. In this section we discuss the calibration first for the single pixel imaging method and then the mosaicing method.

The first step of calibration is to apply sets of voltages on the micro-mirror electrodes while extracting a single data point from each tilt of the micro-mirror. The resulting image for a linear voltage scanning profile is shown in Figure 4.13. On the X-axis, only electrode 1 was activated and took values from 52V-104V with step of 0.4Volts. On the Y-axis, either electrode 3 or 4 were activated one at a given time, in order to give a full scan in the Y direction. The voltage range in this case, on each electrode, was 0-80V with a step of 1.23Volts. The resulting image is 130x130 pixels.

From examining Figure 4.13, it is obvious that the image suffers from distortion. This distortion is a result of non-linearities in the system that are related to the image projection, by imaging a 3D object into 2D (perspective projection), and the non-linearity of the mirrors, in terms of applied voltage and the corresponding mirror

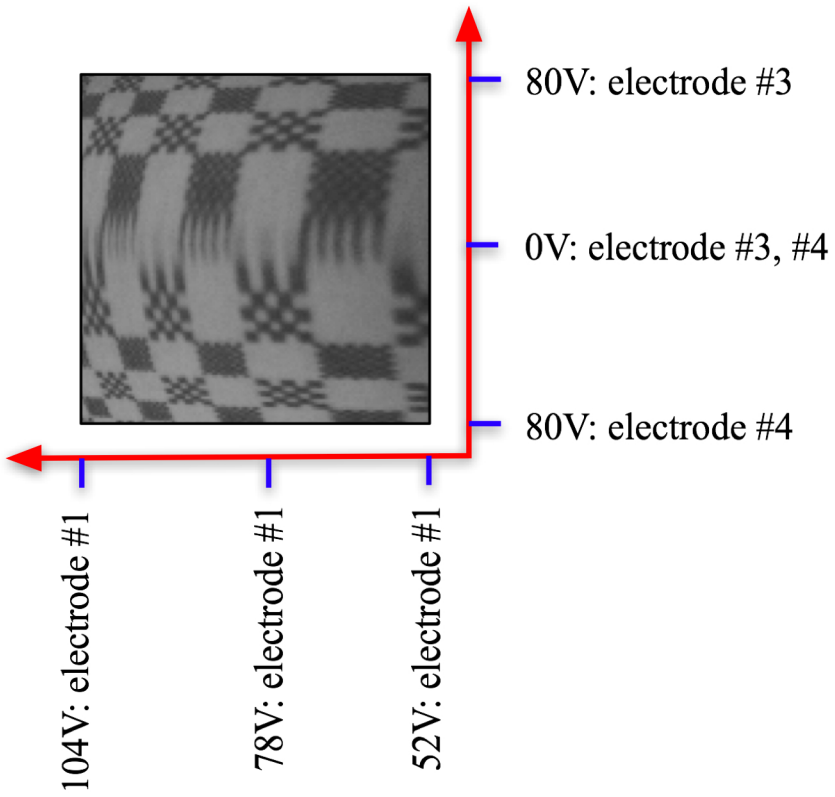

Figure 4.13: Image created by 16,900 discreet points/tilts that were captured as the micro-mirror was scanning the object plane with linear voltage steps on both axes.

tilt.

Projection distortion can be explained through the following example. For instance, lets assume that we want to project a raster scan, as shown in Figure 4.14(a), on a two dimensional surface, located a distance d in front of the micro-mirror, by pointing a LASER beam on the surface of a micro-mirror while the mirror scans. Since the mirror moves around a pivot point in a three dimensional space, the raster path will be translated on the motion shown in Figure 4.14(b). If we rectify the scanning pattern of the micro-mirror in a two dimensional surface then we will see that the image suffers from what is called, pincushion distortion as shown on Figure 4.14(c). Similarly, our system will suffer from the same effect. Therefore, it is very

important to find the relationship between the voltage applied on a the mirror and the projection point on the object plane so that the correct image points get sampled in order to produce *distortion free* images.

The other type of distortion is a result of the non-linearities of the mechanical and the electrical components of the MOEM device. The forces developed in the electrostatic actuators between the electrodes and the mirror plate and mirror frame are capacitive [65]. As a result, it is expected that their behavior won't be linear. Experimentally, it has been shown that the mirror does not tilt significantly until the voltage exceed approximately $\pm$40Volts in either axes. In Figure 4.15, a plot is shown with the experimental relationship between voltage applied on each electrode versus the tilt that the mirror undertook. The graph was data resulting in an experimental configuration of a HeNe LASER, the micro-mirror and the projection plane where the reflected beam was marked on a piece of paper as shown in Figure 4.16.

From Figure 4.15, we observe the non-linear *voltage Vs. tilt* characteristic of the mirror is more dominant at higher voltages. This explains the degree of higher distortions on the edges of the sampled image. Also in the same figure, it can be seen that the mirror doesn't tilt significantly at voltages close to 0 Volts [65]. This is the reason that a large stretch is observed in the middle of the linearly sampled image, as show on Figure 4.13. In this stretch potion of the image, the same point is sampled multiple times.

Apropos what the may cause image distortions, the system calibration is performed by knowing an initial object plane that gets used as the calibration target and the *mirror tilt Vs. actuation voltage* relationship. If we know how to careful choose the voltages applied on the micro-mirror, we can sampled an image in a predetermined fashion that will result on a particular image configurations such as, a *rectified* image. Therefore, there is no need for us to try to identify all the distortions

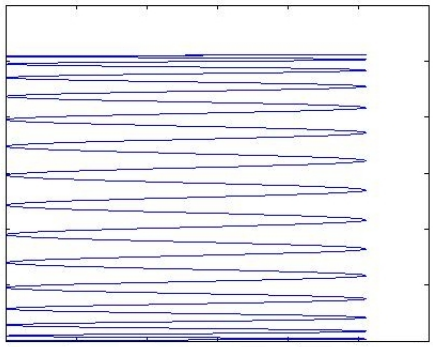

(a) Desired raster scan

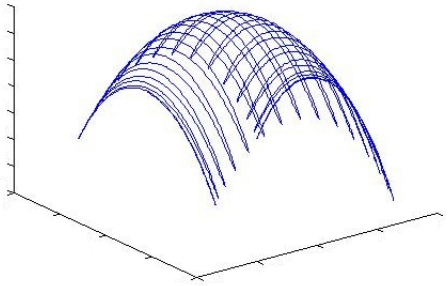

(b) Projection path based on the motion that the mirror undergo in the three dimensional space

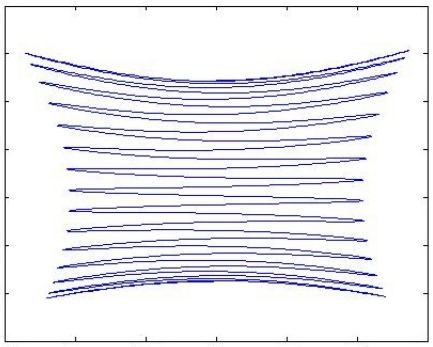

(c) Rectification of the micro-mirrors projection. It is obvious the pincushion effect

Figure 4.14: Raster scan projection going from 2-D to 3-D and then back to 2-D. This conversions have as result the scan path distortions shown on 4.14(c)

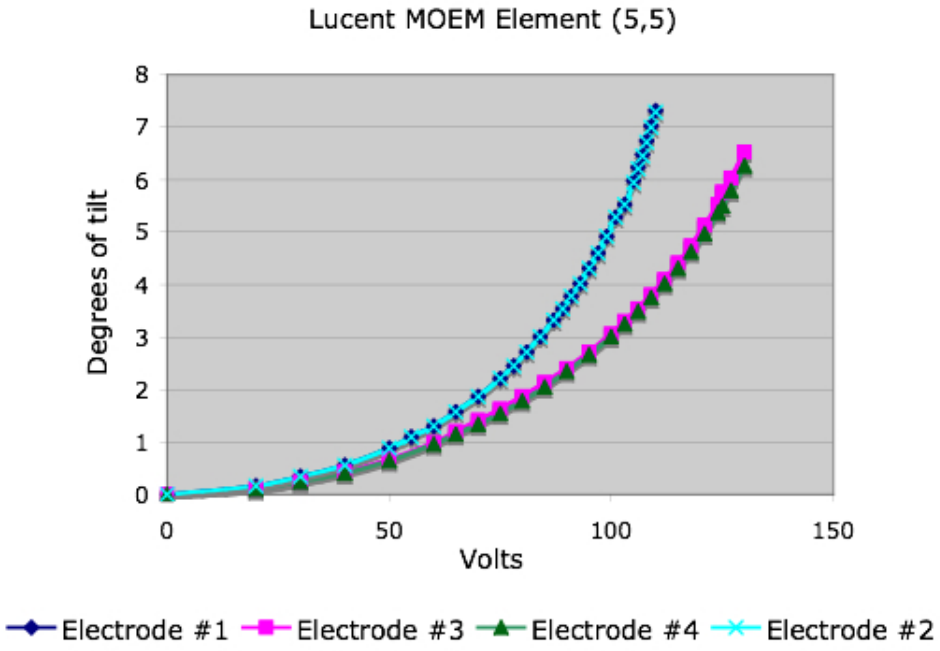

Figure 4.15: We see the non-linear behavior between applied voltage on the actuating electrodes of the micro-mirror and the amount of tilt of the mirror.

of our imaging system or to model them (see Figure 4.17). Simply, we treat all the distortions as a black box and we will address them all with one system calibration using a well known method called *image warping*. It is key to point out that system calibration only needs to be performed one time. Once a mirror calibration is known, programmable imaging can be performed.

In image processing, image warping typically is performed to remove distortions from an image during post processing. Image warps are used by mapping of a set of source image pixels to the destination rectified image. Most geometric correction systems support a limited site of mapping types such peicewise affine, bilinear, bi-quadratic or bicubic mappings. Such mappings are ususally parametrised by a grid of control points.

In our imaging system, we use image warping techniques to calibrate our system

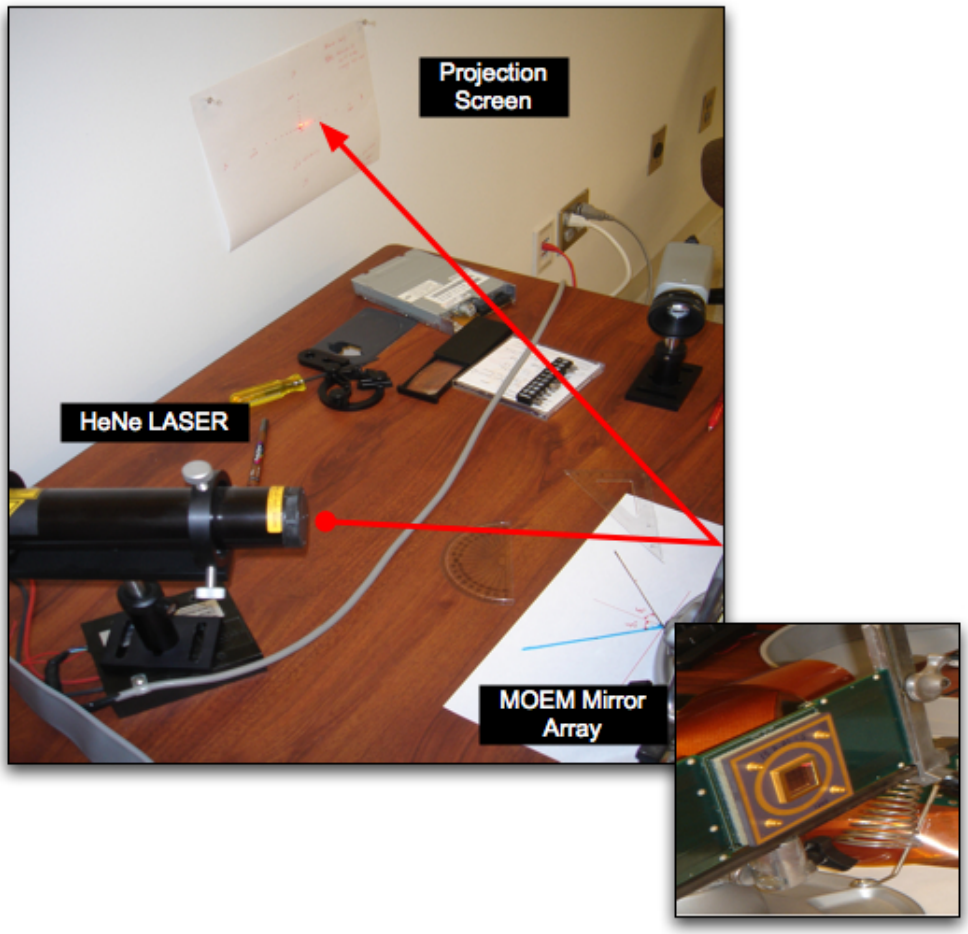

Figure 4.16: System configuration for the study of voltage applied on the micro-mirror versus tilt. Different voltage will tilt the micro-mirror accordingly and the project LASER beam will deviate accordingly on the projection screen.

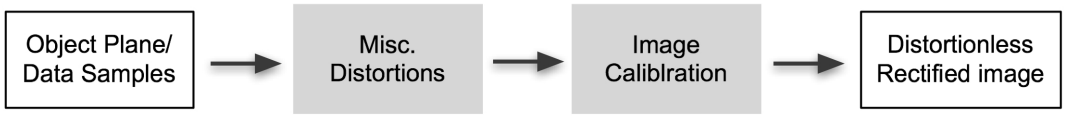

Figure 4.17: All the stages of our imaging system. All the distortions are treated as a black box and treated as one. This way there is no need for complicated modeling and identification of any possible distortion and source of distortion that could affect the sampled image.

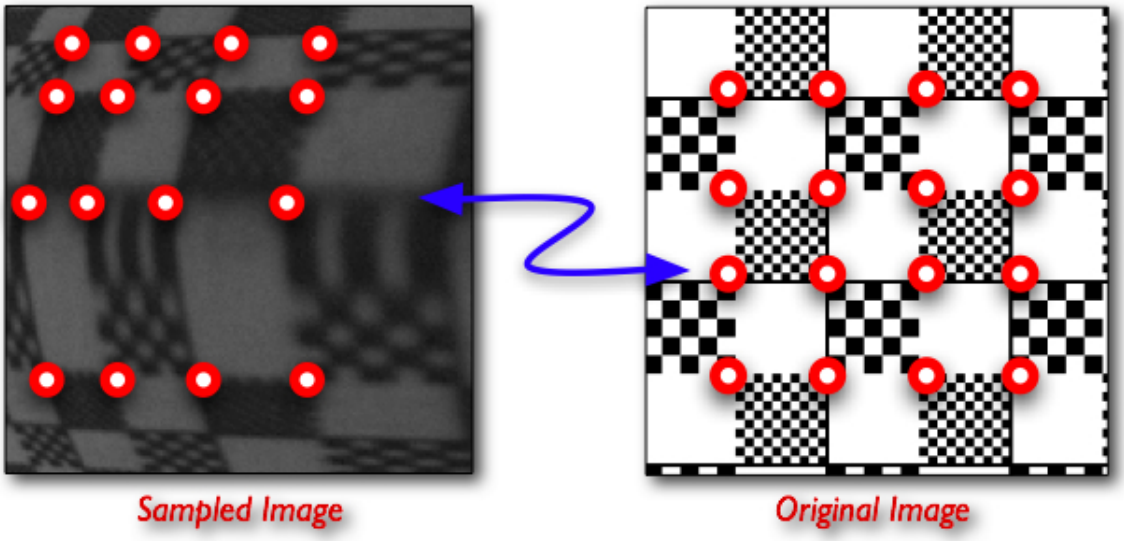

Figure 4.18: Inverse warping procedure. Using control points we can warp the distorted checkerboard to an undistorted one like the object plane one. This will result in non-lineal voltage scanning profile for the micro-mirror.

and correct for any type of system distortions. Knowing that our object plane is a checkerboard in which all corners of the checker are equally spaced, we establish a set of control points. As it is shown, in Figure 4.18 the control points are the corners of each checker on both images. For each of the control points selected, the voltage to achieve that mirror tilt is known. By using a bilinear interpolations between the control points, we are able determine a non-linear voltage sampling table, which will contain voltage sets, that when used to scan an object plane will result in a rectified image. A sampled image with the new calibrated non-linear voltage table is seen in Figure 4.19. The new non-linear scanning voltage profile in a single axis is compared with the original linear scanning voltage profile in Figure 4.20.

Calibration of the system has a significant impact in our work, which exposes some of the system's most unique features. Every pixel on the new unwarped image corresponds to a mirror tilt and particularly to a voltage applied on the mirror. In

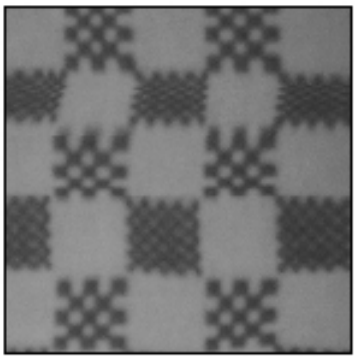

Figure 4.19: This is an image of the object plane captured with calibrated scanning profile. As we can see all the distortions have been eliminated almost entirely.

other words, we now create a non-linear voltage table that will allow the micro-mirror to scan the object plane in any fashion that is desired. We can now create rectified images or other types of images, seen previously in Figure 4.1. We call this process *programmable imaging*, the topic of the next section. However, before that section, we need to state a very important point regarding the resolution of the system.

In the case of single pixel image formation we sample the object plane a pixel at the time. Given that the particular micro-mirrors used can tilt with a precision of 0.05^o and that have about 320 states on each direction, then each mirror could capture an image of 25 megapixels. Depending on how far the object plane is from the mirror it could affect the final image. In Figure 4.19 we see that the minimum we can get out of the targeted checker is 0.25mm points. Even though in Chapter 3 we found that the theoretical resolution of the mirror was about $15\mu m$ we see that experimentally that the maximal resolution for the existing set up under the particular configurations is $250\mu m$. There reason for this big difference on the results is that in the real world estimation there are many other factors that are not and cannot get modeled in order to be taken in to account when calculating that theoretical resolution of a system.

Now lets say few words about calibrating the mosaic images presented earlier in

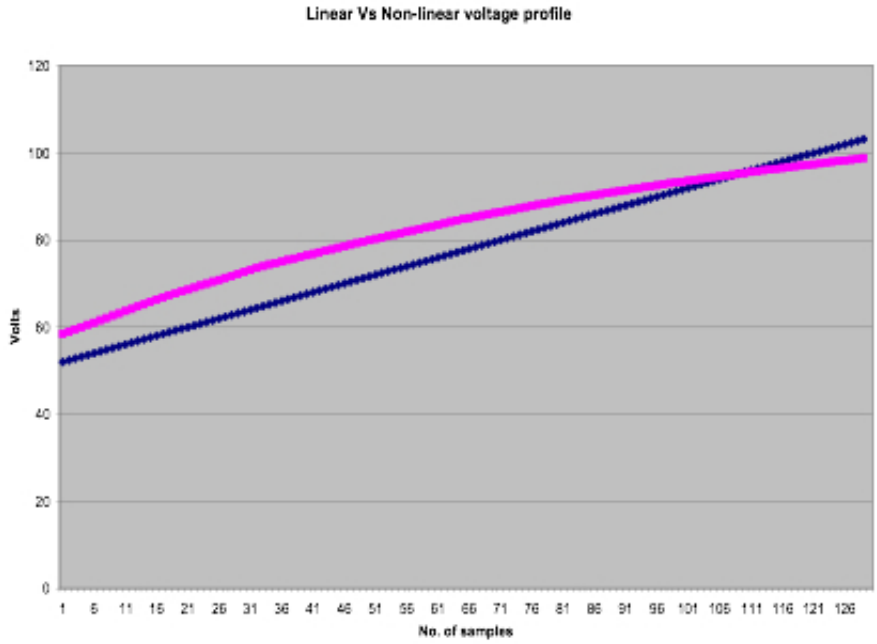

Figure 4.20: This is a direct comparison between a single line of a linear voltage scanning profile versus a non-linear that corresponds to a calibrated scanning profile of a micro-mirror.

this chapter. In the case of multiple pixel extraction for mosaic images, we create images from tiling blocks of data (e.g. 25x25 pixels) together. For the tiling to work, careful calibration is required such that every tilt of the micro-mirror captures adjacent image blocks of the object plane.

For multiple pixel calibration, the first step is to find out how many pixels are to be extracted from each snapshot image from a mirror tilt, as shown in Figure 4.10. In this case, 25x25 pixels were extracted, which correspondes to a distance on the object plane of 1.5mm x 1.5 mm. With this information, we create a calibration target, with dots separated by 1.5mm, as seen to the right in Figure 4.21. If we can sample a 1.5mm image at each spot, the mosaic puzzle pieces will fit together exactly. The calibration target is sampled using the single pixel extraction method described above, with a linear voltage scanning profile. As expected, there are distortions in

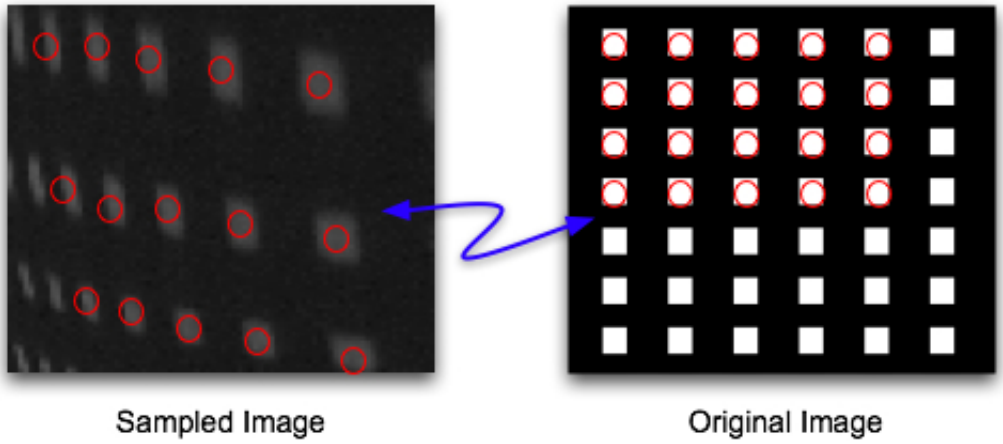

Figure 4.21: System calibration for the case of multiple pixel image formation. The calibration between the original image and the sampled image is necessary in order for the mirror to tilt appropriately and capture the necessary parts of the object plane.

the system, as shown in the left of Figure 4.21. However, all that is required for the mosaicing algorithm is to find the voltage of the center of each calibration dot. We wrote a simple script in Matlab to find the white dots, determine the center, and extract the corresponding voltage. Once this is found, the object is rescanned only at the requested voltage sets, and a snapshot image is taken at every point. Now, the our programmable imaging mosaicing algorithm is performed as described earlier in the chapter. An example of a completed mosaic image is seen in Figure 4.22.

4.3.1 Programmable Imaging

The fact that we can dynamically select the way we sample the image plane gives a new approach to imaging - what we call as programmable imaging. Programmable imaging opens up many opportunities and introduces capacities that were unthinkable until now.

Any conventional imaging systems has to battle distortions either through corrections in optics or through software post processing methods. We showed in Chapter

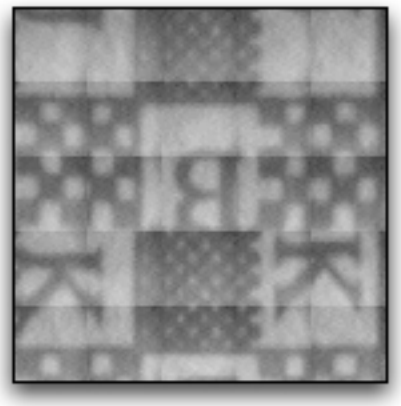

Figure 4.22: The multiple pixel imaging method works like mosaicing. The mirror must tilt only few time and capture certain parts of the object plane and then place them next to each other. No overlapping needed, no sophisticated algorithms.

2 that wide field of view systems suffer from geometrical distortions and only post processing methods can correct it, still without provide perfect imaging. Our method compensates for all distortions by selectively sampling every pixel of the resulting image, as every point/pixel captured from the micro-mirror has it is identification and address on where it is to be placed on the image plane.

This imaging method gives us the opportunity to dynamically control different imaging attributes such as:

Spatial Resolution We can control the number of samples captured from the object plane.

Field of View We can control the field of view of our image by capturing points only from a certain section of the object plane.

Sampling fashion We can manage they way we want to sample the image in order to correct distortions or to resemble effects that could have help us to understand a system better.

In Figure 4.23, we see how from a distorted image we can create a rectified image, as detailed in the calibration section above. We take this programmable imaging a step further, by zooming into a part of the image. It is critical to realize that the system and camera parameters do not change at all. The zoom-in is performed only by a function of the desired sampled points. This is achieved by the creation of a non-linear voltage table, now with a much smaller average voltage step size, compared to average voltage step size used to obtain the original rectified image. In all the images shown in Figure 4.23, the resolution was the same of 130x130 pixels. Through this example we see how we can control, resolution, field of view and sampling through our system.

With conventional commercial digital cameras, the resolution of the captured image can be specified, which equally distributes all of the pixels across the image plane. With our programmable imaging system, we have the ability to select certain areas of the object plane to be imaged at different resolutions. This is a very useful feature, as it allow us to emphasize on certain aspects of the image.

Having reconfigurable control over the resolution and the FOV of an imaging system without the need to change any hardware components and settings, it's unique to our Programmable Imaging System. For example, we assume that in a captured image we want to zoom in to a particular section. With our programmable imaging method, we can do that easily without sacrificing any resolution from the resulting zoomed in image. So, it can have the same (or better!) resolution when compared to the original image. This is not, though, possible with software zooming algorithms. If we were asked to do the same zoom-in using ordinary software post-processing, the algorithm would have to interpolate new points in order to increase the resolution of particular section of the image. Therefore, another advantage of our technique is that each image point is a sampled point in hardware (real sampled point from the object

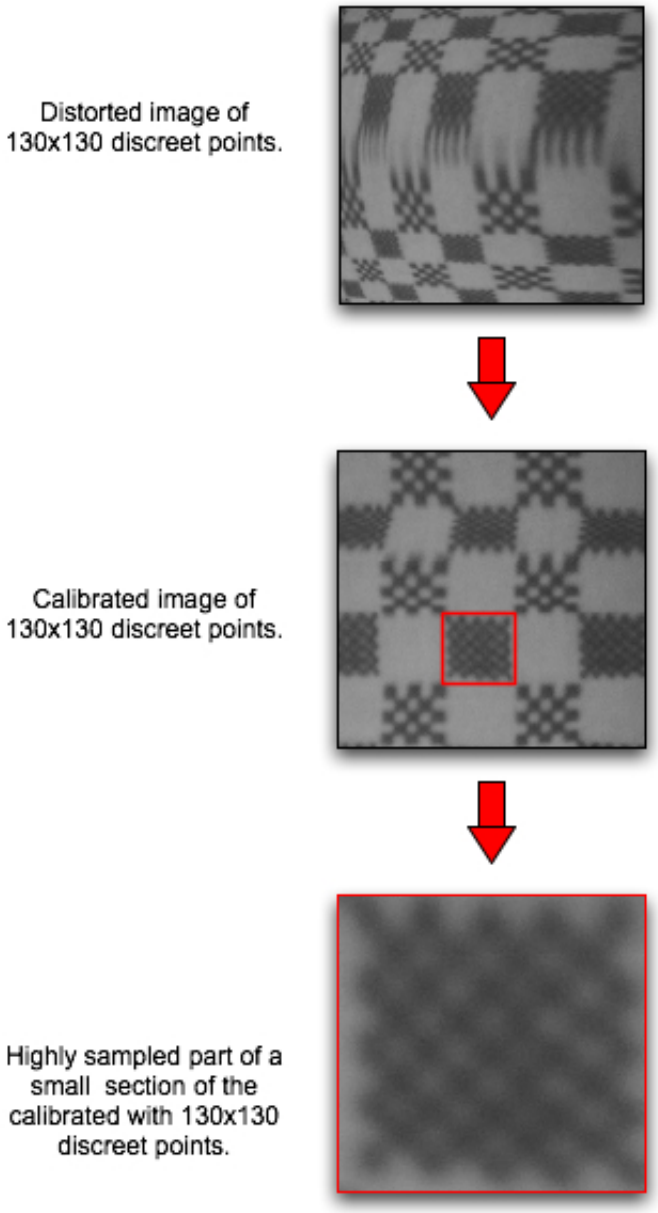

Figure 4.23: In this Figure we see a sequence of images captured by our imaging system. In all cases the images have the same resolution of 130x130 pixels but the sampling pattern and FOV changes. In the first case we see an images sampled with a linear voltage scanning profile. The distortions here are obvious. In the second case we have a calibrated image sampled with a non-linear voltage scanning profile. Last we have a section of the original image fine sampled with small FOV.

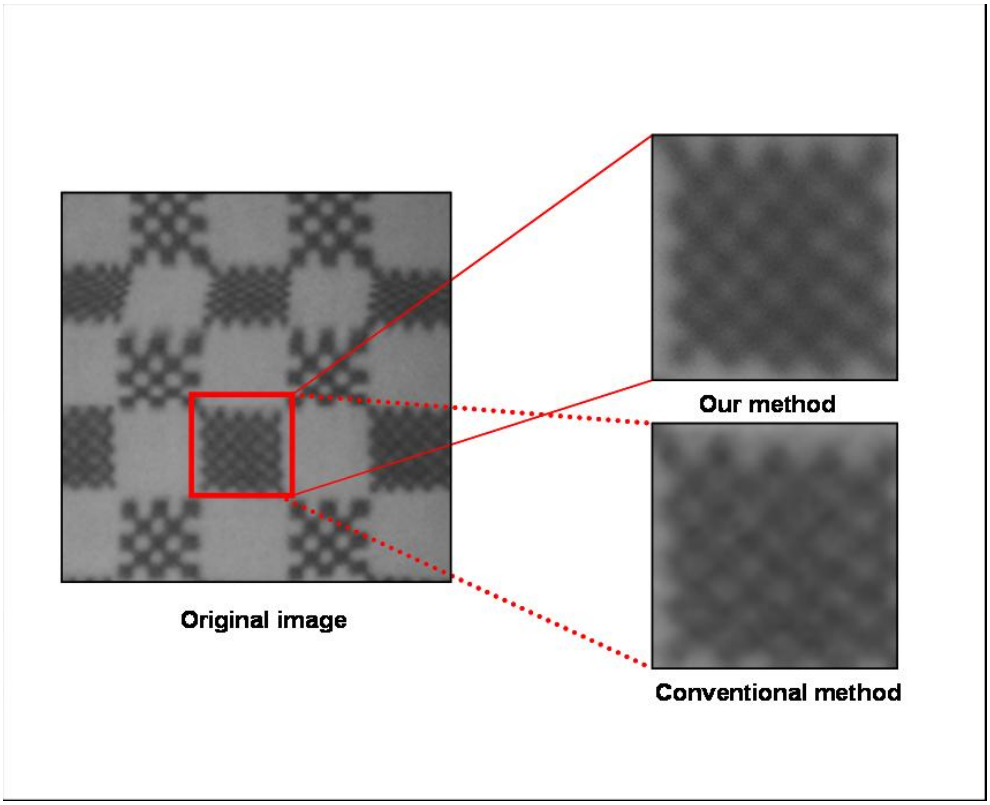

Figure 4.24: With programmable imaging we can easily control FOV and resolution of our imaging system as oppose to conventional methods. In this Figure we show that if you need to zoom in to certain part of the image we can program our camera to do so. With conventional camera we need to apply post zoom methods: crop the image and enlarge it. Such methods introduce artifacts in the image such as aliasing.

plane), with no interpolated image points calculated in software. To complete the example, Figure 4.24 compares a software zoomed-in image, showing artifacts such as aliasing and interpolation, with a zoomed-in image from which every pixel has been sampled.

Another important aspect of programmable imaging is that of dynamic sampling. Using this feature, we previously have seen how we can unwarp distorted images. However, this effect can also mimic various optical systems, all in hardware, without changing any system parameters. This is the most unique advantage of Programable Imaging. For example, we demonstrate an example of a reconfigurable lens, without

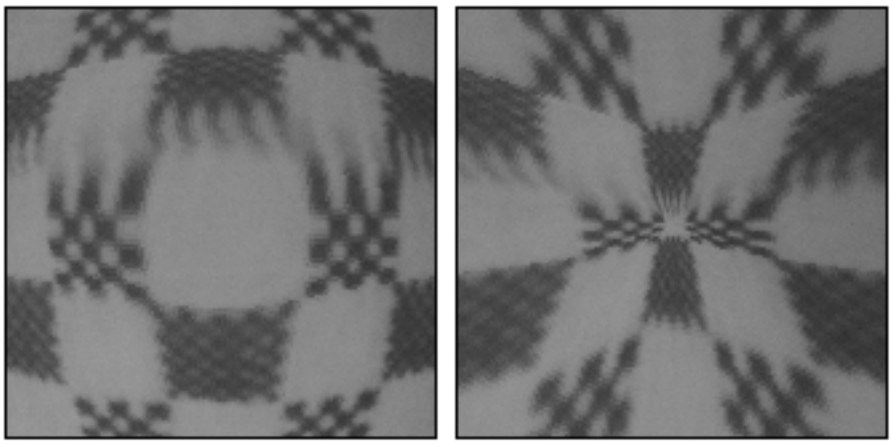

(a) fisheye. (b) whaleeye.

Figure 4.25: One of the features of programmable imaging is the capacity to sample the object plane in a dynamic way. This also let us mimic different optical systems without the need of building them.

the need to have any lens in the system. This *lensless* system does not take into account the imaging lens on the CCD. In this case, the reconfigurable lens is simply represented by the micromirror array. We first sample the object plane as if a fisheye lens is used, as seen in Figure 4.25(a). We created the required voltage sampling table by distributing the data point in some uneven fashion in order to fit the model of a fisheye lens. Similarly, to show the effect of our reconfigurable sampling system, we simple scan the object plan again, however, this time we use a voltage table that samples the object plan as if a whale-eye lens is used, as seen in Figure 4.25(b). Having this reconfigurable capability, we can study the performance of different optical systems in real imaging applications without the need of manufacturing them.

4.4 Summary and Contributions

In this Chapter, we focused on reconfigurable imaging of an object plane with a single MOEMS mirror device and presented our experimental prototype and results.

We described our two methods to imaging with MOEMS: multiple pixel imaging method and single pixel imaging method. We stressed the single pixel imaging method since it gives us more control in imaging. The calibration of the system was critical, and only after this process can programmable imaging occur. We then can associate any point on the object plane to any point on the image plane with a particular voltage/tilt of the micro-mirror. As a result, we can manipulate the sampling pattern of the image in desired fashion.

As we presented, our imaging method demonstrates increased benefits over any other conventional imaging techniques. We showed how we can change the sampling process in a programmable way in order to control dynamically imaging attributes such as the Resolution, the Field of View, and the sampling pattern. Through extensive examples we showed how all this qualities that our system offer can be used for real imaging applications.

We identified the maximum resolution of our current set up experimentally and we compared that to the theoretical one that we found on Chapter 3. We concluded that in the experimental set up there are many other factors that could affect the resolution of the image.

The enabling element in all of this work was the fact that we used a micro-mirror device as our active optical element. As far as we know, no one is performing programmable imaging in the way that we do. From the single pixel extraction, we are developing a single pixel camera that can capture high resolution images as good as a conventional camera, however, have a reconfigurable aspect increasing the capabilities of the system.

5. Imaging with MOEMS Arrays

In this chapter, we expand on our capabilities of imaging an object plane in a programmable and reconfigurable fashion with the use of a single MOEMS device. Here, we explore our ability of our system to image an object plane when an array of MOEMS mirrors is used as the active optical element in the system. We present theoretical and experimental results by using the mirror array, and we investigate their potential applications in the field of imaging. Therefore, our goal is to explore the capabilities of a system that can capture images from many different sources (in this case, micro-mirrors) and combine all this information to form a new type of image that may change the way we think of photography, and in general imaging.

Throughout time, researchers have attempted to work in the area of camera arrays in order to explore images of an object from different perspectives, exposing any hidden aspects of imaging that could make us perceive the world differently [69; 70; 71; 72]. Most of the proposed designs of such systems have offered data fusion captured from the different perspectives that could be used in conjunction with other image processing methods to enhance quality of imaging [73; 74; 68; 75; 72]. The fundamental problem of these camera arrays, though, is that these systems are always physically large since they are composed of arrays of tens or even hundreds of cameras, as can be seen in Figure 5.1. In this figure, there are 100 separate camera, in an 10x10 array [70]. The system is over 1m x 1m in size. In addition, each film or sensor would have to be initially processed and then all the images would have to be post-processed to form the final desired image. Therefore, beyond research curiosity, there is little that is practical about these camera array systems, as there size prohibits them from being useful in many applications and products.

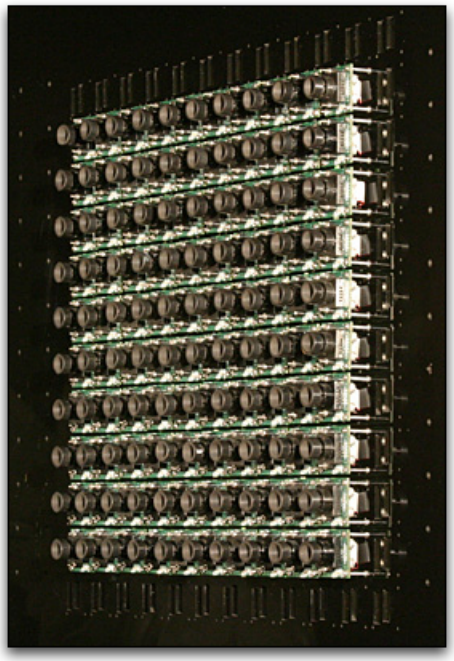

Figure 5.1: An array of 100 cameras used for multi-perspective imaging

However, a micro-mirror array can shrink the entire system to a very small size. One of the benefits of MOEMS fabrication is that the technology allows it to populate many mirrors on the same substrate arrays of elements such as *Lucents' Lambdarouter*. In contrast to the camera array shown in Figure 5.1, the MOEMS mirror array can also be used to take different perspective images. In this case, each mirror acts as a camera, and the entire imaging array can in the size form factor of appoximately 1.8cm x 1.8cm. In Figure 1.3, the LambdaRouter is shown, and you can imagine that each of the 256 mirrors (in a 16 x 16 layout) can act as an individual camera. As a further advantage, only one film or sensor is required, and each of the 256 images can be extracted from the same imaging device. But the most important advantage of our system is that each mirror can be individually controlled, as demonstrated in the previous chapter. Therefore, images created from multiple mirrors can increase image resolution, field-of-view (FOV), dynamic range, frame rate, and the approximation of

a large synthetic aperture. As an example, one mirror can be imaging the complete object plane, while another mirror is imaging a zoomed-in portion of the object plane. This can be seen in Figure 5.2

We use what has been learned in the field of multi-camera arrays for our research in using MOEMS mirror arrays for multiple images. Therefore, we provide a brief description of the current technology of multi-camera arrays.

Multi-camera systems can function in many ways, depending on the arrangement and aiming of the cameras. In particular, if the cameras are packed close together, then the system effectively functions as a *single-center-of-projection system*, which can be configured to provide unprecedented performance along one or more imaging dimensions, such as resolution, signal-to-noise ratio, dynamic range, depth of field, frame rate, or spectral sensitivity [70].

If the cameras are placed farther apart, then the system functions as a *multi-perspective-projection system*, and the data it captures is called a *light field* [6; 70], which is defined as, radiance as a function of position and direction in regions of space free. Of particular interest to us are the novel methods for estimating three dimensional scene geometry from the dense imagery captured by the array, and novel ways to construct multi-perspective panoramas from light fields.

Lastly, if the cameras are placed at an intermediate spacing, then the system functions as a single camera with a large *synthetic aperture*, which allows it to see through partially occluding environments like foliage or crowds [70].

Above, we classified three camera array system based on the physical distance between the image sensors. However, the term *distance* between image sensors is relative, as it also depends on how far the object plane is from the imaging plane. For example, when two cameras are placed 10cm apart and they both image a mountain 100m away, then the distance between the sensors is negligible and the system is

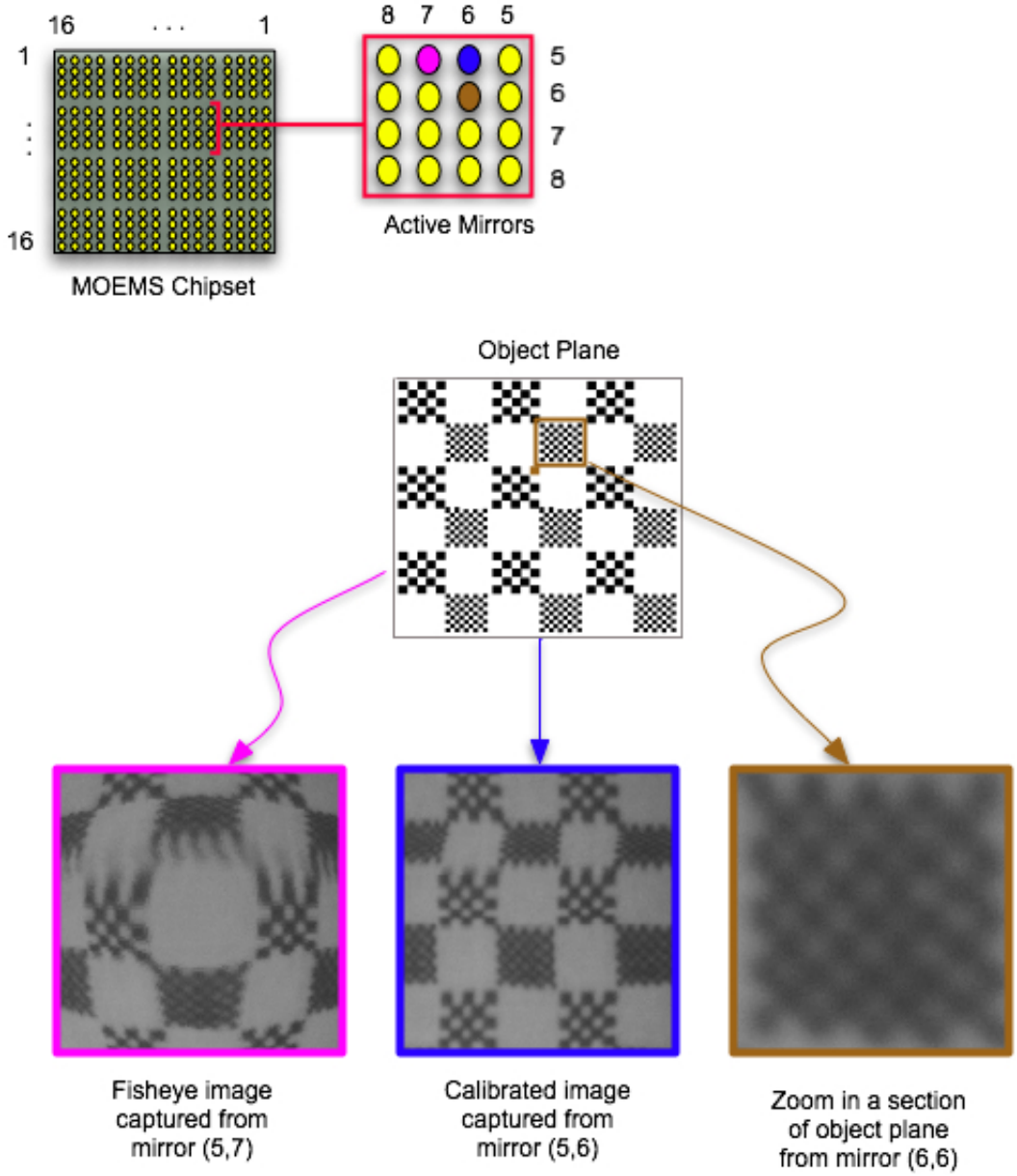

Figure 5.2: An example where multiple mirrors capture the object plane under different settings simultaneously. This demonstrates a unique capacity of our imaging system to do parallel image acquisition.

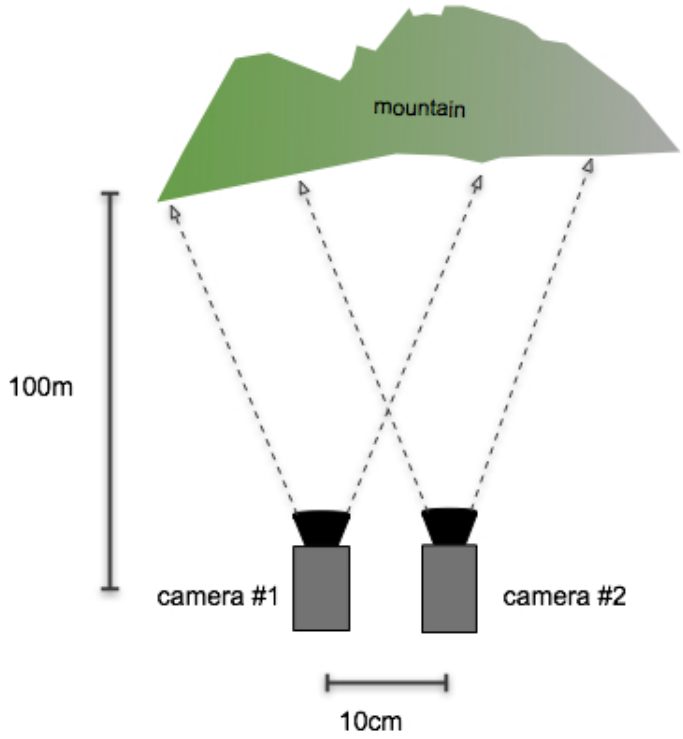

Figure 5.3: The object plane is so large and very far from the two cameras that the system acts like there is not paralax and it is treated as a single projection imaging system.

treated as a single projection system, as seen in Figure 5.3. However, when we image a precious stone 10 cm away from cameras that are space by 10cm apart from each other, then we have a multi-perspective imaging system (Figure 5.4). The difference between this two cases area the fact that in the second case there is a strong parallax presence as oppose to the first case.

With images of an object plane from multiple perspectives (ie, from each of the mirrors in an array), we show virtual environments can be achieved without the need of any post-processing methods, such as morphing. In addition, depth, measured from the image to the object plane, can be calculated from the images with different perspectives (see Figure 5.5). As we will show in the chapter, imaging an object with multiple mirrors opens a huge number of imaging possibilities.

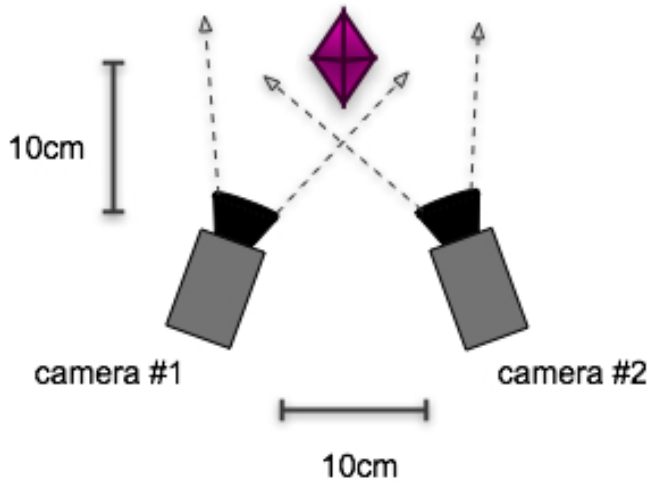

Figure 5.4: The object plane is very small and very close to the sensors. In this case both cameras will act as part of a multi-perspective imaging system since both cameras capture different parts of the object plane.

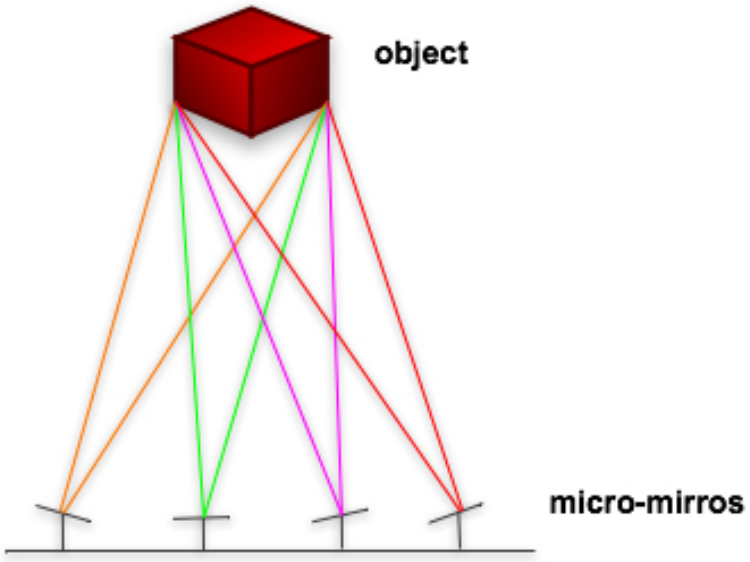

Figure 5.5: MOEMS array have the capacity to view an object from multiple points of view.

5.1 Previous Work on Camera Arrays

In the past decade, digital image sensors have improved in terms of number of pixels and speed, while their physical size and cost have decreased. With these advancements, digital cameras are now everywhere (on cell phones, laptops, etc) and have made photography a part of everyday's life. Yet, even with these achievements, researchers continue to work on new ideas for better imaging. One area is in developing arrays of cameras in order to improve image quality beyond the quality that a single camera can offer. In this technique, more information can be extracted from the object plane than the information captured by an ordinary camera.

The earliest systems for capturing scenes from multiple perspectives used a single translating camera and were limited to static scenes [6]. Dayton Taylor extended this idea to a dynamic scene by using a linear array of still cameras [76]. By triggering the cameras simultaneously and switching from one neighboring camera image to the next, he created the illusion of virtual camera movement through a *frozen* dynamic scene. Taking the work one step further, Manex Entertainment used widely spaced cameras and added an adjustable trigger delay between the cameras to capture images that resulted in the effect of a virtual high-speed camera flying around and through the object plane [77].

For capturing a more general data set, researchers turned to arrays of video cameras [70]. Like the still camera systems, the array of video cameras need to be synchronized and support the enormous amount of data captured. Virtulized Reality™is one of the first multiple video camera array imaging systems. This system uses 49 cameras, which capturing data onto a PC's memory [69]. The cameras used in Virtulized Reality™were relatively high quality, but other researchers have demonstrated the video array system using inexpensive cameras. Yang et al.'s Distributed Light Field Camera renders live dynamic light fields from an 8x8 array of commercial web-

cams [78]. Zhang and Chen's Self-Reconfigurable Camera Array uses 48 commodity cameras with horizontal translation and pan controls to improve interpolation results zhang2004src. More recently, Wilburn et al. presented an array of 100 cameras that perform a number of imaging applications in different array configurations [70].

All of the above examples build camera arrays with the ability to individually control the camera settings of each camera while imaging the object. This leads to the need of sophisticated algorithms to transform all of the captured data into an image that can be used for a specific application. Alternatively, another method of array imaging was presented by Lanman et al. where a system of spherical catadioptric mirror arrays was used in conjunction with a high resolution digital camera in order to produce a wide field of view imaging system [79]. Our system is a combination of these two approaches: on one hand, we use projected images from the micro-mirrors on the image sensor for our imaging needs; and on the other, we can control the way each mirror will sample the object plane, while controlling, FOV, sampling pattern, and imaging qualities of the image sensor for each micro-mirror separately. The uniqueness in our system is that we have a direct relation between each pixel on the image plane with the same on the object plane through a mirror tilt. As a result, we can precisely sample with each mirror independently of the object of interest.

In this chapter, we focus on the use of capturing still objects and only capturing static images from our micro-mirror array while exploring various advantages that our system design offers. We present our method in the next section. Extensions to using video cameras is presented in our Future Work section at the end of the thesis.

5.2 Imaging System Setup and Simulation

In Figure 4.4 from Chapter 4, we showed the experimental setup of our imaging system for capturing images from a single mirror. In this chapter, we are using the

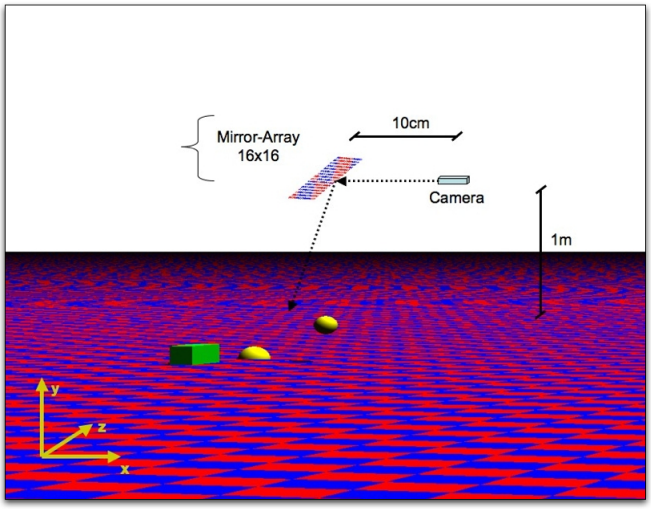

Figure 5.6: POV-ray simulation where a MOEMS array such as Lucents' Lambdarouter is model to be scanning the object plane using 256 micro-mirrors. From each mirror a single pixel gets extracted/tilt, so at each instance we extract 256 pixels from the whole array.

same experimental set up, but more mirrors of the same MOEMS array are engaged so we can achieve higher imaging functionality. In this case, we extract an image from each of the mirrors, as we presented previously in Chapter 4. What is unique about our approach with capturing images from each of the mirrors, is that all of the images are extracted from the same CCD sensor.

In Figure 5.6, we show a diagram from a simulation of our MOEMS array imaging system, using 256 mirrors for imaging. System specifications for the simulation are shown on the diagram. The MOEMS array was modeled based on Lucent's LambdaRouter specifications. The simulation of the system was with homegrown software performed in POVray [80] and MATLAB. POVray is used to image the object plane, and MATLAB is used to calculate which point is sampled off of the object plane due to the mirror position and tilt. In this simulation, we extract a single pixel per mirror tilt for each of the 256 mirror elements. Since only 1 pixel is extracted from each mirror, an image sensor with only 256 photosites (CCD elements) is required.

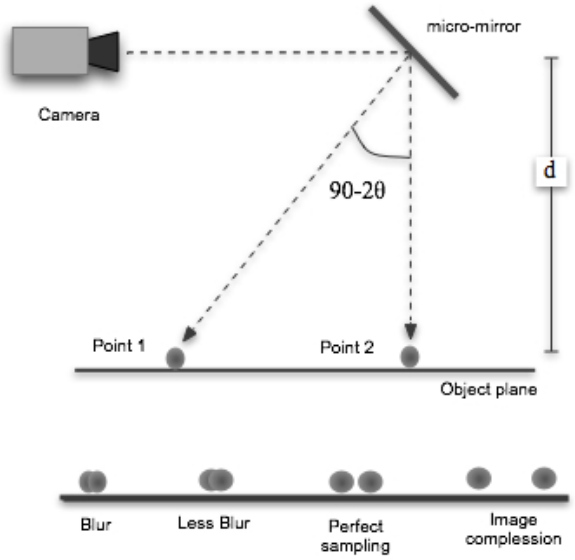

Figure 5.7: We seen the relationship between tilts and captured points. This procedure results anywhere from increasing the blurriness of the image to the other extreme to compress the image.

In Figure 5.9(a), we illustrate an aerial view of the object plane. In Figure 5.9(b), we show the captured image of the object plane. Each mirror samples the image plane with a resolution of 100x100 samples, with the mirror array being sampled a total of 10.000 times. That gives us a total resolution of 2.56 megapixels, an image resolution that was created with only 256 Pixels camera. This shows the magnitude of improvement resolution that can be achieved with MOEMS arrays. We treat this case also also as a Single Center of Projection system. Examining Figure 5.9(b), we can learn about the distribution of our imaging system. As we can see in Figure 5.7 the relationship between each tilt and distribution of captured points is give by the equation:

$$\Delta x = \frac{d}{tan(2\theta)} \tag{5.1}$$

Depending on the consecutive tilts of the mirror, the captured data can have the

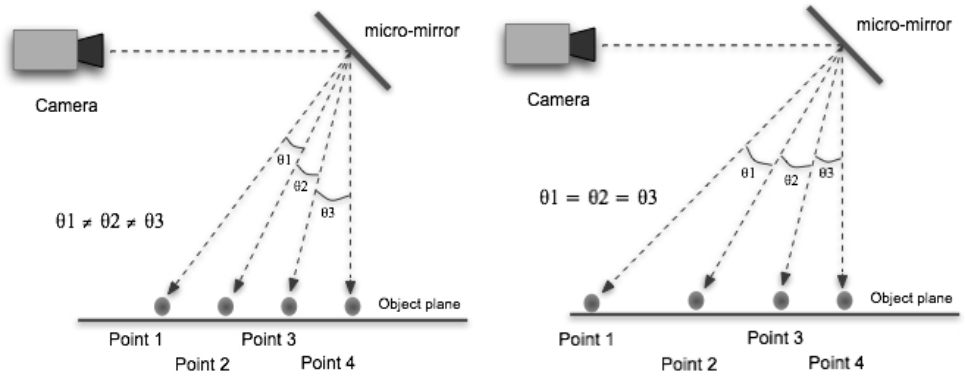

(a) Constant Angle tilting (b) Non-constanct Angle titing

Figure 5.8: Representation of equal angle and non-equal angle tilts versions of our imaging system

characteristics shown in Figure 5.8(b) where we see that depending on the distance between the consecutive points we can have anything from an increase to blurriness up to compression of the captured image.

Therefore, constant angle scanning profiles results in a non-linear captured image whereas non-linear scanning profiles can create images with equally spaced samples. This is summarized in Figure 5.8(a). The advantage in this case is this is that with our programmable system we can interchange between of this sampling procedures without the need to modify any hardware configuration in our system.

When we simulated the above phenomenon in an as close to real situation we collected the following finding. At constant angle angle scans the effects of this non-linearity in sampling can be seen in Figure 5.9(b), as the edges of the image do not have the same resolution as the center of the image.

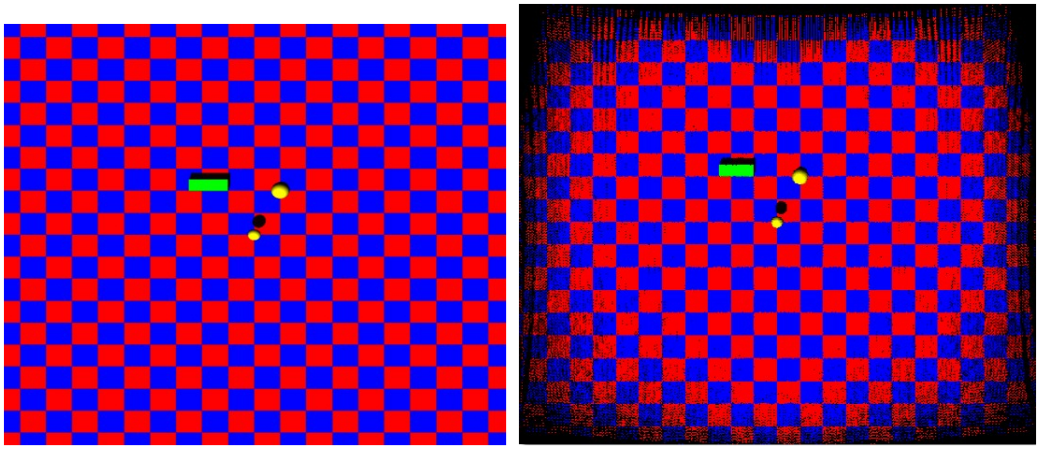

(a) Object plane (b) Reconstructed image

Figure 5.9

5.3 Single-Center-of-Projection system

By combining data from an array of mirrors, we can create an aggregate virtual camera with greatly improved performance. The micro-mirrors are tightly packed together, with every mirror overlapping the field of view of the neighboring mirrors by about 50%. Using this configuration and the existing techniques for the image mosaicing in the literature, we can register and blend the images to create a single image of high resolution. Particularly, if we aim the mirrors inward until their fields of view over lap completely and we use a timing control, then we can create a virtual video camera with a very high frame rate. For the virtual high resolution imager, one can perform exposure metering individually on each camera, which allows us to form a mosaic image with high dynamic range for scenes with spatially varying brightness. This can be explained as each camera can integrate each frame for longer than the frame-rate, thereby capturing more light per unit time. This surpasses the capabilities of a single high speed camera.

We can also do other things that no other single-point-of-projection system can

do. We can do mosaicing with images take from a cluster of mirrors. All this can be performed without any need of mosaicing algorithms and that is due to the precise control that we have over data sampling with the micro-mirrors. This mosaicing has a results to increase the field of view of the camera, when full mirror scans are included, or alternatively allows to focus every mirror in particular section of the object plane for fine scanning and in the end put all the images together like a puzzle.

Furthermore, we can now use a cluster of mirrors where each one of them will be capturing the object space in a different way in order to extract various type of information for the same region of interest on the object plane. So in this case the whole process it is going to be as a collage of images.

As we showed in the earlier on the chapter with MOEMS mirror elements, after careful calibration we have exact control over the position of the mirror. Therefore, we can instruct each mirror to sample distinct, yet neighboring, sections of the object plane. From this selective sampling, a composite image can be formed that is composed from the individual images collected from each mirror. This process can be seen in Figure 5.10. The very interesting thing about it is that the final image is composed with no need of blending and interpolation of its different components. That is due to the precise control of which data point each mirror samples. This procedure is similar to the mosaicing procedure introduced in Chapter 4. The difference is that each image block was captured by the same mirror. In this case, each image block is captured by a different mirror. Therefore, since all the mirrors can be sampled concurrently, the complete image can be created in the same time that it takes to acquire an image from a single mirror.

Since we have precise data sampling control, we can explore unique and exciting features of our system. One such feature is zooming. Zooming is a method that is hardest to achieve without any hardware changes (e.g lens). In most cases it is

achieved by reducing the field of view of the image as data points get interpolated in order to give the impression on the human eye that a more detailed image is produced.

In our case, we can select a region of interest in a captured image and instruct a mirror(s) to scan the area with high resolution. As a result, the magnified image is going to have a smaller field of view and a higher spatial resolution than compared to hardware zooming with a lens. It is important to note that each point in this case, is a real sampled point and not a product of software interpolation.

Experimental results for all of this cases that we dicsussed in this section are shown below. Keep in mind that for all cases there was not done any modfication on the hardware.

5.4 Multi-perspective Imaging system

Multi-perspective imaging has a long and interesting background [6]. Before the Italian Renaissance, virtually all paintings were multi-perspective (see Figure 5.13)[60]. In such painting painters of the Middle Ages paid little attention to making humans and animals look lifelike, creating natural looking landscapes, or creating a sense of depth and space in their paintings. This painting technique transitioned to modern art as well, as can be seen in the works of Picasso and others (see Figure 5.14). Outside of art, multi-perspectives are common in cartography and in aerial and satellite sensing applications. Multi-perspective imaging is also performed in nature, as the most common example in the compound eye of the house-fly.

Human eyes and our brain's interpretation of the images have evolved with perspective optics [5]. Because of this, perspective images seem somewhat natural to our eye. In a perspective image, the objects close to us appear large and in detail, yet we enjoy sweeping wide-range views of distant scenery. Cameras have also evolved with perspective optics. It is natural for camera optics to mimic the human eye-after all,

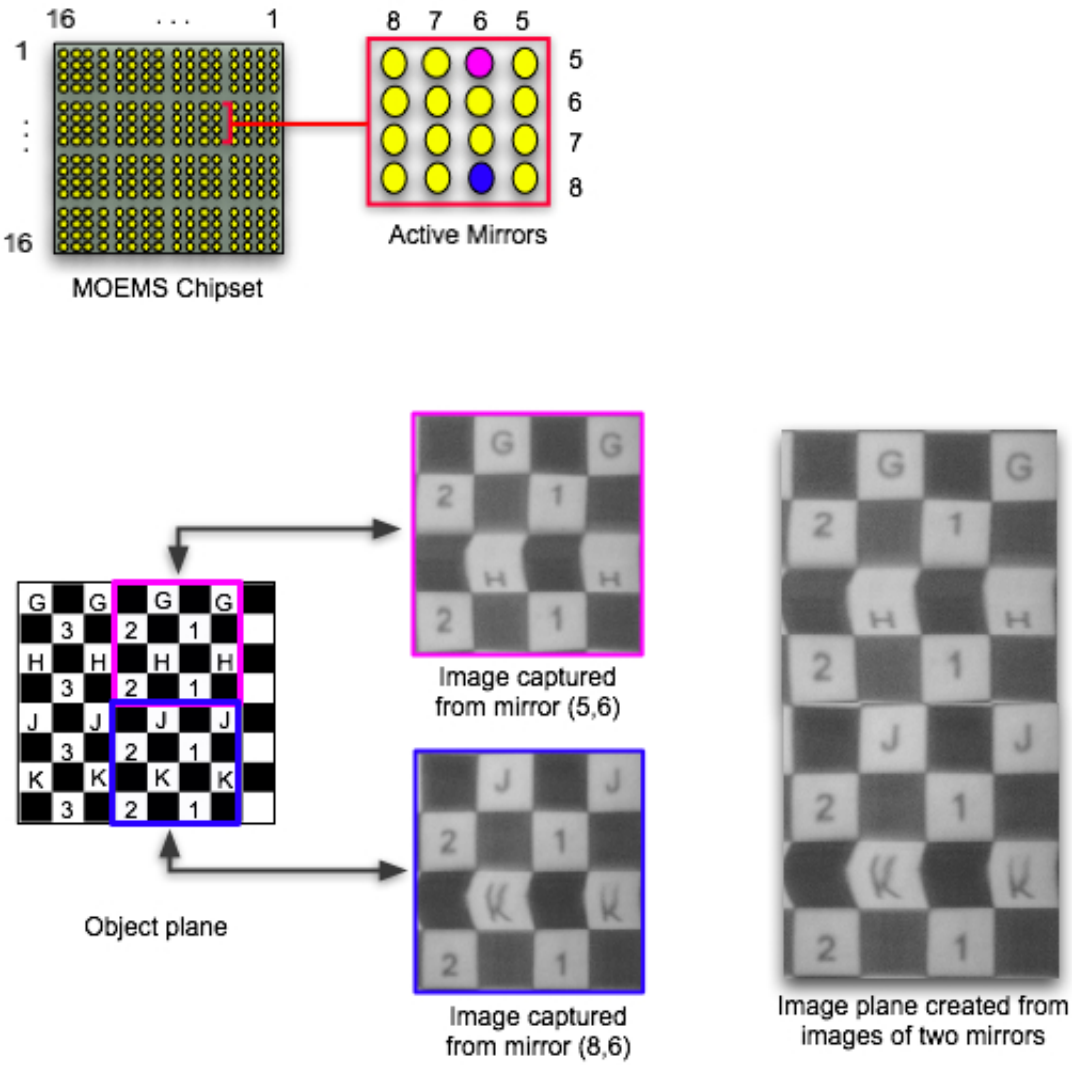

Figure 5.10: Two mirrors scan the object plane in their normal capacity. Knowing the field of view of their scan, we can select mirrors in such a way so when we put the images they capture together we can form a much larger one. In this cases the mirrors used captured image os 130x130 pixels and they were 3mm spaced apart. The resultant image is 130x260 pixels . In this case there is no need for mosaicing algorithnms due to the precise control over the field of view of the scan of each mirror.

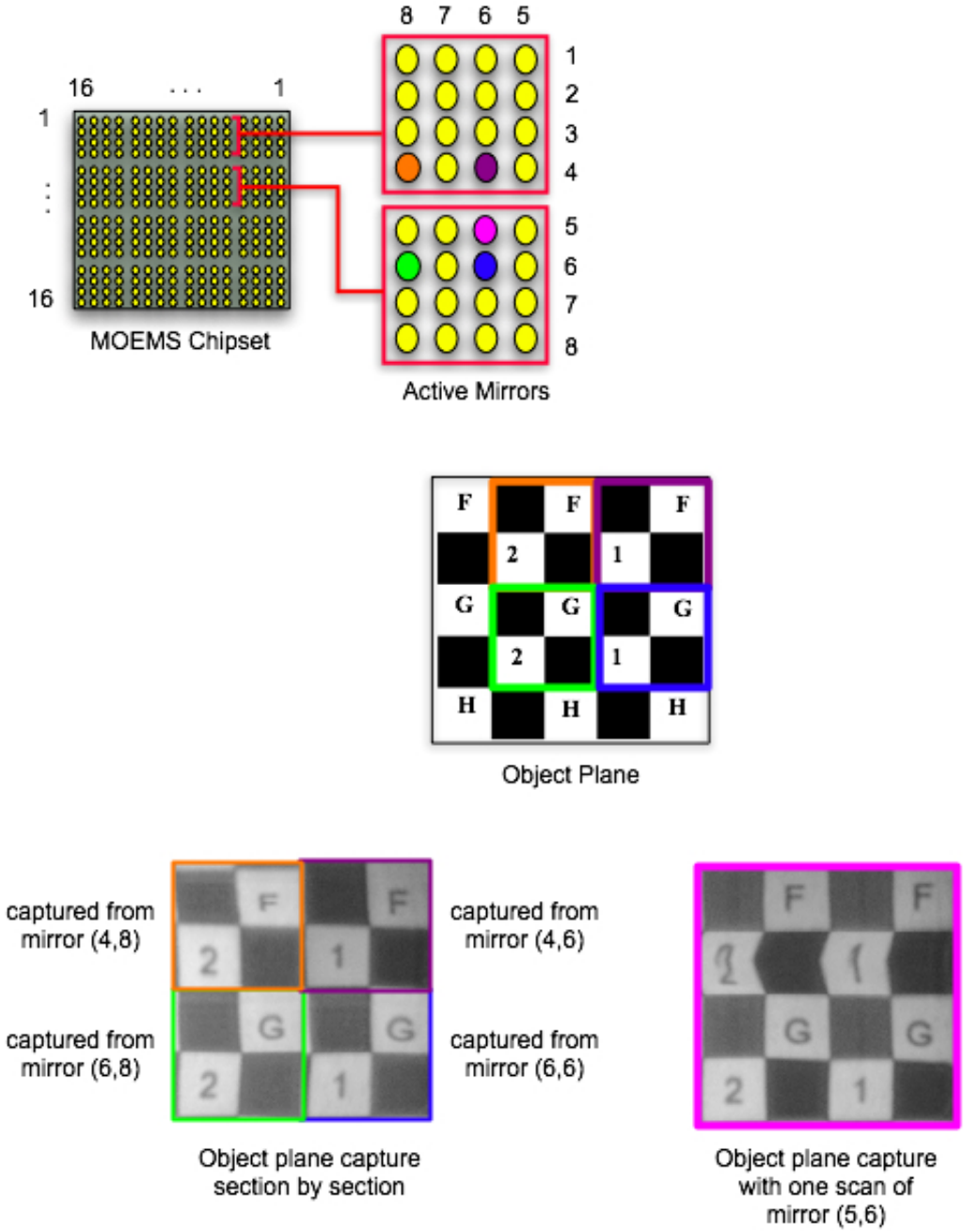

Figure 5.11: In this example we see that mirrors on a small cluster can be used so each one of them is focused on a particular aspect of the object plane. For, instance we see that one mirror captured the whole region of interest of the object plane and then four other mirrors divide that region in four pieces and each one of the focuses on one part of the image.

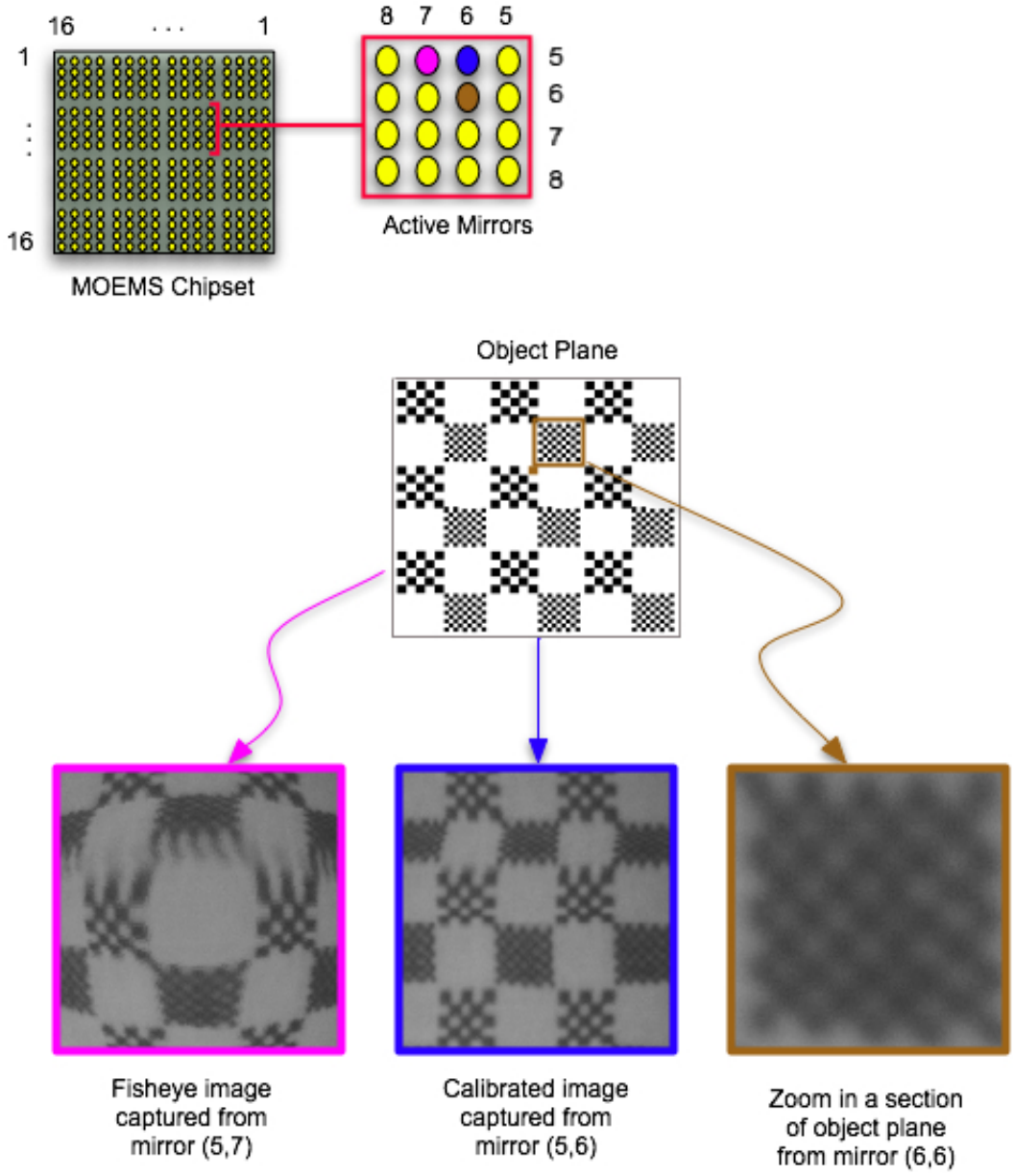

Figure 5.12: In this figure we see a similar example to the one shown in Chapter 4. The difference here is that these images are taken from different mirrors that scan the same region of interest but with different scanning profiles. It is important to notice that since a mirror array is used to perform the imaging task then we more than one images can be captured the same time and as result we can have have "parallel imaging"

Figure 5.13: Even the most talented painters of the Middle Ages paid little attention to making humans and animals look lifelike, creating natural looking landscapes, or creating a sense of depth and space in their paintings (*Giotto, Lamentation Over Christ*)

Figure 5.14: Modern art painting by Pablo Picasso (*Les Demoiselles d'Avignon (1907)*)

as a camera's primary function is to produce images that humans can interpret and enjoy.

However, our eyes perspective has some unfortunate shortcomings. In particular, our eyes have a limited field of view, and we can only see the world in front of us. Ideally, we could see more than one directions at once. Additionally, our eyes are separated by approximately 5 cm, therefore, we can not really get two distinctly separate views of an object. For camera technology, in the last several years, some researchers have investigated techniques that capture multiple perspectives into a single image or an animation - a problem known as *multi-perspective imaging*.

Why is there so much interest in multi-perspective imaging? Multi-perspective images are useful for several reasons. These images have the ability to capture a panoramic field of view of an object, leading to richer and more complete visualizations. Multi-perspective data also opens new opportunities for advanced imaging when applying computer vision techniques such as stereo reconstruction for depth estimation and motion analysis.

Multi-perspective imaging methods many times contribute in increasing the FOV or zooming into an image [5; 70]. In this thesis, we explore multi-perspective imaging through a micro-mirror array. Also we demonstrate how multiple images lead to various applications.

5.4.1 Virtual Environment

A key component in most virtual reality systems is the ability to perform a "walk-through" of a virtual environment from different viewing positions and orientations. The walk-through requires the synthesis of the virtual environment and the simulation of a virtual camera moving in the environment with several degrees of freedom.

Throughout time, there have been many systems developed to accomplish such

tasks. The common denominator between the methods is the trade off between complexity and processing power. One classic example of a virtual walk-through technique is QuickTime-VR [73]. QuickTime-VR is an image-based method for virtual environment navigation that can be used with most personal computers. The processing is relatively quick and the method produces high quality images independent of the scene complexity. In this section, we present our approach towards creations of virtual environments, similar to QuickTime-VR's capabilities, through imaging with MOEMS arrays.

In our approach, each mirror in the array has two degrees of freedom and is separated from neighboring mirrors by a short distance of $1mm$. As a result, each mirror contributes an imaging scene from a different point of view. If you view these captured images in a sequence, each for a quick time duration, a video, of sorts, will be created. Therefore, to render a virtual walk-through, images from neighboring mirrors are placed on top of each other in a time axis. Since the mirrors are physically close to each other, the perspective point changes very little between adjacent mirrors. Therefore, by viewing one image, right after another, a video walk through is created. In this case, we achieve motion through static images. A sample of three different images captured from 3 adjacent mirrors is shown in Figure 5.15. A video walk though of the scene can be seen at **http://sssl3.ece.drexel.edu/moems/publications.php**

5.4.2 Depth Estimation

Image formation takes a 3-D object and transforms its image to a 2-D film or senor plane. The transformation is not one-to-one, therefore the process is not invertible. As a result, the 3D nature of the object cannot be recovered from a single 2-D image, assuming there is no prior information on the object and the system.

Over the years, various methods have been developed for estimating depth through

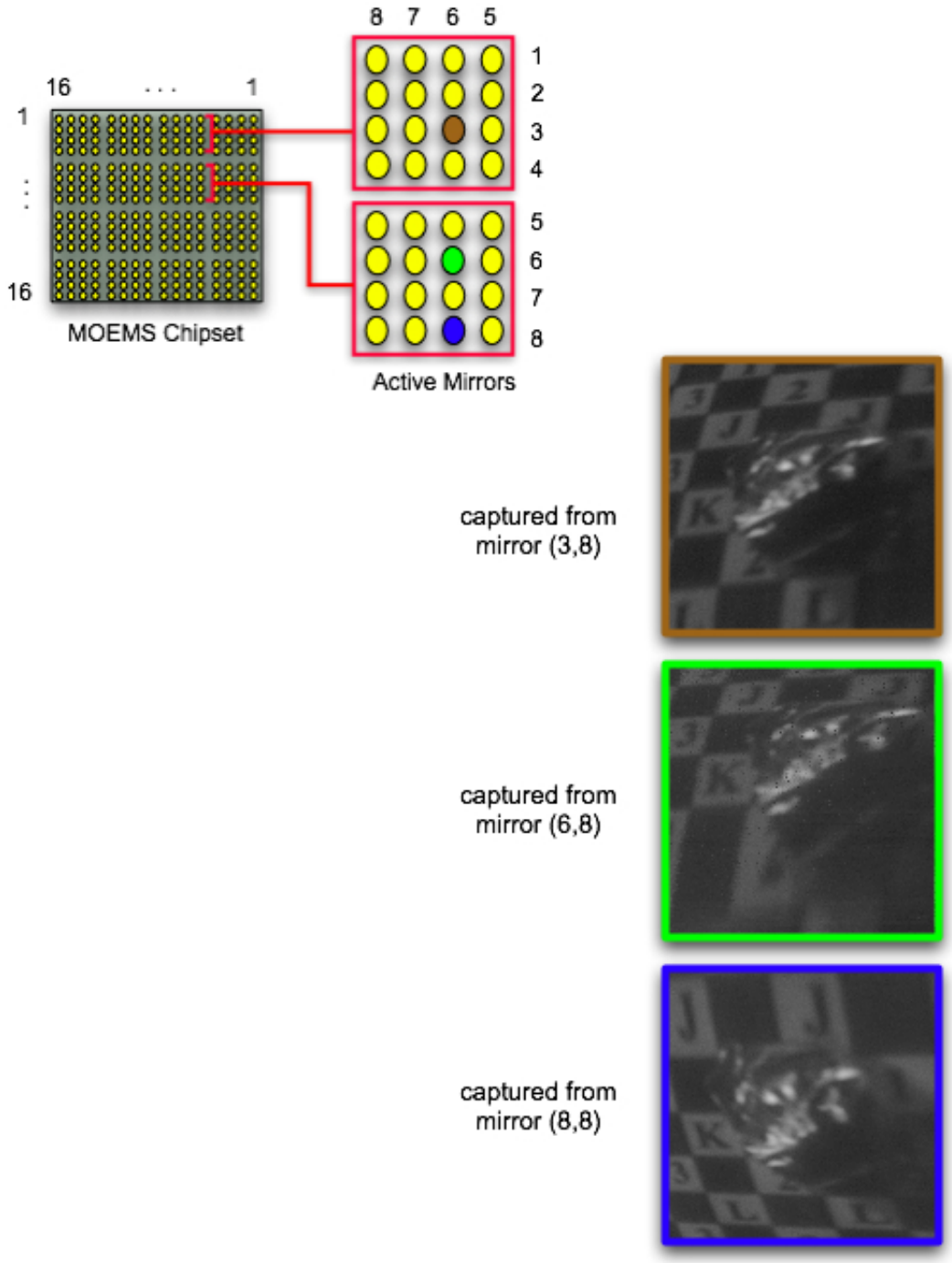

Figure 5.15: We see three images all of the captured from different mirrors. It is obvious that there is significant parallax between the images. That is something that can be used later on for 3-D reconstruction of a scene.

2D images. We showed in Chapter 3 that with perspective projection the projection of a point on an object is inversely proportional to its depth. As such, the range can be estimated by measuring the change in the projection of a point from a different viewing position. That led us to common methods for depth estimation using two images, called stereo depth estimation [9].

The model of a thin lens model suggests a alternative method for recovering range. It is known that with a thin-lens model, an out-of-focus point on an object is imaged as a blurred circle where the radius of the blur is a function of its depth from the image plane. Therefore, range can be estimated by measuring the change of blur as a function of different optical settings. That has results to the development of methods for measuring depth from focus or image defocus [81; 82; 83].

In this section, we show that by using MOEMS arrays for perspective imaging of an object, the depth between the object and image plane can be estimated. We will use classical stereo depth estimation to estimate depth. Details of the stereo method and our experimental results from the micro-mirror array are provided in the next section.

5.4.3 Stereo Depth Estimation

When a point $\vec{P}$ on a 3-D object is projected onto a pair of spatially offset imaging sensors, its image will fall on different relative locations on the two sensors [9]. This can be seen in Figure 5.16. The difference is a function of depth. Points closer to the sensor will be separated more on the image sensor, than points that are further away from the sensor. By measuring the difference or disparity between the projection of the same point onto a pair of imaging sensors, range can be estimated through a process called binocular stereo.

Consider the binocular stereo configuration in Figure 5.17. In this figure, the

sensor nodal points are separated by a distance b, the baseline, and are a distance d_s from the sensor plane. The object point, $\vec{P} = (XYZ)^t$, is a distance Z from the sensor plane, and the disparity between the image $\vec{P}$ in both sensors, $\vec{p_1} = (x_1 y_1)^t$ and $\vec{p_2} = (x_2 y_2)^t$, is denoted by Δ. Similar triangles yields the relationship $\frac{Z}{b} = \frac{d_s}{\Delta}$. Combined with the perspective projection, the equation for determining the position of the point in the 3-D object is [9]:

$$X = \frac{d_s x_1}{Z}, Y = \frac{d_s y_1}{Z}, X = \frac{d_s b}{\Delta} \tag{5.2}$$

Assuming a known baseline and a sensor to sensor point distance, range, can be estimated if the correspondence between the projection of the point in both images is known. Given the projection of the point in one image $I_1(.)$, (centered at (x_1, y_1)), the corresponding projection in the other image $I_2(.)$, can be determined by finding the point (x_2, y_2) that minimizes the following sum of squared differences.

$$c(x_2, y_2) = \frac{\sum_{x=-n/2}^{n/2} \sum_{y=-n/2}^{n/2} (I_1(x_1 + x, y_1 + y) - I_2(x_2 + x, y_2 + y))^2}{n^2} \tag{5.3}$$

where, the summation is performed over a small nxn, image patch centered at (x_1, y_1).

By limiting the geometry of the sensors so that their nodal points are only translated in the horizontal direction (i.e. a parallel optical axis configuration) (see Figure 5.16), the correspondence search can be simplified. Stereo images are frequently displaced horizontally or vertically in order to simplify the correspondence search. In particular, with such configuration, searching is performed along a single horizontal or vertical scan line (i.e. the epi-polar line). In particular, the corresponding match for a point (x_1, y_1) is of the form $(x_2, y1)$, that is, the matching point lies along the

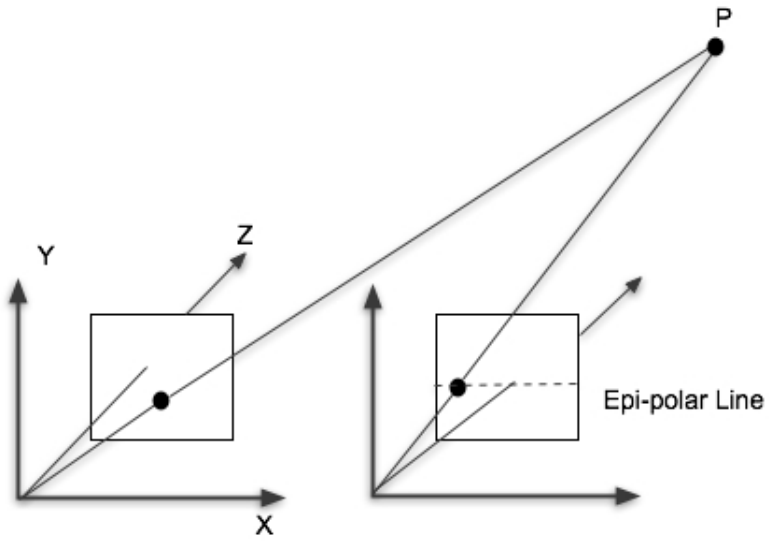

Figure 5.16: Stereo images are frequently displaced horizontally or vertically in order to simplify the correspondence search

same horizontal scan line in the digital image (see Figure 5.17). With such a configuration, the correspondence search will yield a horizontal disparity. By computing the horizontal or vertical disparity at each small image patch in an image, the complete structure of the imaged 3-D world can be determined [9].

After this introduction and theory, we are now ready to proceed to depth estimation with experimental data captured from our MOEMS array.

5.4.4 Experimental Depth Estimation

We have found experimentally with the same setup that we have used throughout this thesis that with at least two images captured from two different mirrors we can estimate depth, as shown on Figure 5.18. It is necessary that there is enough parallax between the two images in order to estimate depth as it was explained in the previous section. To ensure that this necessity is fulfilled we choose for this task mirrors that are further apart

Using one mirror we first capture an image and establish the point to which we

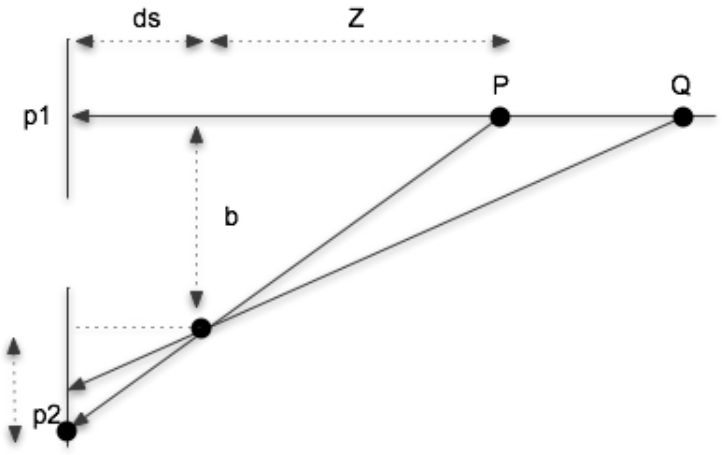

Figure 5.17: With such a configuration, the correspondence search will yield a horizontal disparity. By computing the horizontal or vertical disparity at each small image patch in an image, the complete structure of the imaged 3-D world can be determined

are going to estimate the depth. We then capture another the image, but now from a different mirror. As we see on the second image the point of interest that was identified on first image, it appears shifted. By comparing these two images we identified that shift was approximately 89 pixels or 667.5μm. For this case we also know the physical distance between the two mirrors (3mm)and also the focal length of the camera lens 75mm

Using the above equations, and particularly the method of similar triangles we can now come to the following conclusion about the distance of the image plane from the object plane. From the above it was estimated that the estimated distance between the object and the image plane was 33.7cm. However, when we actually measured that distance with measuring tape we found that the actual distance between the object and the image planes was 36cm. We see that the difference between the two results is less than 3%

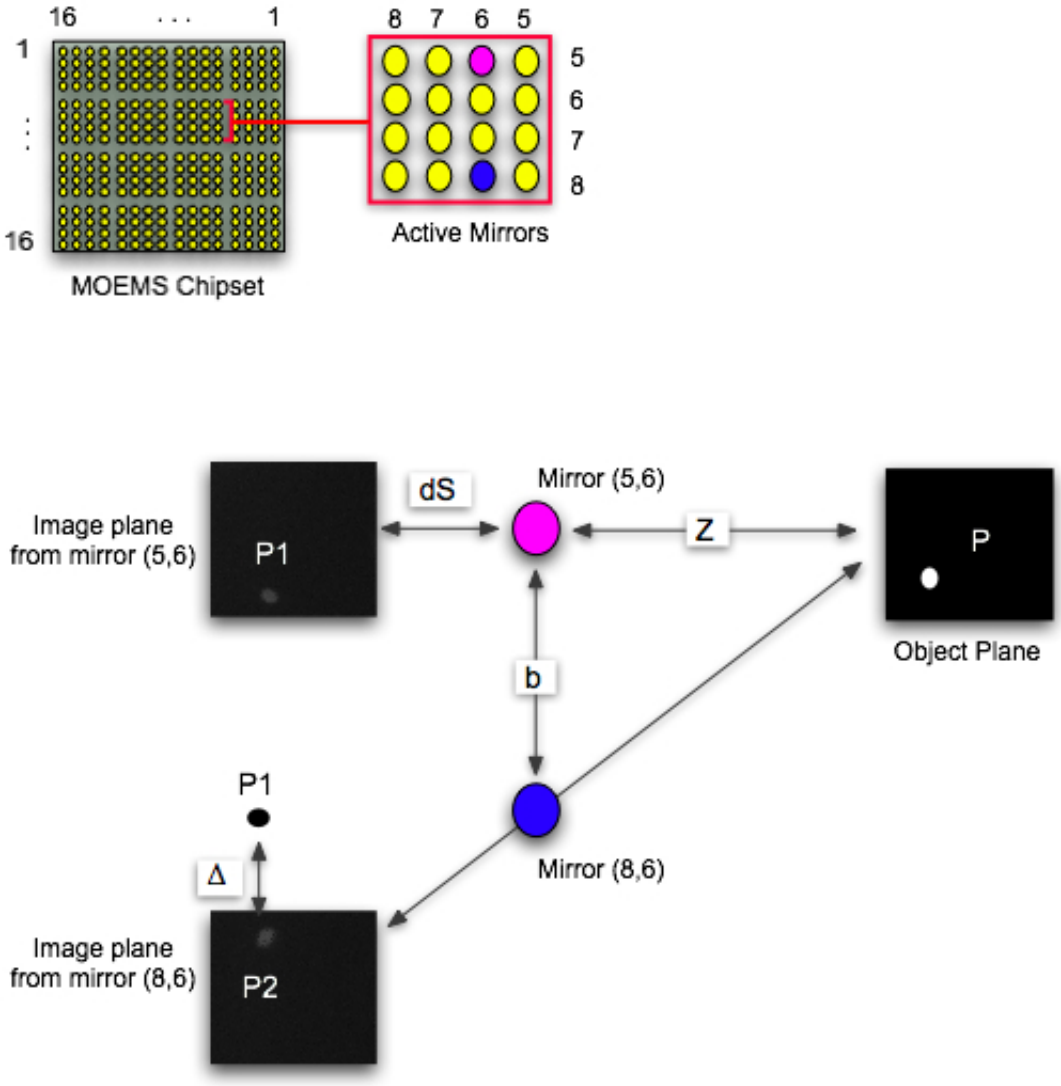

Figure 5.18: Stereo depth estimation. The mirrors that were used were 3mm apart. By looking the images that were captured we can easily notice the shift(disparity) on the point of interest. The parallax in this case is significant to allow depth estimation

5.4.5 Conclusions and Contributions

In this chapter, we have built on the single mirror imaging methods that we discussed in Chapter 4 by the imaging off of mirror arrays. We saw that since micro-mirrors are spaced close together in a small real-estate, the images taken from each one of them can be assumed to be coming from a system of a single-point-of- projection. As a result, we presented that this feature can be used in order to capture simultaneously the same image from different mirrors. In this case, each of the mirrors can image in its own unique fashion. For example, as one mirror provides an image of the complete object plane, another mirror can zoom-in on a particular aspect of the object plane. All this can result, in increasing field of view, dynamic range, mosaicing, fast frame rate but also introduces functionality that cannot be achieved from other camera arrays systems.

We also presented how the mirror arrays can capture multiple perspective images. We demonstrated with experimental results that we can achieve virtual environment effects by capturing the same object from many different point of view. Also we showed some features and applications of multiple perspective imaging, which included depth estimation between the object plane and the image plane. The estimation error in depth was found to be less than 3%.

6. Future Work and Conclusions

6.1 Summary

In the past few decades, a wide variety of novel imaging systems have been developed that have altered the context of imaging. These systems, have shown the ability to enable a high dynamic range and multi-spectral images, as well as omnidirectional and multi-perspective imaging.

In this thesis, we have developed a new paradigm in digital imaging using micro-optical-electro-mechanical system (MOEMS) mirrors. We introduced our method of reconfigurable and programmable imaging by making correspondences between points on the object plane to the image plane. A micro-mirror array is inserted into the optical path between the two planes and tilted to achieve the desired correspondences. Based on this idea, we have developed a programmable imaging prototype using Lucent's LambdaRouter 16x16 mirror array, a quasi-static MOEMS micro-mirror device that can tilt on two axis. In Chapters 3, we theoretically explain the system and discuss its imaging capabilities and performance. In Chapter 4, we showed programmable imaging with the use of a single micro-mirror. In Chapter 5, we take advantage of MOEMS arrays and show images from multiple mirrors, as well as, new imaging capabilities due to the innovation and uniqueness of our system. Next, we briefly summarize the highlights from Chapters 4 and 5.

We showed in Chapter 4 that even a single pixel sensor is capable of producing high quality images. This study, can be significant for the future development of imaging systems. For instance, CCD and CMOS image sensors are close to reaching their limits by trying to squeeze more photosites into small real estate. Our approach, could be used in order to gather multiple data points from each sensor/photosite.

By taking advantage of the MOEMS reliability and controllability, we have shown that we can uniquely manage the way we sample the object plane. We can control the field of view and the resolution. But more importantly, we can compensate for any distortions caused by different components of the imaging system in real time without having any a prior knowledge of the nature and cause of these distortions. In other words, tasks that could previously only be performed using post image processing methods in software, can now be done in real time while the images are captured in hardware.

In Chapter 5, we took our research a step further by exploring imaging capacities with MOEMS mirror arrays. MOEMS technology allows the development of many independent systems on the same substrate. As a result, we studied and developed methods for imaging with more than one micro-mirror at the time. This gave us the opportunity to explore capacities that are not available today by any known imaging system.

In our mirror array work, we first examined the case of a single projection system. Imaging with mirrors that are located close to each other allows us to treat the images as if they were captured by the same mirror because the parallax is negligible. We have showed that this capability allow us to use many mirrors simultaneously to capture different parts of the object plane in a programmable fashion, without the need to change any of the hardware components or settings. This programmable imaging ability, provides many advantages in our imaging system, by increasing the frame rate, the dynamic range, and the resolution, while controlling the field of view, the sampling pattern, and the region of interest in the object plane.

Another use of MOEMS arrays in our imaging system is to enable multi-perspective imaging. In this case, we introduce parallax among the captured images by imaging with the mirrors on the array that are further apart. With this technique, we are

able to explore multi-perspective imaging capacities with our system. We showed that we can create a virtual environment by capturing an object with many mirrors from different perspectives and then having the capability to walk-though, fly around, and zoom-in. In addition, we demonstrated another advantage of multi-perspective imaging, which is depth estimation. Here we use stereo depth estimation to calculate the distance between the object and the image plane. This work is significant, as the depth information was take with *one* image from *one* camera.

6.2 Current Limitations and Applications

One of the drawbacks of our current prototype is the MOEMS device used. The MOEMS array chip that we use was the heart of Lucent's Lambdarouter all-optical switching. It was designed and packaged for telecom applications at a wavelength of 1550nm. The way the chip is packaged makes it almost useless for imaging application. The problem is not only with this particular chip, but is more extensive because we are attempting imaging with analog MOEMS arrays. As a result, there are not optimized analog MOEMS for imaging purposes.

Packaging is not the only problem that we hare facing with our device. These micro- mirrors were designed to tilt in any direction needed, as a light beam bounces off its surface and holds that tilt for as long as needed.

To perform the tilting, the particular device uses capacitive, electro-static actuators. These actuators have a maximum settling time of 5 msec for every tilt they perform. For imaging applications, this time can be a disadvantage for our imaging system, considering the thousand or million mirror states that are required to image an object plane. Another problem with these quasi-static actuators, is the fact that they require high power in order to operate. This makes them very unattractive, especially in the imaging industry.

All of the above contribute in affecting the quality of the image captured and possibly the resolution of our system. At this point, our imaging system has been observed experimentally to reach resolutions of 0.25mm, which is much lower than the theoretical limit that was 0.03mm.

With some optimization, our proposed imaging system can be an excellent candidate for most of the imaging applications that exist in the market. Particularly, it could increase and enhance the photography industry. But, this imaging method can move beyond the everyday common imaging tasks. There is a huge potential in the Biomedical industry. Since our system has the capacity to sample the object plane in a programmable way, it could be used in conjunction with parabolic mirrors in order to increase the field of view of an optical system. In such a case, our technology could be incorporated into endoscopy systems in order to increase their field of view and functionality.

The applications limitations with our proposed imaging system are endless, but bounded within the creativity of the designer or technologist.

6.3 Future Work

Our revolutionized method of programmable imaging with MOEMS has shown great promise in the field of computational imaging. Our initial work in performing software post-processing tasks in real-time hardware can be expanded in many ways. Below, we identify some of the next steps in continuing this research for improving our programmable imaging system.

6.3.1 Imaging with Scanner MOEMS

Alternatively, we could replace the quasi-static mirrors with resonant mirrors, commonly known as scanning mirrors. These types of mirrors, shown in Figure 6.1,

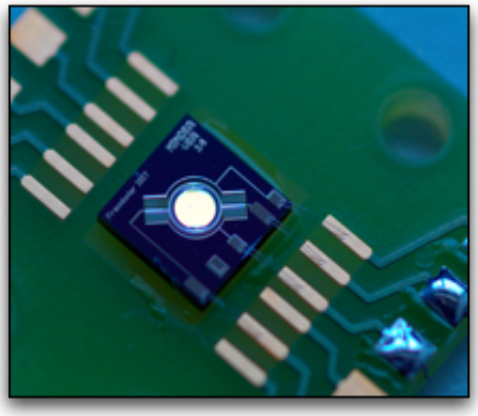

Figure 6.1: Scanning Mirror developed by Fraunhofer ISIT.

operate with low voltage, achieve very high degrees of tilts, and can theoretically have an infinite number of states. Their scanning speed can be controlled from Hz-kHz range.

The challenge with incorporating these devices into our system is to know where the mirror is pointing on any given instant. In this case, our system will work differently than the way we have described throughout this thesis. So far, we were first tilting the mirror towards the particular part of the object plane and then were capturing the piece of data that we needed. However, in the case of the resonant mirror, the mirror is always in motion, and a specific mirror position is not controllable. Since the mirror does scan all states, the imaging device will have to know when to sample, and how this pixel will fit into the rendered image. Therefore, algorithms and hardware will have to be created to know where the mirror is pointing at each instant and capture the data accordingly.

6.3.2 Single Pixel Camera

Another topic of future research is in developing an actual single pixel camera. In Chapter 4, we described the method of a single pixel image formation and introduced the idea that only a single pixel sensor is required to make a complete image. Initial research will be to incorporate a single photo-detector into the system, instead of the CCD sensor. The mirror reflection could be brought to the photo-detector via an optical lensing system, as is currently implemented. However, a single optical fiber could be used, where one end is coupled to the mirror and the other is coupled to the detector.

Image sensor pixel size is another issue that will need to be determined in a single pixel camera. Larger pixels will allow more information to be registered, but will take longer to capture all the data due to the capacitance of the larger photo-detector. However, the smaller detectors might not detect enough light, leaving the images dark.

A single pixel camera could find many applications in different industries such as, in medicine. A single pixel camera could replace conventional cameras that are used today for endoscopy. Such technology will allow the physicians to get a better idea of what they see during an examination.

6.3.3 Light Field Imaging

Light field plenoptic camera, developed at Stanford, is a camera that uses a microlens array (also known as a lenticular lens array) to capture 4D light field information about a scene [84]. This is achieved by inserting a microlens array between the sensor and main lens, creating a plenoptic camera. Each microlens measures not just the total amount of light deposited at that location, but how much light arrives along each ray. By re-sorting the measured rays of light to where they would have ter-

minated, in slightly different, synthetic cameras, we can compute sharp photographs focused at different depths. The problem with this design is that many CCD pixels are sacrificed to capture the image of a lenslet. For example, a team at Stanford University used a 16 megapixel camera with a 90,000-microlens array (meaning that each microlens covers about 175 pixels, and the final resolution is 90 kilopixels.) As a result of this method, even though we end up having a photograph that has all the information for different depths, we sacrifice image resolution.

We proposed a new approach to this design. Instead of using many lenslets, we could use one and through a micro-mirrror we could direct a portion of the object plane so they can get captured by the CCD. Our design could give us the same results in the previous case, but now we don't sacrifice resolution since each portion of the image will be captured using the maximum resolution of the CCD.

6.4 Conclusions and Contributions

New advancements in science are frequently sparked by the invention of new instruments that open opportunities to see the world differently. In this thesis, we have presented a novel method that opens up opportunities to explore unknown aspects of imaging. With our technique, our system can perform in hardware tasks that were previously only available by post-processing in software. Our method is called programmable imaging with MOEMS.

In this thesis, we have presented the idea, the prototype system, and results that support all of our claims. Below are listed some of our contributions in the project:

- Developed theory for our *programmable imaging technique*, which enables dynamic and reconfigurable sampling of the object plane without changing any hardware components or settings of the imaging system.

- *First* and *only* research team to image through MOEMS micro-mirror device

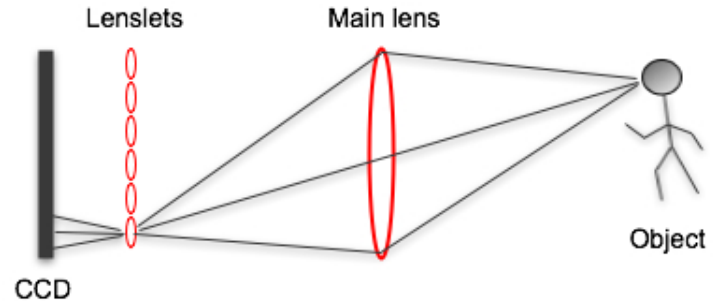

(a) Original Plenoptic Camera Design

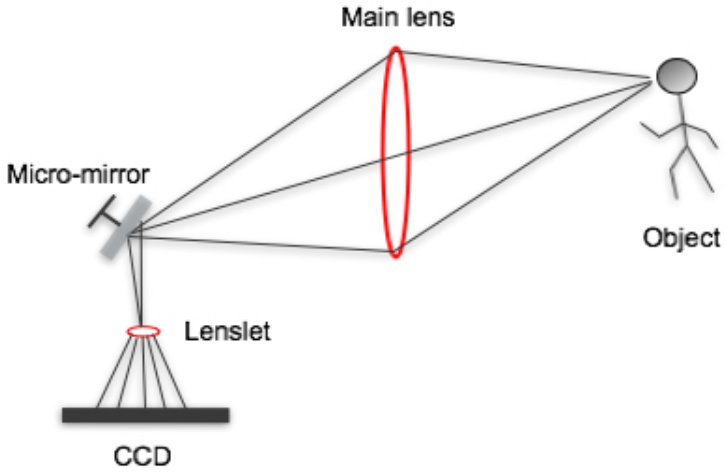

(b) Proposed Plenoptic Camera Design using MOEMS

Figure 6.2: Light field plenoptic camera

and MOEMS array of micro-mirrors, without the need of any special signal processing methods.

- Developed methods for sampling the object plane using both a single and a multiple pixel extraction techniques. *(Chapter 3)*
- Created first ever programmable imaging camera using MOEMS. *(Chapters 4-5)*
- Performed calibration of the imaging system enabling exact pixel sampling. *(Chapter 4)*
- With the use of a MOEMS mirror array, developed a technique to capture multi-perspective images, providing virtual reality 3D images and depth estimation, through the use of a single camera. *(Chapters 5-6)*
- Identified potential limits and use of the technology. *(Chapter 6)*

Bibliography

[1] HC Nathanson, WE Newell, RA Wickstrom, and JR Davis Jr, "The resonant gate transistor," *Electron Devices, IEEE Transactions on*, vol. 14, no. 3, pp. 117–133, 1967.

[2] R.E. Fischer and B. Tadic-Galeb, *Optical System Design*, McGraw-Hill Professional, 2000.

[3] L. Mertz and NO Young, "Fresnel transformation of images (Fresnel coding and decoding of images)," *Optical Instruments and Techinques*, 1962.

[4] S.R. Gottesman and EE Fenimore, "New family of binary arrays for coded aperture imaging," *Applied Optics*, vol. 28, no. 20, pp. 4344–4352, 1989.

[5] S.K. Nayar, "Computational Cameras: Redefining the Image," *Computer*, vol. 39, no. 8, pp. 30–38, 2006.

[6] M. Levoy and P. Hanrahan, "Light field rendering," *Proceedings of the 23rd annual conference on Computer graphics and interactive techniques*, pp. 31–42, 1996.

[7] B. Jähne, *Digital image processing: concepts, algorithms, and scientific applications*, Springer-Verlag London, UK, 1995.

[8] R.A. Hicks and R.K. Perline, "Equiresolution catadioptric sensors," *Applied Optics*, vol. 44, no. 29, pp. 6108–6114, 2005.

[9] H. Farid, *Range Estimation by Optical Differentiation*, Ph.D. thesis, Department of Computer and Information Science, University of Pennsylvania, Philadelphia, PA, 1997.

[10] T. Satoh, N. Mutoh, M. Furumiya, I. Murakami, S. Suwazono, C. Ogawa, K. Hatano, H. Utsumi, S. Kawai, K. Arai, et al., "Optical limitations to cell size reduction in IT-CCD image sensors," *Electron Devices, IEEE Transactions on*, vol. 44, no. 10, pp. 1599–1603, 1997.

[11] J. Bryzek, "Impact of MEMS technology on society," *Sensors and Actuators A: Physical*, vol. 56, no. 1, pp. 1–9, 1996.

[12] M Gad el Hak, *MEMS Handbook*, CRC Press LLC, Boca Raton FL., 2002.

[13] P. Rai-Choudhury, *MEMS and MOEMS Technology and Applications*, SPIE Optical Engineering Press Bellingham, Wash, 2000.

[14] T.R. Hsu, *MEMS & microsystems: design and manufacture*, McGraw-Hill, 2002.

[15] H. Wicht and J. Bouchaud, "NEXUS Market Analysis for MEMS and Microsystems III 2005-2009," .

[16] M.E. Motamedi, *MOEMS*, SPIE Press, Bellingham, WA, 2005.

[17] E. Mounier, Y. de Charentenay, and J.C. Eloy, "New applications for MOEMS," *Proceedings of SPIE*, vol. 6114, pp. 611405, 2006.

[18] D.J. Elliott, *Integrated circuit fabrication technology*, McGraw-Hill New York, 1982.

[19] J. Bouchaud and O. Nowak, "MEMS microdisplays: overview and markets," *Proceedings of SPIE*, vol. 6186, pp. 618605, 2006.

[20] W.C. Tang, TCH Nguyen, and R.T. Howe, "Laterally driven polysilicon resonant microstructures," *Sensors and Actuators*, vol. 20, pp. 25–32, 1989.

[21] W.C. Tang, T.C.H. Nguyen, M.W. Judy, and R.T. Howe, "Electrostatic-comb drive of lateral polysilicon resonators.," *SENSORS ACTUATORS.*, vol. 21, no. 1, pp. 328–331, 1990.

[22] JH Comtois, MA Michalicek, and CC Barron, "Characterization of electrothermal actuators and arrays fabricatedin a four-level, planarized surface-micromachined polycrystallinesilicon process," *Solid State Sensors and Actuators, 1997. TRANSDUCERS'97 Chicago., 1997 International Conference on*, vol. 2, 1997.

[23] L.Q.J.S.P. Gianchandani, Y.B.O. Inc, and CA Campbell, "Bent-beam electrothermal actuators-Part I: Single beam and cascadeddevices," *Microelectromechanical Systems, Journal of*, vol. 10, no. 2, pp. 247–254, 2001.

[24] TY Jiang, TY Ng, and KY Lam, "Optimization of a piezoelectric ceramic actuator," *Sensors and Actuators A: Physical*, vol. 84, no. 1, pp. 81–94, 2000.

[25] P. Schiller and DL Polla, "Integrated Piezoelectric Microactuators Based on PZT Thin Films," *7th International Conference on Solid State Sensors And Actuators*, p. 154, 1993.

[26] H. Toshiyoshi, H. Fujita, and T. Ueda, "A piezoelectrically operated optical chopper by quartzmicromachining," *Microelectromechanical Systems, Journal of*, vol. 4, no. 1, pp. 3–9, 1995.

[27] C.L. Shih, B.K. Lai, H. Kahn, SM Phillips, and AH Heuer, "A robust co-sputtering fabrication procedure for TiNi shape memoryalloys for MEMS," *Microelectromechanical Systems, Journal of*, vol. 10, no. 1, pp. 69–79, 2001.

[28] CC Ma, R. Wang, QP Sun, Y. Zohar, and M. Wong, "Frequency response of TiNi shape memory alloy thin filmmicro-actuators," *Micro Electro Mechanical Systems, 2000. MEMS 2000. The Thirteenth Annual International Conference on*, pp. 370–374, 2000.

[29] H. Guckel, K. Fischer, and E. Stiers, "Closed-loop controlled, large throw, magnetic linear microactuator with 1000 m structural height," *Proc. MEMS98*, pp. 414–418.

[30] A. Garnier, T. Bourouina, H. Fujita, E. Orsier, T. Masuzawa, T. Hiramoto, and J.C. Peuzin, "A fast, robust and simple 2-D micro-optical scanner based oncontactless magnetostrictive actuation," *Micro Electro Mechanical Systems, 2000. MEMS 2000. The Thirteenth Annual International Conference on*, pp. 715–720, 2000.

[31] DV Hale, MJ Hoover, and MJ O'Neill, "Phase Change Handbook," *NASA Contractor Report, NASA-CR-61363, September*, 1971.

[32] et al M.J. Zdeblick, "Thermopneumatically activated microvalves and integrated electrofluidic circuits," *Solid-State Sensor and Actuator Workshop*, pp. 251–255, 1994.

[33] L. Lin, AP Pisano, and AP Lee, "Microbubble powered actuator," *Solid-State Sensors and Actuators, 1991. Digest of Technical Papers, TRANSDUCERS'91., 1991 International Conference on*, pp. 1041–1044, 1991.

[34] KE Petersen, "Silicon as a mechanical material," *Proceedings of the IEEE*, vol. 70, no. 5, pp. 420–457, 1982.

[35] C. Strandman and Y. Bäcklund, "Passive and fixed alignment of devices using flexible silicon elements formed by selective etching," *J. Micromech. Microeng*, vol. 8, pp. 39–44, 1998.

[36] A.R. Mickelson, N.R. Basavanhally, and Y.C. Lee, *Optoelectronic packaging*, Wiley, 1997.

[37] RB APTE, FSA SANDEJAS, WC BANYAI, and DM BLOOM, "DEFORMABLE GRATING LIGHT VALVES FOR HIGH RESOLUTION DISPLAY," *SPIE milestone series*, vol. 153, pp. 171–176, 1999.

[38] RL Clark, JR Karpinsky, JA Hammer, RB Anderson, RL Lindsey, DM Brown, and PH Merritt, "Micro-opto-electro-mechanical (MOEM) adaptive optic system [3008-02]," *PROCEEDINGS-SPIE THE INTERNATIONAL SOCIETY FOR OPTICAL ENGINEERING*, pp. 12–24, 1997.

[39] A. Tran, YH Lo, ZH Zhu, D. Haronian, and E. Mozdy, "Surface micromachined Fabry-Perot tunable filter," *Photonics Technology Letters, IEEE*, vol. 8, no. 3, pp. 393–395, 1996.

[40] MC Larson and JS Harris Jr, "Wide and continuous wavelength tuning in a vertical-cavity surface-emitting laser using a micromachined deformable-membrane mirror," *Applied Physics Letters*, vol. 68, pp. 891, 1996.

[41] H. Goto, "Si micromachined 2D optical scanning mirror and its application toscanning sensors," *Advanced Applications of Lasers in Materials Processing, 1996/Broadband Optical Networks/Smart Pixels/Optical MEMs and Their Applications, 1996. IEEE/LEOS 1996 Summer Topical Meetings:*, pp. 17–18, 1996.

[42] L. Fan, M.C. Wu, K. Choquette, and M.H. Crawford, "Self-assembled microactuated XYZ stages for optical scanning and alignment," *Proc. Int. Conf. Solid-State Sensors and Actuators*, pp. 319–22, 1997.

[43] UD Larsen, O. Signund, and S. Bouwsta, "Design and fabrication of compliant micromechanisms and structureswith negative Poisson's ratio," *Microelectromechanical Systems, Journal of*, vol. 6, no. 2, pp. 99–106, 1997.

[44] D. Ruffieux, MA Dubois, and NF de Rooij, "An AlN piezoelectric microactuator array," *Micro Electro Mechanical Systems, 2000. MEMS 2000. The Thirteenth Annual International Conference on*, pp. 662–667, 2000.

[45] M. Ataka, A. Omodaka, and H. Fujita, "A biomimetic micro motion system," *Transducers— Digest Int. Conf. on Solid-State Sensors and Actuators*, pp. 38–41.

[46] D.K. Cheng, *Field and wave electromagnetics*, Addison-Wesley Reading, 1989.

[47] L.J. Hornbeck, "Digital Light Processing and MEMS: Timely Convergence for a Bright Future," *Micromachining and Microfabrication*, vol. 95, 1995.

[48] MC Wu, "Micromachining for optical and optoelectronic systems," *Proceedings of the IEEE*, vol. 85, no. 11, pp. 1833–1856, 1997.

[49] H. Urey, "MEMS scanners for display and imaging applications," *Proc. SPIE*, vol. 5604, pp. 218–229, 2004.

[50] T. Otto, R. Saupe, A. Weiss, V. Stock, R. Bruch, and T. Gessner, "Principle and applications of a new MOEMS spectrometer," *Proceedings of SPIE*, vol. 6114, pp. 611409, 2006.

[51] B. CHARLOT, F. PARRAIN, S. MIR, and B. COURTOIS, "A self-testable CMOS thermopile-based infrared imager," *SPIE proceedings series*, pp. 96–103.

[52] H. Urey, "Torsional MEMS scanner design for high-resolution display systems," *Proc. SPIE*, vol. 4773, pp. 27–37, 2002.

[53] Y. Silberberg, P. Perlmutter, and JE Baran, "Digital optical switch," *Applied Physics Letters*, vol. 51, pp. 1230, 1987.

[54] DJ Bishop, CR Giles, and GP Austin, "The Lucent LambdaRouter: MEMS technology of the future here today," *Communications Magazine, IEEE*, vol. 40, no. 3, pp. 75–79, 2002.

[55] TS Perry, "Tomorrow's TV-the grating light valve," *Spectrum, IEEE*, vol. 41, no. 4, pp. 38–41, 2004.

[56] S.R. Kubota, "The Grating Light Valve Projector," *Optics and Photonics News*, vol. 13, no. 9, pp. 50–53, 2002.

[57] PF Van Kessel, LJ Hornbeck, RE Meier, MR Douglass, T.I. Inc, and TX Plano, "A MEMS-based projection display," *Proceedings of the IEEE*, vol. 86, no. 8, pp. 1687–1704, 1998.

[58] L.J. Hornbeck, "Digital Light Processing: A New MEMS-Based Display Technology," *Technical Digest of the IEEJ 14th Sensor Symposium*, vol. 6, pp. 297–304, 1996.

[59] MB Wakin, JN Laska, MF Duarte, D. Baron, S. Sarvotham, D. Takhar, KF Kelly, and RG Baraniuk, "An Architecture for Compressive Imaging," *Image Processing, 2006 IEEE International Conference on*, pp. 1273–1276, 2006.

[60] S.K. Nayar, V. Branzoi, and T.E. Boult, "Programmable Imaging: Towards a Flexible Camera," *International Journal of Computer Vision*, vol. 70, no. 1, pp. 7–22, 2006.

[61] R.A. Hicks, V.T. Nasis, and T.P. Kurzweg, "Micromirror array theory for imaging sensors," *SPIE, Photonics West, San Jose*, 2007.

[62] R. Kingslake, *Optical system design*, 1983.

[63] M. Watanabe and SK Nayar, "Telecentric optics for focus analysis," *Pattern Analysis and Machine Intelligence, IEEE Transactions on*, vol. 19, no. 12, pp. 1360–1365, 1997.

[64] VA Aksyuk, S. Arney, NR Basavanhally, DJ Bishop, CA Bolle, CC Chang, R. Frahm, A. Gasparyan, JV Gates, R. George, et al., "238/spl times/238 micromechanical optical cross connect," *Photonics Technology Letters, IEEE*, vol. 15, no. 4, pp. 587–589, 2003.

[65] VA Aksyuk, F. Pardo, D. Carr, D. Greywall, HB Chan, ME Simon, A. Gasparyan, H. Shea, V. Lifton, C. Bolle, et al., "Beam-steering micromirrors for large optical cross-connects," *Lightwave Technology, Journal of*, vol. 21, no. 3, pp. 634–642, 2003.

[66] V.T. Nasis, R.A. Hicks, , and T.P. Kurzweg, "Programmable Imaging with a Single MOEM mirror," *Applied Optics*, vol. to be submitted, 2007.

[67] V.T. Nasis, R.A. Hicks, and T.P. Kurzweg, "Digital photographic imaging using MOEMS," *Proceedings of SPIE*, vol. 6114, pp. 61140N, 2006.

[68] H.Y. Shum and R. Szeliski, "Systems and Experiment Paper: Construction of Panoramic Image Mosaics with Global and Local Alignment," *International Journal of Computer Vision*, vol. 36, no. 2, pp. 101–130, 2000.

[69] T. Kanade, P. Rander, and PJ Narayanan, "Virtualized reality: constructing virtual worlds from real scenes," *Multimedia, IEEE*, vol. 4, no. 1, pp. 34–47, 1997.

[70] B. Wilburn, N. Joshi, V. Vaish, E.V. Talvala, E. Antunez, A. Barth, A. Adams, M. Horowitz, and M. Levoy, "High performance imaging using large camera arrays," *International Conference on Computer Graphics and Interactive Techniques*, pp. 765–776, 2005.

[71] N. Joshi, W. Matusik, and S. Avidan, "Natural video matting using camera arrays," *International Conference on Computer Graphics and Interactive Techniques*, pp. 779–786, 2006.

[72] Y. Nomura, L. Zhang, and S.K. Nayar, "Scene Collages and Flexible Camera Arrays," in *Proceedings of Eurographics Symposium on Rendering*, Jun 2007.

[73] S.E. Chen, "QuickTime VR: an image-based approach to virtual environment navigation," *Proceedings of the 22nd annual conference on Computer graphics and interactive techniques*, pp. 29–38, 1995.

[74] M. Irani, P. Anandan, and S. Hsu, "Mosaic based representations of video sequences and their applications," *International Conference on Computer Vision*, pp. 605–611, 1995.

[75] HS Sawhney, R. Kumar, G. Gendel, J. Bergen, D. Dixon, and V. Paragano, "VideoBrush TM: experiences with consumer video mosaicing," *Applications of Computer Vision, 1998. WACV'98. Proceedings., Fourth IEEE Workshop on*, pp. 56–62, 1998.

[76] D. Taylor, "Virtual camera movement: The way of the future," *American Cinematographer Magazine Online*, vol. 77, no. 9, pp. 93–100, 1996.

[77] A. Ndalianis, "The Frenzy of the Visible: Spectacle and Motion in the Era of the Digital," .

[78] J.C. Yang, M. Everett, C. Buehler, and L. McMillan, "A real-time distributed light field camera," *Proceedings of the 13th Eurographics workshop on Rendering*, pp. 77–86, 2002.

[79] D. Lanman, D. Crispell, M. Wachs, and G. Taubin, "Spherical Catadioptric Arrays: Construction, Multi-View Geometry, and Calibration," *Proceedings of the Third International Symposium on 3D Data Processing, Visualization, and Transmission (3DPVT'06)*, pp. 81–88, 2006.

[80] S. Anger, D. Bayer, C. Cason, CDA Dilger, S. Demlow, A. Enzmann, DFT Wegner, and C. Young, "POV-Ray: Persistence of the Vision Ray Tracer; 1997," *See the POV-Ray WWW home page at http://www. povray. org*.

[81] M. Watanabe and S.K. Nayar, "Rational Filters for Passive Depth from Defocus," *International Journal of Computer Vision*, vol. 27, no. 3, pp. 203–225, 1998.

[82] M. Subbarao and G. Surya, "Depth from defocus: A spatial domain approach," *International Journal of Computer Vision*, vol. 13, no. 3, pp. 271–294, 1994.

[83] J. Ens and P. Lawrence, "An investigation of methods for determining depth from focus," *IEEE Transactions on Pattern Analysis and Machine Intelligence*, vol. 15, no. 2, pp. 97–108, 1993.

[84] R. Ng, M. Levoy, M. Bredif, G. Duval, M. Horowitz, and P. Hanrahan, "Light field photography with a hand-held plenoptic camera," *Computer Science Technical Report CSTR*, vol. 2, 2005.

[85] G.K. Fedder, "Top-down design of MEMS," *Technical Proceedings of the International Conference on Modeling and Simulation of Microsystems (MSM 2000), San Diego, CA, March*, pp. 27–29, 2000.

[86] H. Toshiyoshi and H. Fujita, "Electrostatic micro torsion mirrors for an optical switch matrix," *Microelectromechanical Systems, Journal of*, vol. 5, no. 4, pp. 231–237, 1996.

[87] WC Young, "Roarks Formulas for Stress and," *Strain, 6th Edition. McCraw-Hill*, p. 703, 1989.

[88] L. Dellmann, S. Roth, C. Beuret, G.A. Racine, H. Lorenz, M. Despont, P. Renaud, P. Vettiger, and NF de Rooij, "Fabrication process of high aspect ratio elastic structures forpiezoelectric motor applications," *Solid State Sensors and Actuators, 1997. TRANSDUCERS'97 Chicago., 1997 International Conference on*, vol. 1, 1997.

Appendix A. System Components

A.1 Camera

Sony DFW V300

-Image Sensor 1/3" IT Color CCD

-Effective Pixels768(H) X 492(V) / 752(H) X 585(V)

-Resolution 460(H) X 350(V) TV lines / 450(H) X400(V) TV lines

-LensX12 Power Zoom, ~ f=5.4~64.8mm, F1.8~F2.7

A.2 Lens

75mm Double Gaussian Macro Lens

Focal Length	75mm	
	Min.	Max.
Primary Mag	0.35X	N/A
FOV (2/3" CCD Hor)	26.8mm	6.1°
FOV (1/2" CCD Hor)	19.5mm	4.5°
Resolution in Object Space (1/2" CCD)	>22 lp/mm	N/A
Working Distance	250mm	Infinity
Aperture (f/#)	F4 - F30	
Distance to First Lens*	11.8~37.7mm	
Filter Thread	M49 x 0.75mm	

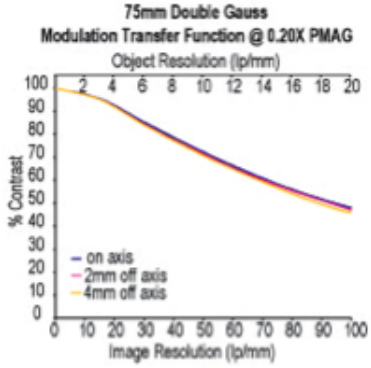

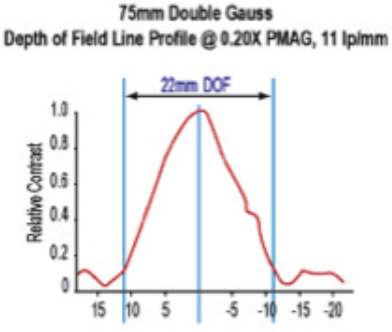

Appendix B. Case Study: Overglass Antireflection Coating

The glass of Lucents MOEMS chip has shown for long time signs of high reflection (see Figure B.1). We have speculated, that the reflection caused by that over glass protection of the chip may be responsible for not allowing the camera to focus on an object through the MOEMS mirrors.

After acquiring from Lucent just the piece of the glass that covers the MOEMS chip we were able to investigate its properties in higher depth. One of the tasks that we wanted to proof experimentally was whether its reflectance prevents us from imaging of any micro mirrors.

In order to proof the above we took one micro-mirror ($700\mu m$ diameter) made by Fraunhofer IPMS and we placed it opposite of an image that contains the word "Drexel University". Opposite of the mirror placed a camera that attempts to focus on the image through the micro-mirror (see Figure B.2).

The Fraunhofer micro mirror was placed on a post and on the same axis with the camera as it is shown above. We first captured an image of just the micro-mirror (Figure B.3) as it is seen from the cameras point of view.

We then attempted to focus on the image through the micro-mirror. As we can see from Figure B.4 we can indeed do so. The result looks like as were imaging with a pinhole camera. As we can see on Figure B.4 we have achieved to focus on the image and as a result we can read back the letter "D" from the word "Drexel University" that is written on the image surface. If we rotate the mirror slowly we will be able to read the rest of the word that is written. Then by doing image mosaicing we reconstructed the entire image.

If we put the piece of glass that was given to us from Lucent, which is the same as the over glass that covers the MOEMS chip surface in order to protect the mirrors, and we placed the glass in front of the micro-mirror that we used previously and we keep the rest of the set up the same as it is described above, then we see a very high reflection. By doing this experiment we were able able to observe that the reflection of that glass was strong enough to prevent us from focusing on an imaging surface through the mirrors and not through the glass surface (Figure B.5).

As we can see on Figure B.5 the reflection of the glass is very significant and it kind of looks like with Figure B.1. The reason that the glass here is a bit more reflective than in Figure B.1 its because the light intensity in this case was much higher and also the camera that the two pictures was take was different as well.

On the next and most crucial step we attempted to focus off the micro-mirror on the image plane. As we see on Figure B.6 such thing is impossible and the only thing that we achieve is to focus on the image plane off the glass surface.

We can observe that the Figures B.5 and B.6 seem to be a little bit distorted. This is due to the fact that the glass plate in front of the mirror was holed by hand and as a result it wasnt able to be kept perfectly still when the picture was captured.

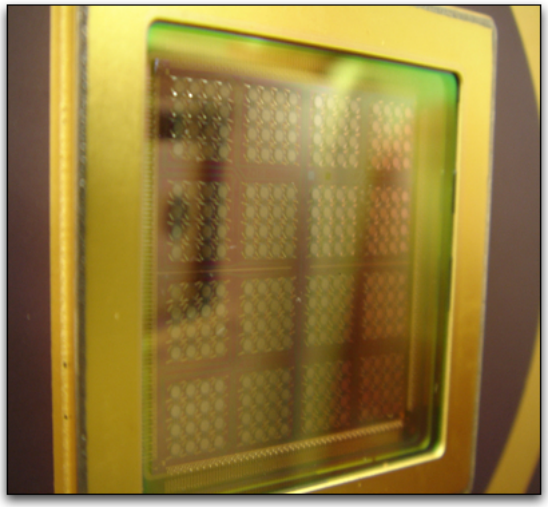

Figure B.1: The Lucent's Mirror MOEMS chip. The reflection from the over glass is very dominant. The overglass has layers of antireflecting coatings in both sides for the wavelength of $1.5\mu m$.

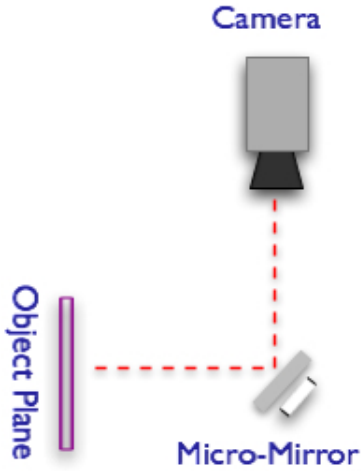

Figure B.2: Diagram of the experiment setup

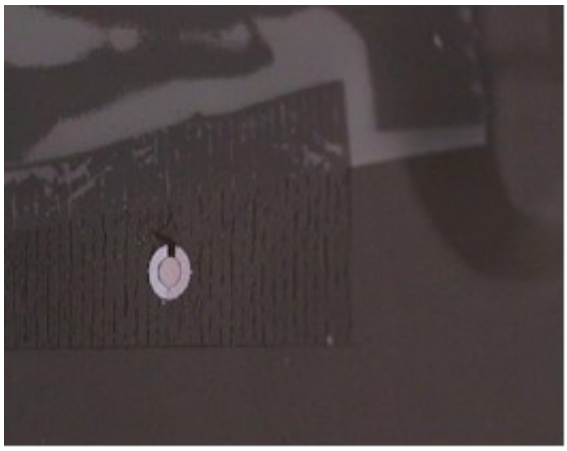

Figure B.3: Close up of the Fraunhofer Micro-mirror placed on a post

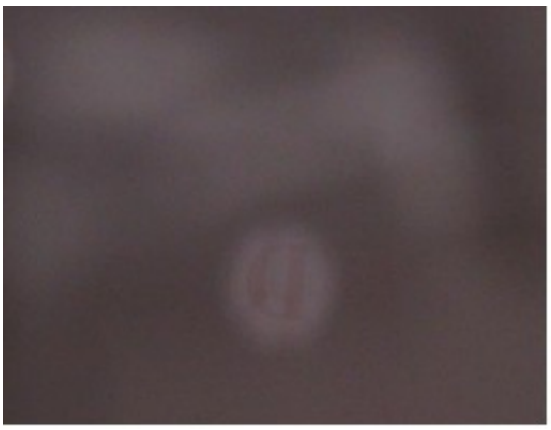

Figure B.4: The camera is focuses on the image through the micro-mirror.

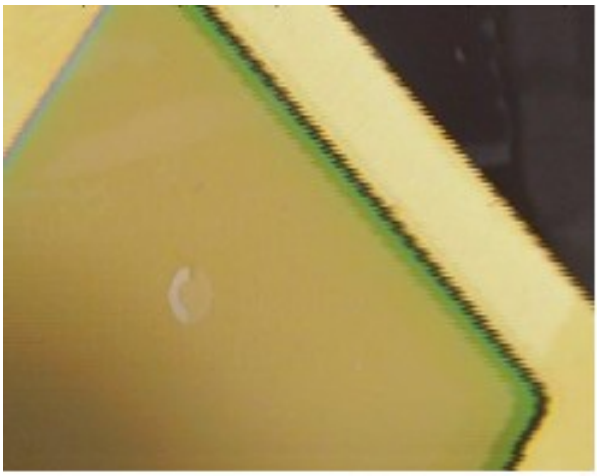

Figure B.5: The glass is placed in front of the micro-mirror.

Figure B.6: The camera is focuses on the image through the glass surface on top of the mirror.

From all the above, we can come to the conclusion that we could do imaging using all of the mirrors on Lucent's Lambdarouter chipset but the reflection of the over glass is preventing us from achieving this task.

Appendix C. Electrostatic Motion of MOEMS

Below we provide a brief description of how most of the electrostatic actuators operate depending on forces acting on them and the type of motion they cause.

Lateral Movement

A system diagram of the lateral movement is shown in Figure C.1. In this case Plate 1 is fixed, while Plate 2 can only move on the x direction. Assuming the applied voltage V between the two plates is constant, the electrostatic force generated between them is only in the x direction and is given by:

$$F_x = -\frac{\partial U_E}{\partial x} = -\frac{1}{2}V^2\frac{\partial C_{overlap}}{\partial x} \tag{C.1}$$

where $U_E = \frac{1}{2}C_{overlap}V^2$ is the system-stored energy and $C_{overlap}$ is the capacitance of the overlap area between the two plates, and W and L are the width in the z direction and length in the x direction of each plate, respectively. Assume the plate thickness T$\ll$ W, L, d_0. Then the fringing effect contributing to the capacitance in negligible, and the overlap capacitance is simply given by

$$C_{overlap} = \frac{\varepsilon_0\varepsilon_{medium}L_{overlap}W}{d_0} = \frac{\varepsilon_0\varepsilon_{medium}(L-X)W}{d_0} \tag{C.2}$$

By using the above equations the generated electrostatic force F_x is given by

$$F_x = \frac{1}{2}\frac{\varepsilon_0\varepsilon_{medium}W_z}{d_0}V^2 \quad for \quad x < L \tag{C.3}$$

Under this condition, F_x is independent of the displacement X of the plate, which means that as long as x is less than the plate overlap L_x, the electrostatic force is a constant. In fact, under certain conditions and particularly for a high aspect ratio plate structure or T/W close to unity, the fringing fields cannot be ignored and a more rigorous model is necessary. This whole movement will classify the particular device as *in-plane*.

Perpendicular Movement

As shown in Figure C.2, perpendicular motion takes place when Plate 1 is fixed and Plate 2 is moveable. If a voltage is applied across them, Plate 2 will move closer to Plate 1 due to electrostatic force. Assume the plate area is A, the original separation between them is d_0, and the applied voltage is a constant V. When separation becomes y, the force exerted on each plate is given by

$$F_y = \frac{1}{2}\frac{\varepsilon_0\varepsilon_{medium}A}{y^2}V^2 \tag{C.4}$$

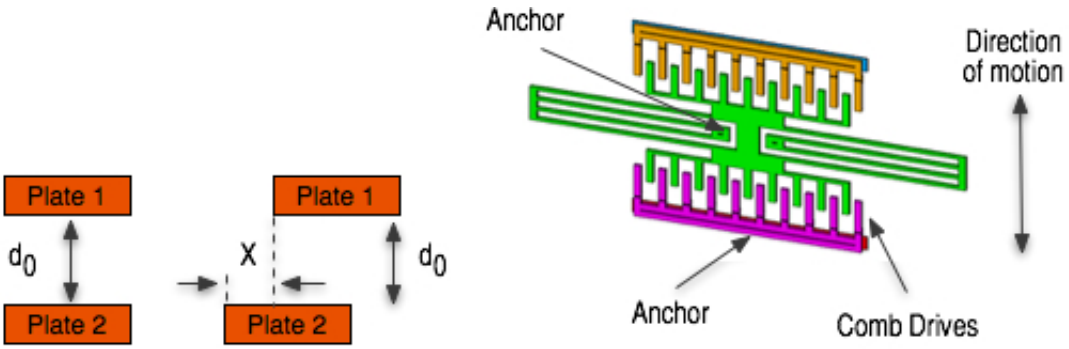

(a) Parallel actuation diagram. (b) Comb drive actuated device.

Figure C.1: In C.1(a) we see a diagram of parallel actuation between parallel plates. Based on this model we see on C.1(b) parallel motion comb drive actuation system

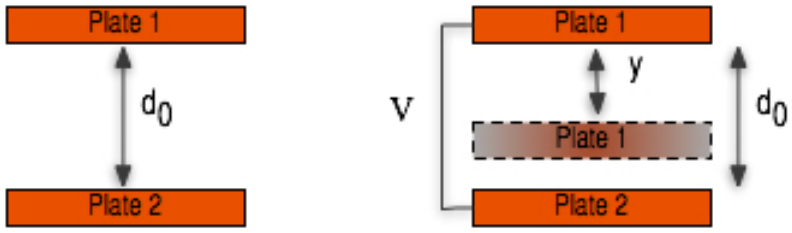

Figure C.2: Actuation of two oppositely charged parallel plates

where ε_0 and ε_{medium} are the permitivity of vacuum and the relative dielectric constant of material between the plates, respectively. The force is directed toward Plate 1, and it increases as y decreases. Equilibrium is usually established by a mechanical restoring force due to a spring. Equilibrium is usually established by a mechanical restoring force due to a spring. However, when y reached a certain value, a *pull-in* effect will occur, in which the electrostatic force overcomes the mechanical force, leading to instability [85].

One major problem of this actuation is the pull-in effect. This effect limits the stable deflection range. Here we use a simple model to describe this phenomenon and discuss how to avoid it and extend the deflection of the micro-plate or mirror.

This idealized model is similar to the system in Figure C.2. The movable Plate 1 is suspended above fixed plate by an elastic spring. The applied voltage between the plates is V. The electrostatic force causes Plate 1 to move downward. The equilibrium position of Plate 1 can be found by equating the electrostatic and mechanical forces. As V increases, at a critical value called the *pull-in* voltage (V_{PI}), the plate suddenly

collapses to the substrate. For a simple parallel plate, the pull-in voltage is

$$V_{PI} = \sqrt{\frac{8kg_0^3}{27\varepsilon_0 A}} \tag{C.5}$$

where k, g_0 and A are the effective spring constant, original gap, and plate effective area respectively. The maximum stable deflection Plate 1 is one third of the original gap g_0, to avoid pull-in.

Out-of-plane electrostatic actuation of a plate or mirror commonly used for several purposes: forming phase grating for display applications, and deforming mirrors for adaptive optics applications or for optical modulation, switching, or even optical variable attenuation applications. Such devices can be plates supported at both edges or hinge-supported micromirrors. When a voltage of sufficient magnitude is applied between the supported structure and the pulldown down electrode, the microplate or mirror is pull down to the substrate. When the applied voltage is removed, the structures are returned to the non-deflected position by the mechanical elastic restoring force.

Torsional Movement

In the Torsional movement case, a plate L_m long, W_m wide, and T thick is supported by two narrow torsion beams, which are L_t long, W_t wide, and T thick, as shown on Figure C.3. The supporting beams provide the pivot beam for the plate. When the plate is electrostatically actuated, it will rotate around the supporting torsion beam either clockwise or counterclockwise, depending on how the actuating voltage is applied. Therefore, it becomes a bit complicated to calculate the capacitance, especially the differential capacitance. So an alternative approach is used to analyze the system.

When the plate is rotated counterclockwise by an angle θ as shown on Figure C.3 the magnitude of the electrostatic field along the plate varies in the x direction. At position x it is given as

$$E = \frac{V}{(d/sin\theta - x)\theta} \tag{C.6}$$

where V is the applied voltage [86]. This equation is also valid for the other two conditions: when the place is rotated clockwise and not actuated. For example, when the plate is not rotated, then $\theta = 0$, and the electrostatic field is given by

$$\lim_{\theta \to 0} E = \frac{V}{d} \tag{C.7}$$

which is the electrostatic field for two parallel plates with separation d. The force on the actuated plate is also position-dependent. The average force can be estimated by integrating the force distribution along the x axis, and is given by

$$F_A = \int_0^{L_m/2} PW_m dx = \frac{\varepsilon_0 W_m}{2} \int_0^{L_m/2} E^2 dx \tag{C.8}$$

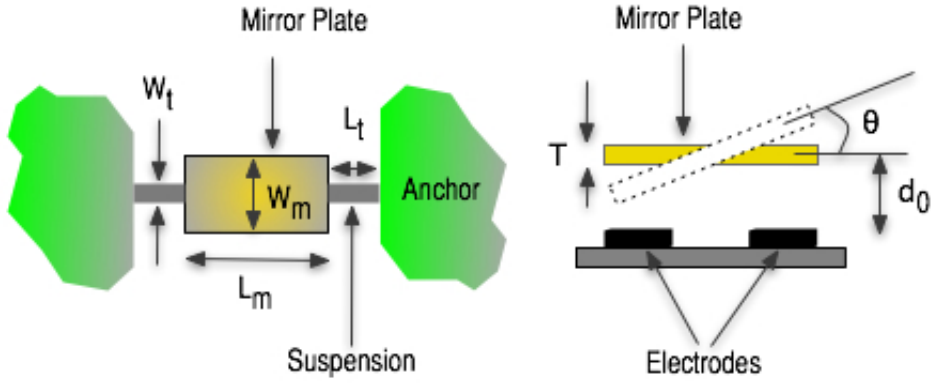

(a) Torsional Actuated Device.

(b) Cross-section of torsional actuated device.

Figure C.3: In C.3(a) we see a typical torsional actuated devices. The particular device is using electrodes to initiate motion shown on Figure C.3(b).

where $P = \varepsilon_0 E^2/2$ is the electrostatic pressure on the plate surface. Similarly, the total torque by electrostatic attraction exerted on the plate can be obtained as

$$T_E = \int_0^{L_m/2} xPW_m dx \tag{C.9}$$

This torque, on the other hand, is balanced by the restoring torque of the torsion supporting beams, which is

$$T_R = \frac{2GW_b T_b^3}{3L_b}\theta\left[1 - \frac{192}{\pi^5}\frac{T_b}{W_b}tanh\left(\frac{\pi W_b}{2T_b}\right)\right] \tag{C.10}$$

where G is the elastic constant of the plate material, and W_b, T_b, and L_b are the width, thickness, and length of the torsion beam, respectively [87]. From the above equations the maximum rotation angle can be obtained for each applied voltage.

In resonance mode, the equation describing the motion for small oscillation amplitudes is given by

$$\ddot{\theta} + \frac{2k}{Ih}\theta = 0 \tag{C.11}$$

where $k = 2Gt^3/3h$, and I is the movement of inertia ($Lt \gg w,\ t$) and is given by

$$I = \frac{M}{12}(W_m^2 + r^2) = \frac{\rho L_m W_m t}{12}(W_m^2 + t^2) \tag{C.12}$$

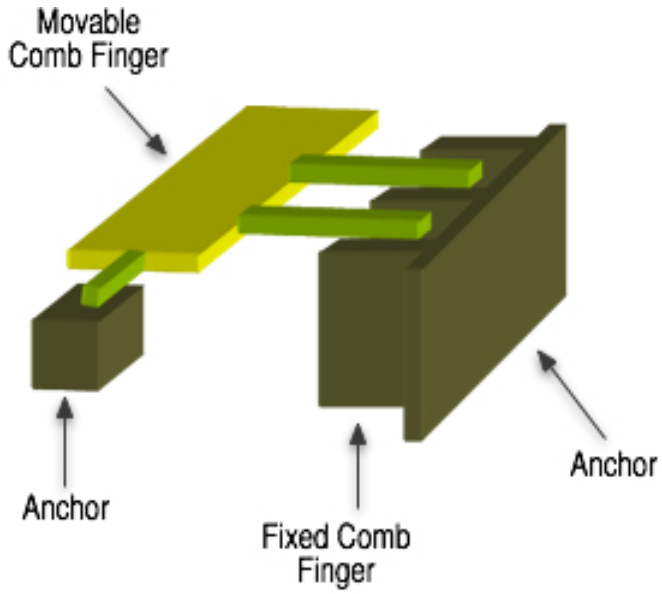

Figure C.4: Asymmetric Comb Drive structure

Therefore, the resonant frequency is

$$\varpi_R = \sqrt{\frac{Gt^2}{L_t}\frac{72}{\rho L_m(W_m^2 + t^2)}} \tag{C.13}$$

Similar to the parallel plate, if the applied voltage reaches a certain value, a pull-in effect can occur for the torsion plate [88].

Torsional motion by electrostatic actuation can be achieved in a plate or a mirror that has a suitable suspension about which the structure may rotate. The actuation force may be applied from an electrode placed under one side of the mirror as show in Figure C.4. Alternatively, another option is to use *asymmetric* comb drives to actuate the plate or mirror attached to one side of the comb fingers. The type of motion that the device has results in classifying it as *out-of-plane* actuated device.

Unlike, the conventional symmetric comb drive, the asymmetric comb drive has finders on one comb with different thickness and in a different plane from those on the other comb. When the voltage is applied between the comb fingers, the force resulting from the fringing electric field pulls the movable comb down to the substrate. The difference of the height and thickness of the comb fingers leads to a differential capacitance, which is related to the position of the movable comb fingers. Similarly to the *in-plane* comb drive, this structure also has two actuation modes: *static* and *dynamic*.

The *pull-in* effects have been studied extensively for torsional actuators and particular for torsional plates. When a voltage is applied to the plates, an electrostatic

torque T_E upon the top plate is generated. Since, the top plate is suspended by the torsion beams, it is also subjected to a mechanical torque T_R. When T_E overcomes T_R, pull-in causes the two plates to touch each other. Assuming the applied voltage is time-variant, the torsion angles ca be obtained by solving the following equation:

$$K_a\alpha = T_E \tag{C.14}$$

where K_a is the spring torque coefficient and α is the rotation angle.

At low voltages the above equation. has two solutions, but only one is stable. When the applied voltage reaches a certain value, the two solutions become equal. This voltage is called the $pull-in$ voltage. If the applied voltage is bigger than $V_{pull-in}$ the electrostatic torque becomes bigger than the mechanical restoring torque at any angles. That means the torsion plate collapses to the substrate. The pull-in voltage can be calculated with the following formula.

$$V_{PI}(\beta,\gamma) = \sqrt{\frac{2K_a d^3}{\varepsilon_0 a_3^3 b} f(\beta,\gamma)} \tag{C.15}$$

where $f(\beta,\gamma)$ is given as:

$$f(\beta,\gamma) = \frac{\theta_{PI}^3}{\frac{1}{1-\beta\theta_{PI}} - \frac{1}{1-\gamma\theta_{PI}} - ln\left(\frac{1-\beta\theta_{PI}}{1-\gamma\theta_{PI}}\right)} \tag{C.16}$$

In the above equations d is the gap between the two plates at the axis of rotation, α is the angle between the two plates, $\alpha_{max} = d/3$, $\beta = \alpha_2/\alpha_3$, $\gamma = \alpha_1/\alpha_3$, $\theta = \alpha/\alpha_{max}$ and α_1,α_2, α_3 are the distances from the axis of rotation to the nearest edge of the plate, to the end of the plate and the end of the proof mass, respectively.

Vasileios T. Nasis

Drexel University
Electrical and Computer Engineering
vtn23@drexel.edu +1 (267) 237 3380

Education

Doctor of Philosophy in Electrical and Computer Engineering
Drexel University, 2008
Master of Science in Electrical and Computer Engineering
Drexel University, 2004
Bachelor of Science in Electrical and Computer Engineering
Drexel University, 2002
Associate of Science in Engineering Science
Camden County College, 1997

Professional Profile

Creative problem solver, decisive team leader and persuasive communicator with well-developed presentation and negotiation skills. Able to develop productive relationships with colleagues, customers and staff at all levels.

Employment

Photonics, Inc - Philadelphia, PA, USA *Spring 2008 to present*
Chief Operating Officer (COO)
Responsible for product development, customer relations and investor relations in one of the most promising start-up companies in the Telecommunications sector that develops switches, couplers and modulators directly on the fiber based on proprietary technology

Drexel University - Philadelphia, PA, USA *Winter 2008 to present*
Adjunct Assistant Professor
Teaching courses in the Electrical and Computer Engineering mainly on the field of Telecommunications, Electronics, DSP and Optics.

Netronix, Inc. - Philadelphia, PA, USA *Fall 2006 to present*
President and CEO

Leading the company that develops the most unique and comprehensive solutions in the industry for monitoring remotely sensors that measure environmental pollution.

Drexel University - Philadelphia, PA, USA *Summer 2002 to Winter 2007*
Research Assistant

- Developed an innovative systems level digital imaging device using Micro- Electromechanical Mirrors for programmable imaging. Proposed applications of this innovative technology.
- Developed algorithm for automatic Breast Cancer Detection and tumor classification using digital signal processing on ultrasound signals.
- Developed algorithm for automatic landmine detection in all fields using Ground Penetrating Radar. This algorithm was proposed for application to the Department of Defense.
- Participate in research on wireless network protocols.

Drexel University - Philadelphia, PA, USA *Summer 2002 to Winter 2007*
Teaching Assistant
Participate in teaching various undergraduate courses in the field of Electrical and Computer Engineering. Also participated in designing electric circuits labs for undergraduate students.

Fraunhofer Institute ISIT - Itzehoe, Germany *Summer 2006 to Fall 2006*
Visiting Researcher
Developed models and methods that described the motion of a single micro-optical electromechanical (MOEM) mirror laser projector system. The model helped in resolving some fundamental distortions caused by the micro-mirrors system design and the physics of projection.

Marconi Communications - Warrandale, PA, USA *Fall 2000 to Spring 2001*
Product Integrity Engineer
Developed automated testing procedures for systems such as: Ethernet 10/100, SONET, ATM. Also developed automation of Thermal-chambers by the use of a self-developed GUI program. Interfaced with vendors (HP, Agilent, Tektronix, LeCroy), institutions (University of New Hampshire) and international government offices (Ministry of Telecommunications, Greece) for the acquisition and set-up of new products, procedures, and configurations.

Publications

- R. Andrew Hicks, **Vasileios T. Nasis** and Timothy P. Kurzweg, *"Programmable Imaging with two-axis Micromirrors* Optics Letters, Vol. 32, Issue 9, pp. 1066-1068

- Petropulu, A.P.; **Nasis, V.T.**; Tretiak, O.; Piccoli, C.W.; *"Benign versus malignant classification of breast tumors based on the the PLSN model for the ultrasound RF echo and homomorphic filtering* Engineering in Medicine and Biology Society, 2004. EMBS 2004

- **V. Nasis**, G. Ford and A. Hirebet, *"ECSPLOD:Elimination of Clutter Through signal Processing for Landmine/Ordnance Detection.*, IEEE Region 2 Student Paper Contest Proceedings, April 2002

- **Vasileios T. Nasis**, *"Benign vs Malignant Classifications of Breast Tumors Based on the PLSN Model for the Ultrasound RF Echo*, Masters in Science Thesis 2004, Drexel University Hagerty Library.

- **Vasileios T. Nasis**, *"A Novel Approach to Programmable Imaging Using MOEMS*, Doctor of Philosophy Thesis 2007, Drexel University Hagerty Library.

Awards and Honors

- Research Award for Research, Innovation, Scholarship and Creativity Day 2007 Drexel University

- Honorary mention Research Day competition 2004- Drexel University

- UNYSIS Award for Best Senior Design Project 2002 Drexel University

- Recipient of Best Student Paper Award (IEEE Region 2 April 02)

- Member of the Golden Key National Honor Society

- Recipient of Deans Scholarship Drexel University

- Two-time recipient of Math Scholarship Camden County College